Catalytic RNAs as a target and a tool for the control of gene expression in mammalian cells and bacteria

Doctoral thesis for obtaining the

academic degree

Doctor of Natural sciences

(Dr. rer. nat.)

submitted by

Kläge, Dennis

at the

Universität Konstanz

Faculty of Sciences

Department of Chemistry

Konstanz, 2024

Tag der mündlichen Prüfung: 14.06.2024

1. Referent: Prof. Dr. Jörg Hartig

2. Referent: Prof. Dr. Valentin Wittmann

Prüfungsvorsitz: Prof. Dr. Martin Scheffner

Notes to the reader

The presented doctoral thesis is organized in three chapters that can be read independently and an additional conclusion that involves future prospects of catalytic RNAs as a tool and target to control gene expression.

In Chapter I a general introduction to the discovery and function of catalytic RNA is given as well as an overview of mRNA processing in eukaryotes and bacteria that is important for regulation of gene expression. Moreover, the relevance and specific mechanisms of artificial riboswitches are included and described.

Chapter II and Chapter III show results of two independent projects:

Chapter II highlights the potential of catalytic RNAs as a tool to control gene expression. A comparative examination of naturally occurring self-cleaving RNAs was conducted within different genetic contexts. Furthermore, it includes the design and optimisation of tetracycline-dependent riboswitches for the regulation of gene expression in HeLa cells.

Chapter III highlights the potential of catalytic RNAs as a target to control gene expression in bacteria. Newly synthesized glucosamine-6-phosphate mimics were examined on their efficiency to trigger the self-cleavage of the *glmS* ribozyme *in vitro* and their potential use as antimicrobial compounds for gram-positive bacteria.

Both chapters include an introduction, the results with a respective discussion and a conclusion. The used materials and methods are summarized separately in another section. All described experiments were conducted in the laboratory of Prof. Dr. Jörg S. Hartig (Department of Chemistry, University of Konstanz) from February 2020 until December 2023.

The synthesis of the investigated compounds in Chapter III was conducted by Dr. Bjarne Silkenath in collaboration with the laboratory of Prof. Dr. Valentin Wittmann (Department of Chemistry, University of Konstanz).

Parts of Chapter I and II are published in “A comparative survey of the influence of small self-cleaving ribozymes on gene expression in human cell culture” D. Kläge, E. Müller, J. S. Hartig, *RNA biology* **2024**, *21*, 1-11.

Parts of Chapter III are published in “Phosphonate and Thiasugar Analogues of Glucosamine-6-phosphate: Activation of the glmS Riboswitch and Antibiotic Activity” B. Silkenath, D. Kläge, H. Altwein, N. Schmidhäuser, G. Mayer, J. S. Hartig, V. Wittmann, ACS Chemical Biology **2023**, 18, 2324-2334.

Table of Contents

1. Abstract

RNAs with catalytic functions were discovered over 40 years ago. Since then, major advances were made investigating the biological function of catalytic RNAs and exploiting them as tools for artificial systems. Especially, the self-cleaving ribozymes are a suitable element for synthetic riboswitch design. Generally, riboswitches consist of a ligand-binding aptamer domain that is fused to an expression platform via a communication module. Upon ligand-binding, due to a conformational change of the expression platform, the information is transferred and gene expression can be regulated. Over the years, the interest in controlling transgene expression increased dramatically and artificial riboswitches are useful tools in versatile applications ranging from synthetic biology for basic research interests to potential therapeutic approaches.

Therapeutic contexts involve for instance the controlled expression or induction of cytokines like interleukins or interferon-gamma. Therefore, synthetic riboswitches require to be transferrable between different contexts maintaining their dynamic range, while regulating the expression of the respective gene of interest. Moreover, the system has to be sensitive and highly selective to the chosen ligand. Thereby, side effects from unspecific binding events or leaking background expression in the uninduced state can be prevented. Common therapeutic approaches involve viral vectors, such as Adeno-associated virus or Measles virus, as carriers to bring the synthetic riboswitch directly into the target cells. This poses limits to the switching system in order to be combinable with the viral context, like the small coding space. Moreover, for instance, transcription-dependent RNA-switches are difficult to apply to negative-sense single-stranded RNA-viruses, as Measles virus vectors. Therefore, it is important to develop always new switching systems to exploit them for different therapeutic strategies.

Riboswitches differ a lot in size and complexity. The simplest design utilizes an aptamer as *cis*-regulatory element to act as a roadblock for the ribosome or to control the accessibility of essential sequence elements within the mRNA upon ligand addition. Combining multiple elements, the dynamic range increases and the background expression in the OFF-state can be reduced. One common strategy is to fuse an aptamer to small self-cleaving ribozymes to create allosteric ribozymes. These so-called aptazymes can be inserted in either of the untranslated regions (UTR) of an mRNA to control its stability in a ligand-dependent manner. By now, several systems with high dynamic ranges exploiting aptazymes were designed. However, their context-dependent performance poses an obstacle to use them in therapeutic approaches. In this study, we implemented a comprehensive and comparative survey of the effect of inserting different self-cleaving ribozymes into mRNAs in human cell culture to expand the toolbox of ribozyme platforms. Furthermore, we used the obtained results to create new

tetracycline (Tet)-dependent aptazymes, based on the hepatitis delta virus-ribozyme (HDV). Although their induction levels upon ligand addition were lower than expected, we found strategies to optimize the system. Following different approaches, we were able to generate a set of ON-switching HDV-based aptazymes.

Moreover, we could show their great combinability with other synthetic riboswitches. By developing a Tet-dependent splice-based system, which is residing in the 5'-UTR of the mRNA of the gene of interest, we could develop combinations with aptazymes showing increased dynamic ranges. The splice-based system controls the presence of an upstream open reading frame (uORF) within the mRNA, which is effectively downregulating gene expression. By investigating different uORF sequences, aptamer structures and splice site properties, we were able to create a set of ON-switches. These show Tet-dependent switching on the protein level as well as on the RNA level. Additionally, we could show that this system is easily transferrable to another gene context maintaining its switching ability. The systems presented in this thesis add up to the already existing toolbox of synthetic riboswitches for human cell culture and our data can be used to improve future aptazyme designs.

However, we did not only examine self-cleaving ribozymes on their potential as a tool for controlling gene expression. We were also investigating the *glmS* ribozyme as it exploits another molecule to enhance its biological function. It uses glucosamine-6-phosphate (GlcN6P) as a coenzyme for self-cleavage. The presence of the *glmS* ribozyme almost exclusively in gram-positive bacteria makes it a convenient target for antibiotic drug development. Using artificial mimics of the natural ligand, which are not metabolized but efficiently trigger the self-cleavage of the ribozyme, we were able to interfere with cell metabolism and inhibited the growth of multiple different species, including human pathogens such as *S. aureus*. Thus, within this thesis we were able to develop genetic devices important for therapeutic strategies in human cell culture as well as to study the pathogenicity of different gram-positive bacteria using GlcN6P mimics.

2. Zusammenfassung

Schon vor über 40 Jahren wurden RNAs mit katalytischen Funktionen entdeckt. Seitdem wurden große Fortschritte bei der Erforschung der biologischen Funktion und ihrer Nutzung als Werkzeuge für künstliche Systeme erzielt. Insbesondere die selbstspaltenden Ribozyme waren für die Entwicklung synthetischer Riboswitches geeignet. Im Allgemeinen bestehen Riboswitches aus einer ligandenbindenden Aptamerdomäne, die über ein Kommunikationsmodul mit einer Expressionsplattform verbunden ist. Bei der Bindung des Liganden findet eine Konformationsänderung der Expressionsplattform statt, die die Information weiterträgt und so die Genexpression regulieren kann. Im Laufe der Jahre hat das Interesse für die Expression von Transgenen stark zugenommen. Riboswitches finden Platz in vielfältigen Anwendungen, die von der Grundlagenforschung bis hin zu potenziellen therapeutischen Ansätzen reichen.

In therapeutischen Ansätzen wird z.B. die Expression oder Induktion von Zytokinen wie Interleukinen oder Interferon gamma kontrolliert gesteuert. Daher sollten synthetische Riboswitches idealerweise zwischen verschiedenen Kontexten übertragbar sein, ohne ihre Schaltbarkeit zu verlieren. Außerdem muss das System sehr empfindlich und selektiv für den gewählten Liganden sein, um Nebenwirkungen durch unspezifische Bindungen oder zu hoher Basalexpression im nicht induzierten Zustand zu vermeiden. Übliche therapeutische Ansätze verwenden virale Vektoren, wie Adeno-assoziierte Viren oder Masernviren. Die dienen als Träger, um die synthetischen Schalter direkt in die Zielzellen einzuschleusen. Dadurch entstehen jedoch Einschränkungen für die RNA-Schalter, da sie in den viralen Kontext integriert werden müssen, z.B. darf der Schalter nicht zu groß sein. Darüber hinaus könnten beispielsweise transkriptionsabhängige RNA-Schalter in einsträngigen RNA-Viren mit negativer Polarität, wie Masernvirus-Vektoren, Probleme verursachen. Daher ist es wichtig, immer neue und verschiedene Schaltsysteme zu entwickeln, damit sie für verschiedene therapeutische Strategien einsetzbar sind.

Riboswitches unterscheiden sich stark in Größe und Komplexität voneinander. Das einfachste Design ist ein Aptamer als *cis*-regulierendes Element, welches das Ribosom beim Abscannen der mRNA blockiert oder die Zugänglichkeit essenzieller Sequenzen in Abhängigkeit vom Liganden kontrolliert. Durch eine Kombination mehrerer Elemente kann der Schalteffekt vergrößert und die Basalexpression im Aus-Zustand verringert werden. Eine oft verwendete Strategie besteht darin, ein Aptamer mit kleinen selbstspaltenden Ribozymen zu verknüpfen, um ligandenabhängige Ribozyme zu schaffen. Diese so genannten Aptazyme können in die untranslatierten Regionen (UTR) einer mRNA eingesetzt werden, um deren Stabilität selektiv zu steuern. Inzwischen wurden mehrere Systeme mit hohem Schalteffekt entwickelt, die auf Aptazymen basieren. Aber die Effizienz der Aptazyme ist kontextabhängig, was ihre

Verwendung in therapeutischen Ansätzen behindern kann. Daher haben wir in dieser Arbeit eine umfassende Untersuchung durchgeführt, um die Auswirkungen verschiedener selbstspaltender Ribozyme in der mRNA von menschlichen Zellen zu vergleichen. Damit zielen wir darauf ab, die existierenden Ribozym-Plattformen zu erweitern. Darüber hinaus nutzten wir diese Ergebnisse, um neue Tetracyclin (Tet)-abhängige Aptazyme zu entwickeln basierend auf dem Hepatitis-Delta-Virus-Ribozyms (HDV). Obwohl die Induktionslevel geringer als erwartet waren nach Zugabe vom Liganden, konnten wir das Systems weiter verbessern. Durch verschiedene Ansätze gelang es uns, eine Reihe von anschaltenden HDV-basierten Aptazymen zu erzeugen.

Außerdem konnten wir zeigen, dass sich Aptazyme hervorragend mit anderen synthetischen Riboswitches kombinieren lassen. Wir modifizierten ein Tet-abhängiges spleiß-basiertes System so, dass es in die 5'-UTR der mRNA einer Luciferase einsetzbar ist. In Kombination dieser Spleiß-Kassette mit den Aptazymen konnten wir höhere Schalteffekte beobachten als beide Systeme einzeln erzielen würden. Im hier verwendeten Kontext kontrolliert die Spleiß-Kassette das Vorhandensein eines upstream open reading frames (uORF) in der 5‘-UTR der mRNA. Dieses Element verhindert die Expression des nachfolgenden Zielgens. Durch die Untersuchung verschiedener uORF-Sequenzen, Aptamer-Strukturen und Spleißstellen-Eigenschaften konnten wir eine Reihe von anschaltenden Spleißschaltern entwickeln, die sowohl auf Proteinebene als auch auf RNA-Ebene eine Schalteffekt in Abhängigkeit von Tet zeigen. Darüber hinaus konnten wir zeigen, dass dieses System leicht auf einen anderen Genkontext übertragbar ist und die Schaltfähigkeit beibehält. Mit den in dieser Arbeit vorgestellten Systemen können wir die Sammlung der bereits vorhandenen synthetischen Riboswitches für die menschliche Zellkultur erweitern und Hilfestellung in der Konstruktion neuer Designs geben.

Wir haben die selbstspaltenden Ribozyme jedoch nicht nur auf ihr Potenzial zur Kontrolle der Genexpression analysiert. Ein Vertreter unter ihnen, das *glmS* Ribozym, nutzt ein weiteres Molekül, um seine biologische Funktion zu erweitern. Es verwendet Glucosamin-6-Phosphat (GlcN6P) als Coenzym für die Selbstspaltung. Da das *glmS* Ribozym fast ausschließlich in grampositiven Bakterien vorkommt, welche auch viele pathogene Stämme umfassen, ist dieses Ribozym ein geeignetes Ziel für die Entwicklung von Antibiotika. Durch die Nutzung von Mimetika des natürlichen Liganden, die nicht verstoffwechselt werden, aber effizient die Selbstspaltung des Ribozyms induzieren, konnten wir in den Zellstoffwechsel eingreifen und das Wachstum verschiedener Spezies hemmen. Darunter befanden sich auch humanpathogene Keime wie *S. aureus*. Im Rahmen dieser Arbeit konnten wir somit genetische Werkzeuge entwickeln, die einerseits für therapeutische Strategien in menschlichen Zellen einsetzbar und wichtig sind, und andererseits ein ideales Ziel ausmachen, um die Pathogenität verschiedener grampositiver Bakterien näher zu untersuchen.

3. Chapter I: General introduction

3.1 Properties and structure of RNA

Ribonucleic Acid (RNA) is a fundamental molecule found in all living cells, comprising chains of nucleotides. Each nucleotide consists of a ribose sugar molecule, a phosphate group, both forming the backbone of the RNA and one of four nitrogenous bases: adenine (A), cytosine (C), guanine (G), or uracil (U). The sequence of these bases contains information, crucial for protein synthesis and various cellular functions.

The exploration of RNA's significance dates back to the mid-20th century, marked by the advancing discoveries of scientists such as Francis Crick posing the Central dogma [3], Alexander Rich and David R. Davies for the first crystal structure of RNA [4] and Roger Kornberg for revealing the structure of the RNA polymerase and showing how RNA is synthesized [5]. Besides, the ground-breaking discovery of ribozymes, catalytic RNA molecules [6], challenged the long-held belief that only proteins could possess catalytic activity, revolutionizing our understanding of RNA's functional capabilities. RNA exhibits a high structural diversity. The single-stranded nature of RNA allows it to fold back on itself, forming complex secondary and tertiary structures (Figure 1A-B). These structures include stem loops, bulges, and multiloops. They are crucial for enabling RNA to perform its roles affecting gene expression directly [7], catalysis [8], and interactions with RNA-binding proteins [9]. Next to the frequently encountered kissing-loop and pseudoknot structure, the ribozyme-zipper and tetra loop-receptor motif are pre-eminently present in larger RNA structures such as group I introns.

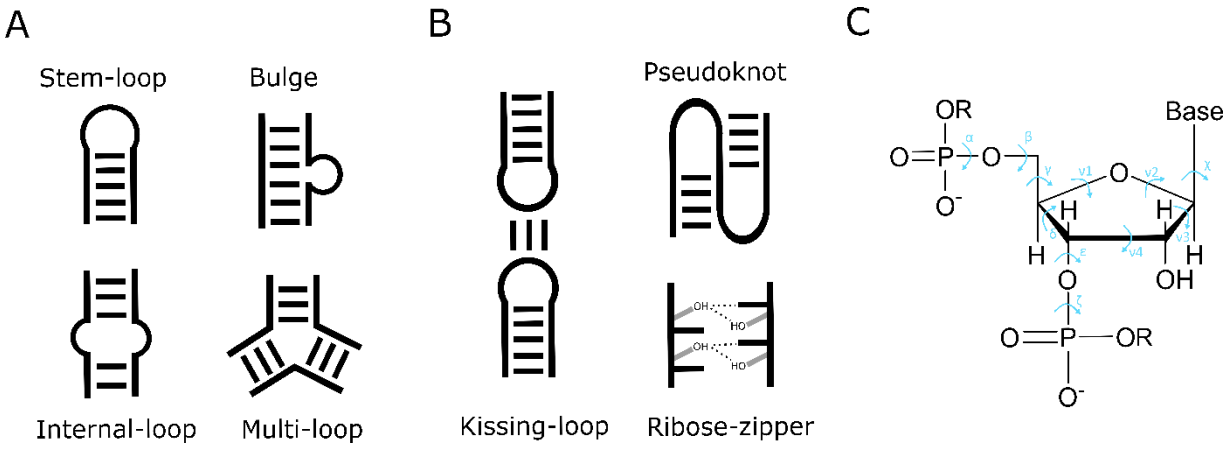

Figure 1: Overview of RNA structures. A) Different secondary structures formed by base pairing. B) Common tertiary structure motifs encountered in catalytically active RNAs. C) Depicted nucleotide within the RNA with annotated angles of torsion for the bonds of the RNA backbone (α–ζ), the nucleosidic bond (χ). The pseudo-rotation angles within the ribose ring are shown as v0–v4. The figure is adapted from Marek et al. [2]

Especially in larger molecules, the folding causes conformational heterogeneity depending on the environmental conditions. RNAs can form into more possible conformations than peptides of the same size due to the large number of dihedral angles [2] (Figure 1C). Subsequently, it could be shown that multiple native states can exist for one specific RNA [10], which regulate its function and affect its activity.

RNA exhibits unique chemical properties. Within the DNA, the uracil base is replaced by thymine. This way, frequent mutations are prevented in the replication process, as thymine cannot be formed easily by spontaneous deamination of cytosine. However, the uracil base present in RNA was found to exert less stable stacking interactions contributing in formation of bulge-out structures [11] being advantageous for RNA structuring. Besides, with the remaining 2'-hydroxy group of the ribose, RNA is susceptible towards base-catalysed hydrolysis, and it can easily be cleaved. Therefore, the presence and concentration of these polynucleotides is controlled as well and adds to the fine-tuned regulation processes they are involved in [12].

Moreover, RNA encompasses a spectrum of subclasses, each with distinct functions and roles within the cell. Messenger RNA (mRNA) serves as the intermediary carrier of genetic information from DNA to protein synthesis machinery. Transfer RNA (tRNA) plays a pivotal role in translating the genetic code and delivering specific amino acids to the ribosome during protein synthesis. Ribosomal RNA (rRNA) forms an integral part of the ribosome, the cellular machinery responsible for protein synthesis. Beyond that, there are less prominent members of non-coding RNAs, for instance: small nuclear RNA (snRNA) are involved in RNA maturation processes and have been shown to be a crucial part within the spliceosome [13]; circular RNA (circRNA), which can also encode polypeptides but mostly serve as protein scaffold or sponges for micro RNAs [14]; Ribozymes and Riboswitches, which are described and discussed more detailed within the next sections of this thesis.

Understanding the nuances and distinctions in RNA's structure, composition, and function highlights the remarkable versatility of this pivotal molecule within cells and across various organisms.

3.2 Transcription and mRNA processing in eukaryotes

Eukaryotic gene expression orchestrates the flow of genetic information from DNA to functional proteins, encompassing complex regulatory mechanisms at the transcriptional and translational level. In order to use catalytic RNAs as a tool to control gene expression in mammalian cells, one has to become aware of the exact mechanisms they are involved in.

RNA is produced from DNA within a cell in a process called transcription. It is a tightly regulated process and can be divided in three main stages: initiation, elongation, and termination. First, as the DNA is stored in a condensed state, the correct section of DNA has to be unwounded in order to be transcribed. The respective promoter must be accessible to proteins, such as transcription factors and the transcription apparatus including RNA polymerase II. This way, all different classes of RNA are made. In particular, the *de novo* transcribed pre-mRNA can be divided in different sections, the 5'-UTR, the 3'-UTR and the coding sequence (CDS) in-between. The CDS in turn contains segments coding for proteins (exons) but also interspersed regions, which are non-coding (introns).

Prior to translation, the introns must be removed. The precise joining of the exons is achieved in a process called splicing, which happens already co-transcriptionally [15]. The spliceosome, a dynamic macromolecular complex comprising small nuclear ribonucleoproteins (snRNPs) and associated proteins, governs the splicing process. To excise an intron from the pre-mRNA, two consecutive transesterification reactions are required [16] (Figure 2A). Highly conserved sequences at exon-intron boundaries, the 5' splice site (5'ss), branch point, polypyrimidine tract, and the 3' splice site (3'ss) guide the spliceosome in recognizing the splice sites for precise excision of introns and ligation of exons. The 5'ss is complementary to the U1 snRNP and is binding for initial detection [17]. Variations from the consensus motif decide on the strength of this site by reducing the binding affinity and make the intron less likely to be spliced out [18]. This strength can additionally be regulated by the presence of splicing enhancers or silencers, small sequences that reside within the exons and affect the spliceosome in its work [19].

The meticulous orchestration of sequential splicing steps: first, the splice site recognition, then intron excision and last, exon ligation; ensures accurate mRNA maturation. However, not every exon has to be included in the mature mRNA and can be removed (Figure 2B). Alternative splicing, a widespread mechanism across eukaryotic organisms, allows the generation of multiple mRNA isoforms from a single gene. By selectively including or excluding exons, cells produce a diverse array of protein isoforms with distinct structures and functions [20]. Using genome-wide analyses almost 95 % of all human genes were associated with alternative splicing [21]. Particularly, tissue-specific splicing patterns, including varying splice site strength,

RNA-binding proteins, and different splicing enhancers/silencers, carefully control this process in mammals, impacting development [22], cellular differentiation [23], and disease [24].

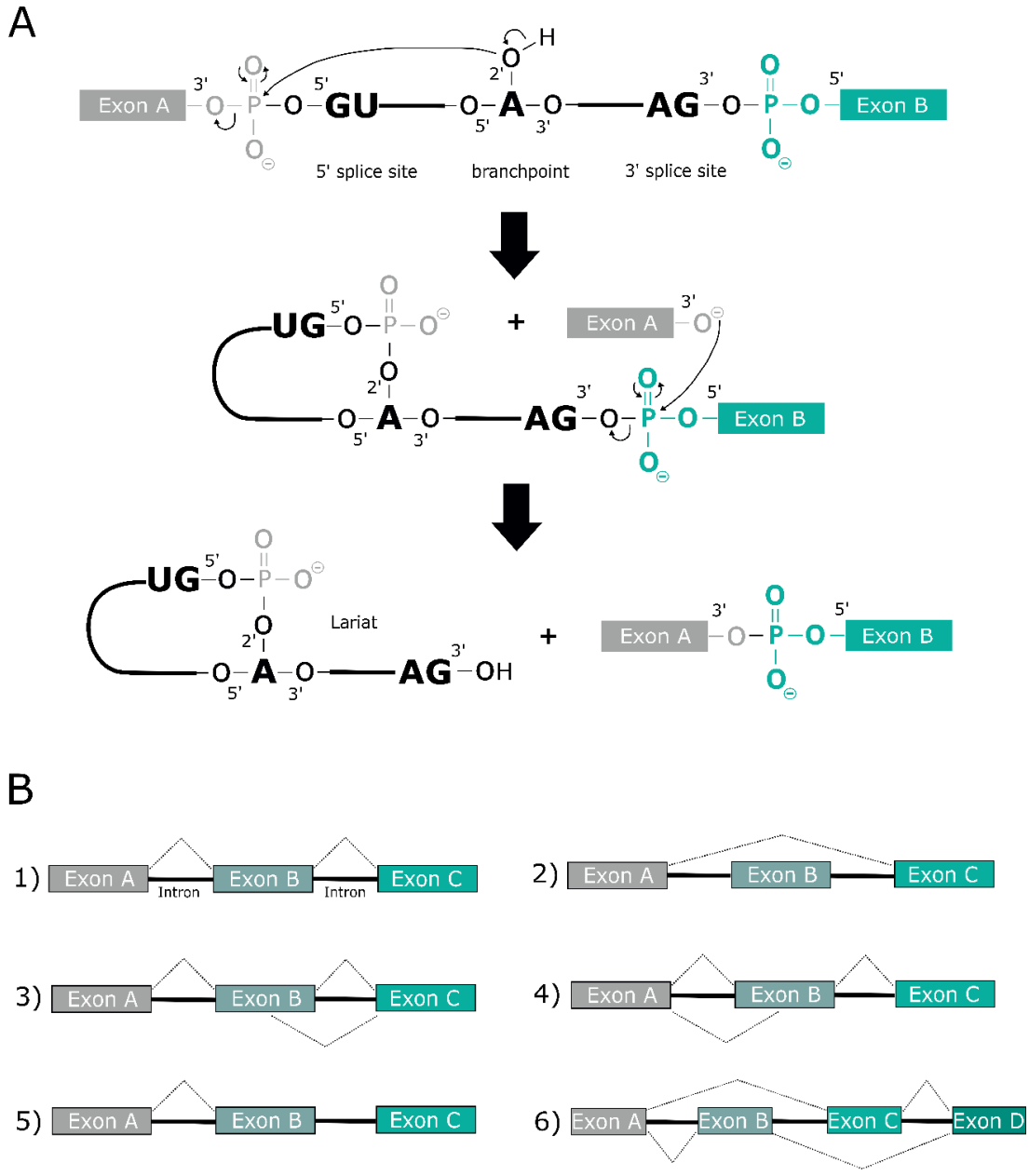

Figure 2: A) Reaction scheme for the two steps of nuclear pre-mRNA splicing. Electron transfer is indicated by arrows. The 2′ hydroxyl-group of the adenosine base residing at the branchpoint makes a nucleophilic substitution type 2 (SN2) attack on the phosphodiester moiety at the 5′ splice site. As an intermediate the 5′ exon in a free form (grey) and the 3′ exon-intron-lariat motif are formed. Subsequently, another SN2-type reaction of the free 3′ hydroxy anion of the 5′ exon attacking the phosphodiester moiety at the 3′ splice site (green), yields in a spliced RNA and the removed intron in the lariat form. Figure derived from [25]. B) Major types of alternative splicing encountered in mammalian cells: 1) constitutive splicing; 2) exon skipping; 3) use of alternative 5'ss; 4) use of alternative 3'ss; 5) intron retention; 6) mutually exclusive exons.

Additional processing steps of the pre-mRNA aim for the UTRs. As unprotected RNA is susceptible towards degradation, its stability is increased by protecting its 5' end with a cap group to distinguish it from cell foreign RNAs [26]. The 5'-cap is introduced by a guanylyltransferase to form a 7-methylguanosine which is involved as well e.g. in splicing [27], polyadenylation [28] and degradation [29]. On the other end, the RNA is cleaved and a poly-(A) tail, which is added by the poly-(A) polymerase protects the RNA from degradation [30]. The

length of this tail can vary and directly influence the translation rate [30]. Finally, the processed RNA is exported as mature mRNA through the nuclear pore into the cytoplasm [31].

In the cytoplasm, translation of the mature mRNA then takes place, which is managed by the ribosome. The 80S eukaryotic ribosome consists of two subunits, the 40S and the 60S subunit. Next to a set of other protein factors, the 40S subunit must bind to the 5'-cap of the mRNA and is scanning in 5’-3' direction along the mRNA, searching for the start sequence [32]. After the initiating tRNA interacts with the start codon, the large 60S subunit is recruited. The now catalytically active ribosome can translate the mRNA into a protein sequence. The factors that bind to this machinery such as initiation, elongation, and termination factors regulate the protein synthesis, ensuring accurate translation [32].

Moreover, the UTRs contain several regulatory sequences either *cis*- or *trans*-acting [33]. The 5’-UTR affects mostly translation efficiency exploiting structural features [34], e.g. hairpins [35], G-quadruplexes [36] or internal ribosomal entry sites (IRES) [37]. Besides, the presence of uORFs – sequences coding for small peptides with mostly no function – can reduce protein production severely [38]. The 3’-UTR can accommodate different miRNA target sites and AU-rich sequences impacting mRNA stability [39]. Furthermore, this part is important to determine the subcellular localization of the mRNA using zip-codes or the length of the poly(A)-tail to interact with protein partners [33]. Previous studies unveiled splicing events occurring within UTRs [21, 40]. Thus, alternative UTR splicing mechanisms contribute to the fine-tuning of gene expression by varying 5' or 3' UTR lengths, adding another layer of complexity influencing mRNA stability, isoform diversity, and protein output. Nucelotidewise, the conserved splice sites are almost identical [40a]. However, compared to the coding region, the length, distribution and prevalence of introns seems to differ severely within the 5’-UTR [21]. From the 35 % of human genes containing introns in their 5’-UTRs, a correlation of having short introns within the 5’-UTR and highly expressed genes was found, suggesting that they are positively affecting transcription or mRNA stabilization [21]. Furthermore, it could be shown, exploiting 5’-UTR isoform-specific translation can be a robust mechanism to control protein production in human cells [41]. However, as non-coding exons and cryptic splice sites complicate the detection of the exact transitions between introns and exons, current prediction tools are not as reliable here as they are in conventional CDS splice sites [21]. Although the 3’-UTR is larger than the 5’-UTR, splicing events are less prevalent [42]. This could be linked to the direct degradation of the mRNA via the non-sense mediated decay (NMD), if an exon-exon junction is formed 50 nt downstream of a stop codon [43]. The stop codon is then recognized a premature signal causing the degradation. Nevertheless, indeed some splicing events are also found here e.g. to regulate the insertion of the penultimate exon, causing a frameshift event in its absence to extend the CDS into the 3’-UTR using another out of frame stop codon. This mechanism generates isoforms, which are assumed to take over maintenance functions [44].

3.3 Catalytic RNAs

In synthetic biology, the family of small self-cleaving ribozymes is of particular interest. They catalyze RNA strand cleavage via intramolecular transesterification reactions of the phosphodiester backbone [45] (Figure 3). They can be found in all kingdoms of life. Until to date, 12 classes of natural self-cleaving ribozymes are known mostly with detailed information about their cleavage mechanisms, structure, and natural environments [45-46].The family of self-cleaving ribozymes includes (in order of discovery) the hammerhead (HHR) (1986) [47], hairpin (1986) [48], hepatitis delta virus (HDV) (1988) [49], Varkud satellite (VS) (1990) [50], glucosamine-6-phosphate synthase (*glmS*) (2004) [51], Vg1 (2008) [52], twister (2014) [53], twister sister, hatchet and pistol (all 2015) [54], epigenetic (B2)n (2020) [55] and the most recently discovered hovlinc (2021) [46c] ribozymes. For some, only a single or few instances of the motif were found in genomes, while for others, numerous natural variants were identified [45].

Considering the broad distribution of self-cleaving ribozymes and the recent and ongoing developments of *in vitro* selection methods and bioinformatic analysis approaches, it is likely that further ribozyme classes will be discovered [53]. In addition, several artificial self-cleaving ribozyme classes generated by *in vitro* selection strategies have been reported [45, 56].

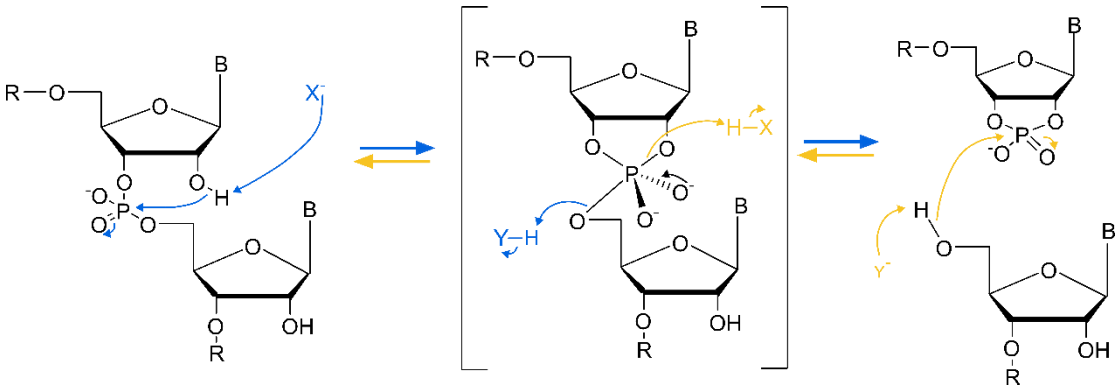

Figure 3: General mechanism of ribozyme supported cleavage reaction (blue) and ligation (yellow). Electron transfer indicated by arrows. X^- and Y^- show general base and X-H and Y-H general acid.

Although the primary, secondary, and tertiary structures of those natural small self-cleaving ribozymes vary, they share common features, such as helical segments (stems) connected by unpaired nucleotides (loops) that are often conserved (Figure 5B-J). Many comprise tertiary interactions between distal parts of the ribozymes to support or enable the folding of the catalytically active conformation [45]. In case of the HHR the comparably late discovery of such tertiary interactions explained how fast-cleaving ribozymes are obtained even in physiologically low Mg^{2+} concentrations [57]. Solving the crystal structure of the full length *Schistosoma mansoni* HHR revealed non-canonical interactions that align stems I and II and thereby stabilize the overall conformation and proper folding of the catalytic core [58].

Despite their similarities, each class favors slightly different sequence specific requirements for activity [46b]. Besides, computational investigation of the active sites revealed details of respective catalytic strategies, exploiting ions or water molecules or using certain co-factors [46b, 59]. A theoretical examination of these different catalytic strategies enabled predictions for the speed limit of the respective ribozyme class. By introducing alterations to the catalytic strategy, the acceleration of the internal phosphoester transfer could be optimized [60].

In contrast to these comparably well-studied catalytic properties of natural self-cleaving ribozymes, their physiological functions remain largely unknown. However, their abundance and wide distribution in nature imply important functions [45]. The best-characterized function of small self-cleaving ribozymes is the processing of concatemeric copies of RNA genomes of subviral particles such as viroids, satellites and HDVs by hairpin, VS, some HHRs, and HDV-like ribozymes [45-46].

Interestingly, in the case of newly discovered HDV-like circular RNAs, self-cleavage can be provided by either HDV-like ribozymes or HHR motifs (until recently the human HDV was the sole representative of such infectious RNA agents) [61]. Some HHRs and HDV-like ribozymes were found to be associated with retrotransposons [45-46]. Additionally, isolated cases of intronic HDV-like ribozymes and HHRs in amniotes have been proposed to be involved in gene regulation or mRNA biogenesis [62]. Weinberg *et al.* suggested that the function of some genomic ribozymes may depend on their interaction with endogenous proteins, an aspect that is not yet well understood [45]. In contrast, the *glmS* ribozyme found in some bacteria is well-known to facilitate a negative feedback regulation in gram-positive bacteria using glucosamine-6-phosphate (GlcN6P) as co-factor, hence acting as a riboswitch to control gene expression [63].

Most natural riboswitches reside in the 5'-UTR of bacteria and archaea and are usually *cis*-acting elements to control gene expression tightly. With over 28 different classes, they are very versatile in the ligands, which they are recognizing and their expression platform [64]. That is why, research is focusing on understanding these systems and how to exploit them for other uses. Especially, since many pathogenic bacteria harbor mechanisms like the *glmS* ribozyme to regulate gene expression [65], the ribozyme cleavage, if triggered constantly, can be targeted for antibiotic strategies. Synthetic mimics of the natural coenzyme GlcN6P are already used to suppress expression of the *glmS* gene crucial for cell growth [66]. Besides, there are more catalytically active RNAs than the self-cleaving ribozyme classes presented here. Over the last decades, also inhibitors were discovered and developed to impair their activity. As for the group I intron, already in 1991, first descriptions of small molecules selectively impairing self-splicing of the td intron *in vitro* were reported [67]. Also for the ribosome, which uses the rRNA for catalysis of the aminolysis to form peptide bonds and of the peptidyl hydrolysis to release

the complete protein from the peptidyl tRNA [68], several small molecules were discovered, which are directly impairing the catalytic function [69]. With all these molecules reported, there are already many ways to effectively go against pathogens. However, due to rising multiple-drug resistance in bacteria, finding new strategies for antibiotic mechanism is of great interest and still challenging [70].

3.4 Artificial riboswitches for control of gene expression in eukaryotes

As already described in the previous chapter the 5'-UTR of the mRNA contains many regulatory elements. Thereby, it is not surprising that most naturally occurring riboswitches reside in this region distributed across all kingdoms of life [71]. Within eukaryotes, also intronic regions are found to accommodate these regulators [72]. Riboswitches contain at least one aptamer domain, an RNA sequence binding a particular small molecule with high specificity and sensitivity. A signal-dependent change in RNA structure of the overlapping expression platform then transfers the information to the gene expression machinery to affect transcription translation or other gene expression related processes [73]. This way, they achieve to unite the sensing and transduction of a signal that is tightly coupled to the metabolism of the cell, without need of additional protein factors. Due to their conservation and their widespread occurrence, riboswitches are thought to have existed prior to the evolution of ribosomal protein synthesis in the so-called RNA-world [74].

Over two decades ago, the first ligand-induced riboswitches were described [75]. However, the concept of aptamers was discovered already earlier [76]. Hence, first artificially riboswitches were constructed in 1998 by inserting an aptamer into the 5′-UTR of an mRNA allowing repression of its translation upon ligand addition in the test tube as well as in mammalian cells [77]. This discovery sparked curiosity among scientists, who envisioned exploiting these molecular switches as customizable tools for controlling gene expression in other artificial systems.

In the course of developing artificial riboswitches, researchers have engineered molecular RNA-switches to respond to a range of molecules that exceed what their natural riboswitches recognise [78]. However, there are only a few aptamer-ligand partners exerting both: high specificity and sensitivity, which is the bottleneck in applying these systems for therapeutic purposes. Nevertheless, already today, these customisable genetic tools hold promise in diverse fields, such as metabolic engineering [79], biomedical research [80] and gene therapy [81], as they enable complex and tuneable control of gene expression for a variety of applications.

Not only the choice of new aptamers expanded the diversity of synthetic riboswitches but also the combination with several new expression platforms gave rise to new possibilities.

According to the signal-induced conformational change the switches can either upregulate gene expression upon ligand binding (ON-switch) or reduce gene expression (OFF-switch). Until now, within eukaryotic cells multiple commonly adapted expression platforms are known (Figure 4). In yeast, aptamers were successfully introduced as a roadblock for the ribosome during the scanning process [78c] (Figure 4A).

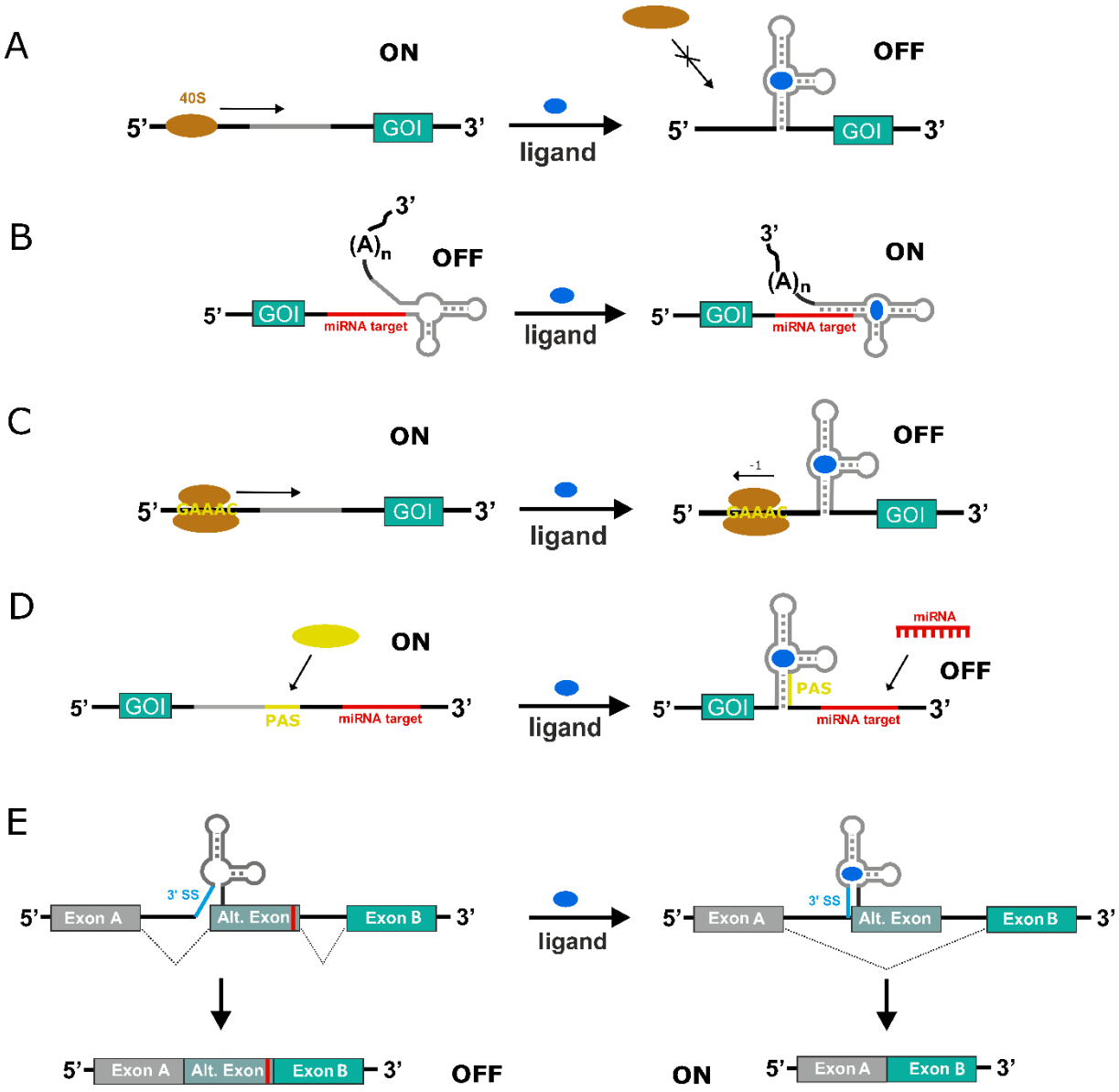

Figure 4: Common expression platforms for artificial riboswitches in eukaryotic cells: ON and OFF indicate the upregulation and downregulation of gene expression, respectively. A) Aptamer added into 5'-UTR as a roadblock for the 40S ribosomal subunit to impair scanning process upon ligand binding. B) Aptamer introduced to 3'-UTR containing complementary sequence to miRNA target site. Upon ligand-binding miRNA target site is sequestered within stem structure impairing RNAi and enabling gene expression. C) Aptamer introduction in 5'-UTR downstream of a slippery sequence causing a frameshift of the ribosome creating a non-sense product upon ligand binding. D) Aptamer inserted into 3'-UTR to sequester poly(A)-binding signal (PAS). Without ligand the PAS is recognized, the miRNA target site is cleaved off and mRNA gets poly-adenylated. In presence of the ligand miRNA target site resides in mRNA and is degraded. E) Splicing cassette with an alternative exon containing a premature stop codon flanked by two introns. Masking the 3'ss of the first intron inclusion of alternative exon can be controlled upon ligand binding.

Another strategy was to mask important regulatory sequences within a stable stem of the aptamer to make them not accessible for its target molecules or proteins [82]. Here, the poly-adenylation signal (PAS) and a miRNA target site was masked, respectively (Figure 5B and 5D). Moreover, the frameshifting mechanism can be used to actively force the ribosome to change the frame within a slippery sequence (Figure 5C) [83]. Another design involved alternative splicing. By actively regulating exon skipping controlling the accessibility of either the 5'ss or 3'ss, an alternative exon containing a premature stop codon is spliced into the mRNA leading to immediate degradation (Figure 5E) [84]. The usage of ribozymes as elements for riboswitch design is discussed in detail in Chapter II.

For aptamers to be efficient *in vivo,* they need to undergo a conformational change that is sufficient to transfer the signal onto the expression platform. Although RNA aptamers can be evolved *in vitro* using Systematic Evolution of Ligands by EXponential Enrichment (SELEX) against potentially any small molecule and ligand of interest, they often lack this ability [85]. This problem can be tackled using selection methods like Capture-SELEX, which is reducing the probability of non-specific binding [86]. As an advantage, if a suitable aptamer has been found, it can often be used in many different constructs in a very modular way. Next to neomycin [85] and ciprofloxacin [87], in 2001 the widely used Tet aptamer was obtained by *in vitro* selection by Berens et al. [88]. The structure consists of three helices P1-P3 (Figure 8). The Tet-binding site resides within the three-way junction, and it is bound as a magnesium ion chelate. Upon ligand binding, the P1 stem is stabilized. As the P1 stem is not directly involved in binding, its sequence is variable. [89] This enables the great potential to combine this aptamer with the RNA in multiple ways, as long as the stem structure is maintained. Moreover, the K_D was determined to be in the sub-nanomolar range indicating a very high affinity [89]. In combination with its strong discrimination between closely related derivatives e.g. doxycycline [88], the aptamer is ideal for *in vivo* applications. However, experimental data suggest that higher concentrations (>1 µM) are needed to induce the riboswitch specific effects [54b, 90]. In this work, we used Tet concentrations that do not interfere with cell viability [54b]. Since Tet as a drug is already approved by the FDA, together with the exceptional properties of the Tet-aptamer this is a promising starting point, to develop synthetic riboswitches for therapeutic applications.

In general, artificial riboswitches provide ideal traits to be used for regulation of gene expression. The modularity of elements enables a plug and play driven design strategy. This way, as an example, insertion of multiple copies of the aptamer is increasing the dynamic range significantly [91]. Moreover, condition-responsive or effector-responsive transcription factors are circumvented and due to the rather small coding space, artificial riboswitches are applicable in almost any context within mammalian cells [81b].

4. Chapter II: Functional RNAs as a tool to conditionally control gene expression in human cells

4.1 Introduction

In synthetic biology, new biological systems are developed from existing natural components. Conditional control of gene expression can be achieved by using artificially constructed riboswitches. Such systems are especially interesting for future applications in gene therapy due to their small size and the absence of potentially immunogenic regulatory proteins.

One commonly used element, which can be additionally exploited for riboswitch design was presented in the previous chapter – the self-cleaving ribozymes. With their small size (<200 nt), compact and often simple structures, self-cleaving ribozymes are appealing to be utilized for the construction of artificial systems in synthetic biology. In 2004, Yen *et al.* showed that self-cleaving ribozymes can be used to control mRNA stability in mammalian cells and mice [92]. Here, ribozyme cleavage provides permanent translation repression by removing motifs relevant for translation such as the 5'-cap or poly-A tail, thereby generating unprotected ends susceptible to exonuclease digestion [93] (Figure 5A). By combining self-cleaving ribozymes with aptamers so-called aptazymes are created. Already in 1997, Tang and Breaker constructed a functional allosteric ribozyme in the test tube by fusing an HHR with an ATP binding aptamer [94]. However, as for their ribozyme platforms, the function of such aptazymes was not transferrable from the test tube into cells. The primary reason for the lack of functionality was the use of slow-cleaving HHR versions that lacked stem-I/stem-II interactions. When these tertiary interactions were included, it enabled the construction of artificial riboswitches based on the HHR as expression platform [95]. However, even in these cases it proved that the developed sequences were often context-dependent and could not be transferred easily from e.g. bacteria or yeast to mammalian cells [96]. Hence, context-dependent optimization is often required to utilize small self-cleaving ribozymes for the construction of artificial switches of gene expression.

Until now, aptazymes for mammalian cells are mostly based on the HHR and are predominately derived from HHR sequences from *S. mansoni* [54b, 96b, 96c, 97] or the satellite tobacco ringspot virus (sTRSV) [98]. Lately, aptazymes based on the HDV [96c, 99], pistol [100] and twister [96c, 101] ribozyme were developed. Artificial aptazyme-based riboswitches do not rely on the expression of specific protein factors, do not interfere with cellular mechanisms, and are easy to implement by inserting them into the UTRs of a gene of interest.

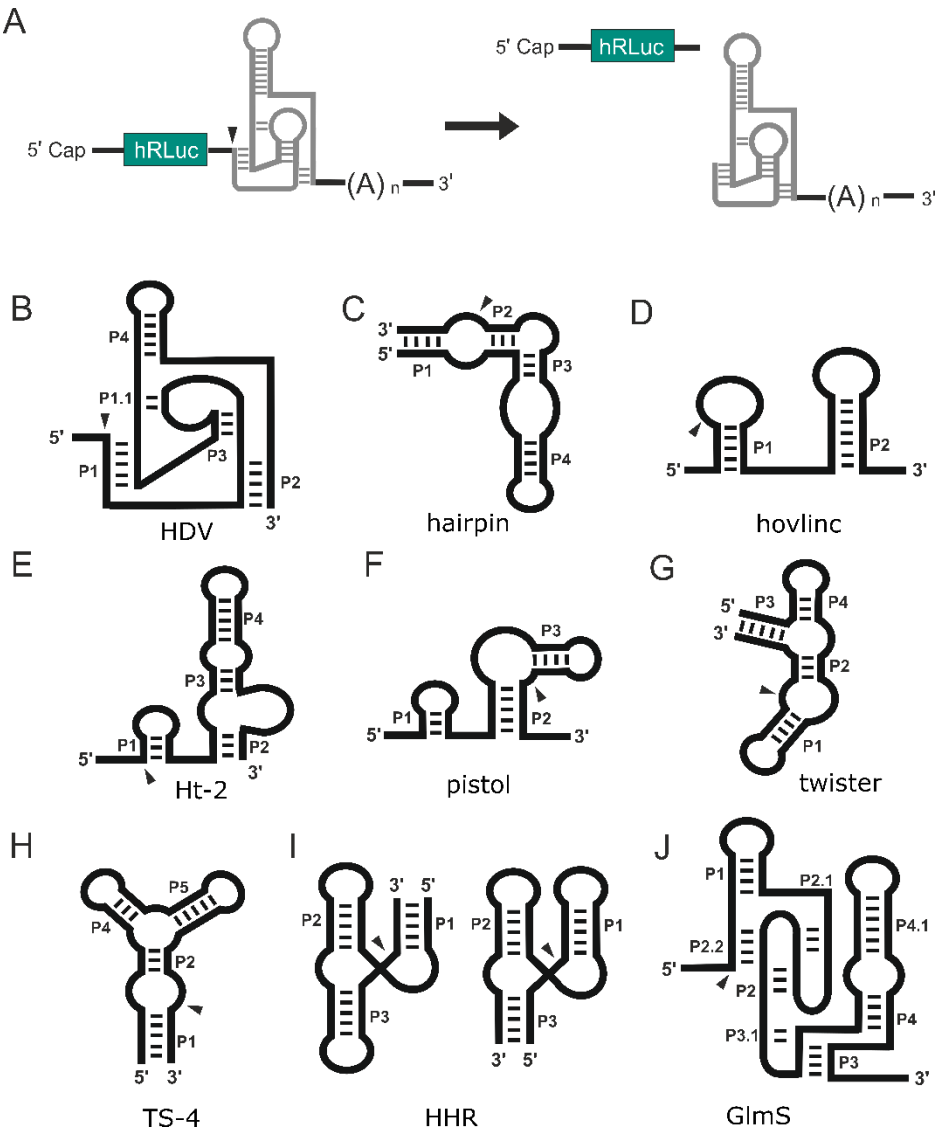

Figure 5: A: Exemplary mRNA containing a ribozyme in the 3'UTR. After cleavage, the unprotected RNA is subjected to degradation. B-J: Schematic secondary structures of small self-cleaving ribozymes. Figure derived from [1] B: HDV ribozyme, C: Hairpin ribozyme, D: Hovlinc minimal structure, E: Hatchet ribozyme, F: Pistol ribozyme, G: Twister ribozyme, H: TS-4 ribozyme, I: Hammerhead type I (left) and type III (right) ribozymes, J: GlmS ribozyme. The arrowhead depicts the location of the cleavage site within the RNA motifs, respectively. Figure adapted from [1].

Multiple proof-of-principle studies have demonstrated that ribozymes and aptazymes can be used to regulate therapeutically relevant biological outcomes such as T-cell proliferation [98b], adeno- and AAV-vectored transgene expression in cell culture as well as mice [81a, 96c, 97a, 100b, 102] and direct regulation of viral gene expression and replication [103]. These studies, demonstrate the transferability of aptazymes to different genetic contexts. However, high variability of the regulatory range and fold-change is commonly observed. Optimization of aptazymes and generation of novel aptamer-ribozyme pairs, therefore, remains an important area of research. Remarkably, apart from the *glmS* ribozyme mentioned above, natural examples of aptamer-regulated ribozyme activity are restricted to a single case of a c-di-GMP-dependent self-splicing group I ribozyme in *Clostridioides difficile* [104]. To expand the toolbox of ribozyme platforms for aptazyme development, a comprehensive and comparative survey

on the effect of inserting several different self-cleaving ribozymes into mRNAs in human cell culture was conducted in this thesis.

4.2 Results and discussion

4.2.1 Systematic comparison of self-cleaving ribozyme efficiency in mammalian cells

To further expand the available toolbox of small self-cleaving ribozymes, we included all known ribozyme classes that show favorable properties for straightforward aptazyme design (Figure 5). For that reason, we focused on small (<100 nt) and independently self-cleaving ribozymes that excluded the epigenetic ribozyme B2 [55] as well as the VS ribozyme, due to their rather large sizes [50]. We also excluded the *glmS* ribozyme [105], due to the necessity of the endogenous glucosamine-6-phosphate as coenzyme. As an endogenous metabolite, this sugar activates the ribozyme already at low concentrations. Moreover, multiple intracellular hexose and aminohexose derivatives interact with the *glmS* ribozyme [106]. The Mn^{2+}-dependent Vg1 ribozyme was also not examined as it has already been shown to be non-functional in cells and is proposed to be a molecular fossil [52].

The insertion of structured elements within the mRNA alone can interfere with gene expression. Hence, as a control, ribozymes inactivated by small, defined mutations were tested respectively to visualize structure-induced effects. All constructs were inserted into the 3'-UTR (30 nt downstream of the stop codon) of a Renilla luciferase (hRLuc) with a flanking sequence of $(CAAA)_3$ to minimize interactions with the surrounding sequence context. This insertion site is especially relevant for a potential therapeutic use since the 3'-UTR has already been shown to be easily exchanged between target genes and naturally occurring regulatory elements are found to be enriched in the UTRs [107]. We used the psiCHECK-2 vector that encodes a second luciferase (Firefly) that can be utilized for normalization in order to control for transfection efficiency. In a dual luciferase assay (DLA) as used by Beilstein *et.al*. [54b], the luciferase activities are measured (Figure 6A). Ribozyme cleavage-induced reduction of luciferase expression results in lower activity. Hence, the difference in luciferase activity between the active and inactive ribozyme reflects its regulatory potential and can be quantified as ON/OFF-ratios.

To further support the obtained data, the relative activity of the ribozyme classes was evaluated in another reporter assay (Figure 6B). Controlling eGFP expression, the selected ribozymes show comparable trends to the DLA-based screen. However, the DLA-based assay is considered more sensitive and reliable since cells show natural auto-fluorescence and high expression levels of GFP can interfere with cellular fitness [108]. For that reason, statements about hRLuc activity are concerning the data obtained by DLA if not stated otherwise.

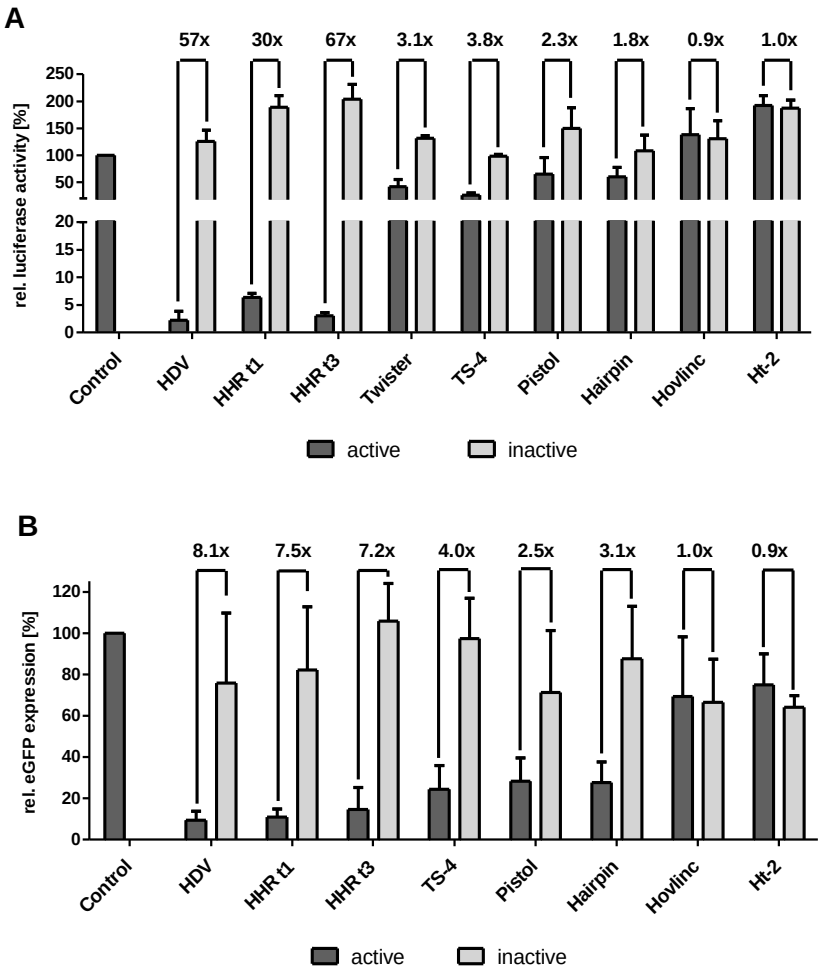

Figure 6: A) Dual Luciferase Assay (DLA) and B) eGFP/mCherry based assay results examining different ribozyme classes on their self-cleaving activity in HeLa cells. Relative hRLuc activity is shown for constructs containing the active and inactivated ribozyme version. Ribozymes were tested within the 3'-UTR 30 nt after the stop codon. Error bars show the standard deviation from three independent measurements. The respective ON/OFF-ratios between active and inactive constructs are displayed above. Respective sequences are shown in Supplementary Table 1.

One highly active ribozyme occurs in the Hepatitis Delta Virus (HDV) (Figure 5B). It is stated to be the fastest naturally occurring self-cleaving RNA [109], and functions efficiently in the test tube and in cell culture using the wild type sequence [110]. Moreover, its structure is very robust to denaturants [109]. A unique feature is the position of its terminal cleavage site directly at its 5'-end. Notably, within our context, the active ribozyme decreases luciferase activity to about 4 % (Figure 7). In nature, the HDV ribozyme often occurs with additional sequences flanking the catalytic core. They are presumed to facilitate correct folding but are not critical for the catalytic activity [110]. Our results show that by further reducing the HDV sequence to only the catalytic core (Figure 7) its activity is not impaired but enhanced and it even outperforms the HHR. The shortened version effectively reduces hRLuc activity to 2 % (Figure 7B). Interestingly, in 2006 an HDV-like ribozyme was found in human cells, the CPEB3 ribozyme, which exerts strong structural similarity with the HDV ribozyme [62b]. As some would also define HDV-like ribozymes as another distinct class, we wanted to include this in the comparative

survey. Despite their similarities, the CPEB3 ribozyme can only reduce gene expression to minor extents and cannot keep up with the HDV ribozyme. This indicates that the efficiency of the HDV ribozyme wild type sequence resides in its optimized structure, as already minor changes to the sequence result in a loss of activity.

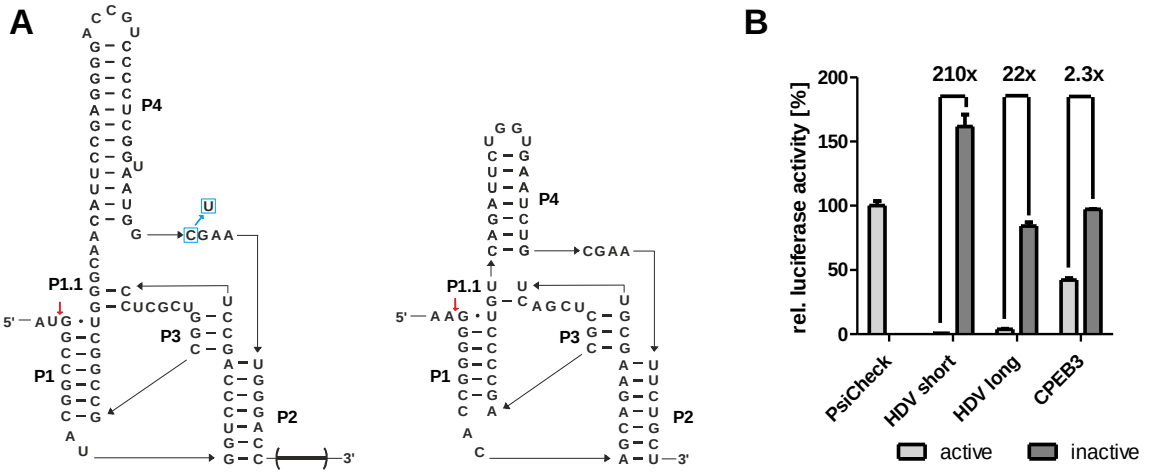

Figure 7: A) Nucleotide sequence of the HDV ribozyme [110] (left) and the CPEB3 ribozyme [62b] (right). Cleavage site is indicated with a red arrow. Point mutation used for inactivation of the HDV ribozyme depicted in blue. Brackets in the HDV ribozyme indicate additional nucleotides in the long version that are deleted in the HDV short version. B) Relative luciferase activity obtained from DLA comparing the HDV and CPEB3 ribozyme on their activity in HeLa cells. Error bars show the standard deviation from three independent measurements. The respective ON/OFF-ratios between active and inactive constructs are displayed above. Full sequences are listed in Supplementary Table 1.

The hairpin ribozyme (Figure 5C) belongs to one of the earliest described ribozyme classes. Here, a sequence derived from the chicory yellow mottle virus (sCYMV1) was used [111]. Although every catalyzed reaction is an equilibrium between cleavage and re-ligation, the equilibrium of most known ribozymes is predominantly found on the side of the cleavage products. In case of the hairpin ribozyme, harsh conditions can favor the ligation reaction [112] and stabilization of the tertiary structure can promote ligation over cleavage [113]. Although the hairpin ribozyme from sCYMV1 was engineered to cleave efficiently in the test tube [113-114], within the cells only minor effects contributing to stabilization of the tertiary structure could be responsible for this poor reduction of luciferase activity. This causes the equilibrium to shift. With the hovlinc ribozyme (Figure 5D) we also included a ribozyme originating from mammalian cell lines, which was only recently discovered as a new ribozyme class. It is stated to be a hominin-specific ribozyme comprised of 168 nt with its pH optimum between 9 and 10 [46c]. Since we were focusing on shorter constructs in this study, we used a proposed minimal version of 83 nt which has been demonstrated to still show cleavage activity [46c]. However, it is stated to lose about 90 % of efficiency compared to the full length construct because of slower or improper folding [46c].

For the hatchet ribozyme (Figure 5E), a wild type sequence from a metagenomics search was selected (Ht-2) [115]. In 90 % of the environmental sequences the ribozyme is associated with

an additional P0 stem upstream of the P1 stem. Since the P0 stem was shown not to contribute to the cleavage activity, it was removed from the construct used in this study. Derived from the annotated sequence [115], the P4 stem was closed with a tetraloop (GAAA). For this motif, the presence of Mg^{2+} is crucial and metal ion concentrations varying from the natural environment could impair its activity [115]. Besides, when examining the crystal structure an equilibrium of dimeric and monomeric ribozymes was observed [116]. Further studies revealed that dimerization is not crucial for ribozyme activity; however, it could impair correct folding in the cellular environment. The hatchet ribozyme was shown to be cleaving efficiently in the test tube [115], however in the context of the mammalian cells studied here it does not seem to exert a significant influence on gene expression (Figure 6). For all three ribozyme classes, hairpin, hovlinc and hatchet, only small changes in hRLuc activity were observed (0.9-1.8 ON/OFF-ratio).

The pistol ribozyme (Figure 5F) was discovered along with the hatchet ribozyme. Multiple environmental sequences exist for the pistol ribozyme. The motif derived from *Alistipes putredinis* exerts fast and efficient cleavage in experiments in the test tube [54c]. In the past, this class of ribozymes was rather inefficient when brought into the mammalian cell context [101a, 117] and we observed a rather weak performance as well. However, its compact structure and tertiary interactions provide several potential aptamer connection sites. Recently, the Yokobayashi group developed artificial sequences of pistol ribozymes cleaving with high efficiency within mammalian cells [117]. This already led to the construction of well-performing aptazymes [100a].

For the twister ribozyme (Figure 5G) many natural sequences have been characterized already. One well-studied example is the environmental sequence 9 (*env9*), which has been used for the design of functional aptazymes in different organisms [96c, 101b, 118]. Since the twister motif consists of multiple stem-loop structures, many permutations are possible depending on which stem the ribozyme is connected to the mRNA (P1 and P3 have been realized already for *env9*) [53]. A study in yeast showed better performance and a higher ON/OFF-ratio when connected via the P3 stem [101b]. In our experiments, the twister *env9*-derived sequence shows a three-fold reduction in luciferase activity. However, the remaining hRLuc activity of about 40 % is still rather high in respect of most applications. Nevertheless, it has been shown that inserting a twister ribozyme from *Nematostella vectensis* strongly reduced reporter activity in another context [101a]. Thus, other motifs could potentially be identified within this class that result in more pronounced reduction of reporter gene activity. Due to problems during the cloning process and time constraints, the twister ribozyme regulating *gfp* expression could not be tested.

The rather newly discovered twister-sister (TS) ribozyme (Figure 5H) class is divided in four different subgroups, each forming multiple stem-loop structures [54a], resulting again in a variety of possible permutations. We focused here on the TS-4 P1 construct closing the P4 stem with a (GGAAA)-loop. The TS-ribozymes exhibit numerous similarities with the twister motif [54a]. Here, they show a comparable performance although the overall expression levels of the active and inactive TS-variant are slightly lower. The ON/OFF-ratio of 3.8 shows a clear change in hRLuc activity. Despite the high OFF-state, both classes, twister and TS ribozyme, offer a lot of structural options to be combined with an aptamer structure. Thus, for applications, which do not require a low OFF-state but a significant absolute change in gene expression, these two motifs could be suitable. Moreover, in contrast to the twister ribozyme no data on the performance of the TS ribozyme within cells of different permutations and the other subgroups exist, to our knowledge. For that reason, we also compared the active version respectively in the DLA (Figure 8). The hRLuc expression varies between 6 and 30 % for the different motifs. Whereas the TS2 and TS4 are performing better, the TS1 and TS3 show only moderate reduction of gene expression. The connection to the RNA via P1 or P5 stem seems to have a slight influence on efficiency as well. For TS1 and TS2 the P1 connected motifs reduce hRLuc noticeably more. Nevertheless, even a reduction to 6 % is inadequate for most therapeutic applications, as a much lower background is required there.

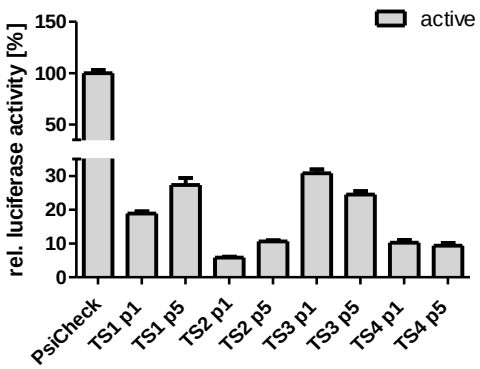

Figure 8: Relative luciferase activity obtained from DLA comparing two different permutations (connection to mRNA via P1 or P5 stem) of the four TS ribozyme subclasses on their activity in HeLa cells. Error bars show the standard deviation from two independent measurements. Only active versions of the ribozymes were tested here.

The most prominent class of small self-cleaving ribozymes is the HHR (Figure 5I). HHRs are categorized into types that indicate which stem is connecting the ribozyme to the surrounding RNA. The most prevalent permutation encountered in natural environments is the type II HHR directly followed by type I [119]. However, optimization studies in cell culture showed that the highest activity can be obtained if the HHR is connected to the mRNA via its P3 stem (type III) [81a]. Here, two frequently used topologies of the *S. mansoni* HHR (type I N107 & type III N79 derived sequences) [54b, 81a, 92, 96b] were examined. The HHR has already been used for the design of various aptazyme constructs [54b, 96b, 97a]. For either ON- or OFF-switches the HHR provides a high dynamic range, which was successfully exploited to control reporter gene

expression. Similarly, in our context, active HHRs of both topologies reduced the hRLuc activity with high efficiency. For the type III variant a relative *Renilla* signal of only 3 % was obtained. An ON/OFF-ratio of 66-fold represents a high dynamic range. Optimizing these sequences, the Farzan group was able to increase the ON/OFF-ratio to 1200 within a different context [81a]. By testing all these different ribozyme classes within the same context, we were able to identify motifs with high performance in human cells being ideal starting points to develop novel aptazymes.

As mentioned before, the performance of a construct often depends on the context in which it is tested. However, it should be possible to derive some general trends on how to adjust parameters like position or distance to the ORF to increase the performance in certain designs. Since it would be impossible to vary and test all different parameters, we started to examine the efficiency of two well-performing ribozymes with regard to their position within the 3'-UTR (Figure 9). For this purpose, we designed HDV-(short) and HHR (type I N107)-based constructs in positions ranging from 1 to 50 nt downstream of the ORF of the hRLuc reporter (Figure 9A). We also tested the +19 position (19 nt downstream of the ORF) for comparison with well-performing aptazymes that have been applied successfully at this location by the Suess group [54b]. Additionally, we tested if the flanking spacer sequences are necessary for proper function and indeed in their absence the performance of the ribozyme decreased largely (Figure 9C).

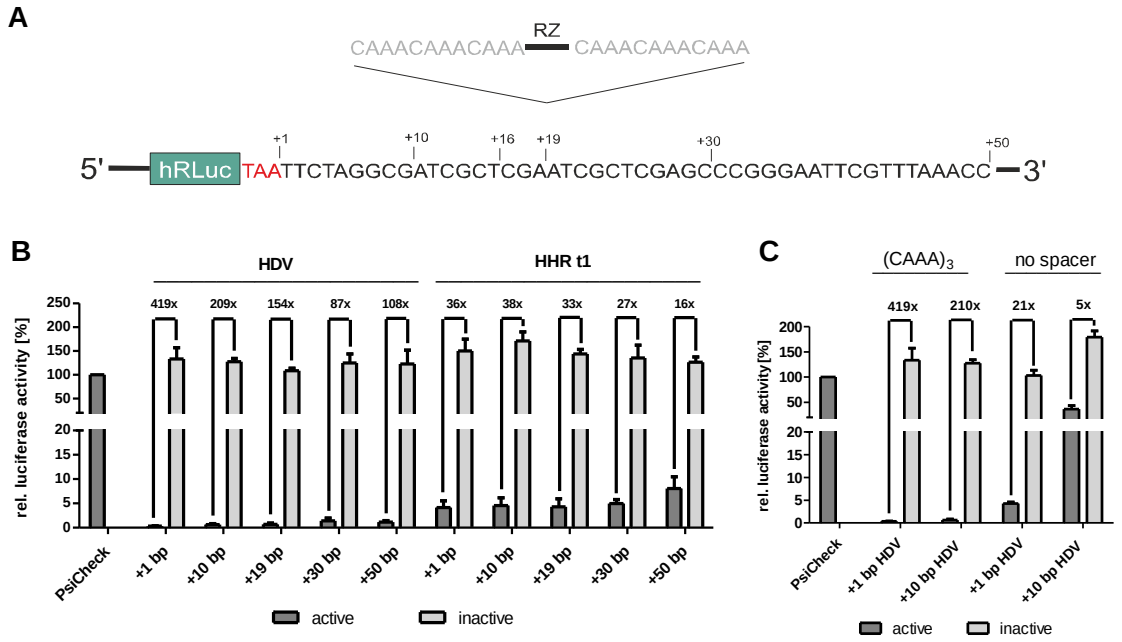

Figure 9: A) Schematic depiction of the mRNA of the Renilla luciferase (hRLuc). The numbers indicate the respective insertion sites within a 3'-UTR. The flanking spacer sequences were adapted from [54b]. B) Dual luciferase assay of constructs containing the HDV ribozyme (shortened) or the N107 type I hammerhead ribozyme (HHR t1) in different positions of the 3'-UTR of the hRLuc. The relative hRLuc activity is shown for the active and inactive ribozyme, respectively. Shown are mean and standard deviation of three independent measurements, each performed in technical triplicates. The respective ON/OFF-ratios are indicated above the bars. C) Relative luciferase activity in presence and absence of the spacer sequences flanking the ribozyme. Shown are mean and standard deviation of two independent measurements, each performed in technical triplicates. The respective ON/OFF-ratios are indicated above the bars.

Again, the relative reduction of luciferase activity was compared with a DLA for a series of different constructs and positions (Figure 9B). Interestingly, the ON/OFF-ratio increases rather consistently with increasing proximity of the ribozyme to the ORF. For the HDV ribozyme inserted immediately after the stop codon the hRLuc activity is abolished almost completely to 0.3 % compared to the parental construct lacking a ribozyme. With a dynamic range of about 419, the HDV ribozyme seems to be an ideal candidate as well when a low OFF-state is required. The same trend is also observed for the type I HHR, although the general performance as well as the distance effect are both comparably less pronounced.

These findings are in accordance with a previous study examining the effect on translation of varying lengths of 3'-UTRs in absence of a poly(A)-tail. It was found that the length of the 3'-UTR affects translation efficiency severely - the shorter the 3'-UTR the lower the translation efficiency observed [120]. This finding could also explain the low background reached by the HDV ribozyme which cleaves at its 5'-end leaving a short 3'-end. In contrast, the cleavage sites of HHRs are located in the center of the structure and a less pronounced effect was observed. However, it cannot be excluded that other RNA motifs could differ in their behavior. This finding is important as it allows for the optimization of existing aptazymes. Additionally, it provides valuable insight for the design of future aptazymes emphasizing the importance of placing the cleavage site as close to the end of the ORF as possible.

4.2.2 Aptazyme-based design of riboswitches

When comparing the different self-cleaving ribozyme classes on their efficiency to reduce gene expression, the HDV ribozyme tends to outdo every other class. A unique feature is the cleavage site directly at its 5'-end, leaving almost no trace to the upstream RNA. This can be suitable for more complex applications requiring a defined 3'-end of the RNA. In literature only a few HDV-based aptazymes are described [96c, 99], and they often rely on ligands, natural metabolites such as guanine, which could cause unspecific effects. Moreover, to date all HDV-based aptazymes are OFF-switches to our knowledge. We aimed for combining the highly sensitive Tet aptamer with this ribozyme to design ON-switches. Therefore, the aptazyme was inserted into the 3'-UTR of hRLuc with a flanking spacer of $(CAAA)_3$, analogous to the comparative survey. It can be challenging to design an ON-switching aptazyme, as the aptamer has to be placed within a ribozyme without a detriment to its catalytically active structure. The active conformation of the ribozyme should be disrupted, solely upon ligand binding. We used different strategies to achieve this (Figure 10).

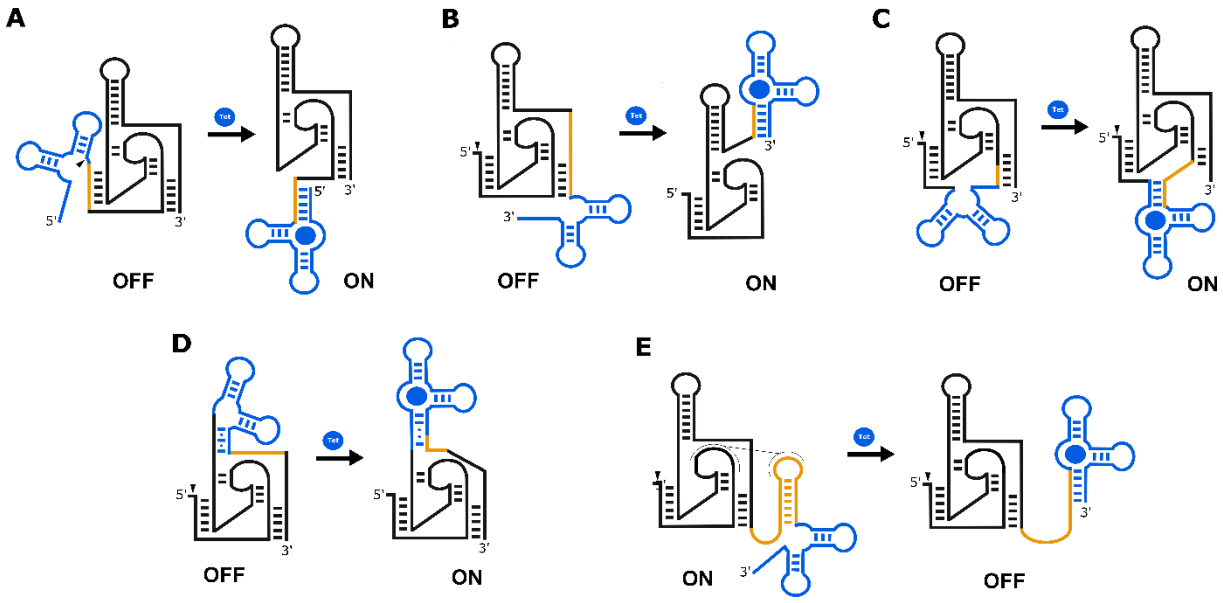

Figure 10: Schematic depiction of different design strategies of Tet-dependent and HDV-based ON-switching aptazymes. Ribozymes are depicted in black, aptamers in blue. A) Tandem design inserting the aptamer at the 5'-end of the ribozyme to compete with stem formation. B) Tandem design inserting the aptamer at the 3'-end of the ribozyme to compete with stem formation. C) Insertion of the aptamer within loop regions of the ribozyme, which disrupts internal stem structures upon ligand binding. D) Slippage constructs designing 'weak' stems that slip into alternative conformation upon ligand binding, masking the catalytic site of the ribozyme. E) Exploiting stem loop to disrupt tertiary interactions.

As a first approach 'tandem' designs were constructed, fusing the aptamer either at the 5'end (Figure 10A) or at the 3'-end (Figure 10B) of the HDV ribozyme wild type motif. Thereby the P1 stem of the aptamer is complementary to the P1 or the P2 stem of the HDV. Thereby, they compete in stem formation. The binding of Tet should stabilize the P1 stem of the aptamer, impede with HDV folding and reduce its cleavage activity. Consequently, gene expression should be upregulated upon ligand binding.

As the P1 stem of the HDV comprises 7 bp with high G-C content, the aptamer was designed to disrupt the whole stem upon ligand binding (Figure 11). We observed that the reduction of gene expression was lost even in absence of the ligand. This indicates that the P1 stem of the aptamer is too stable disrupting the ribozyme structure already without the ligand. To decrease the stability, we shortened the P1 stem of the aptamer successively starting from the full length stem (FL). The obtained variations (V1-V5) showed increasing reduction of gene expression in absence of Tet. Especially V3 showed almost two fold switching upon Tet addition. Further shortening of the P1 led to the loss of switching activity. The aptamer as well as the ribozyme are rather stable structures, finding the sweet spot of both stem is crucial to enable switching between the two states.

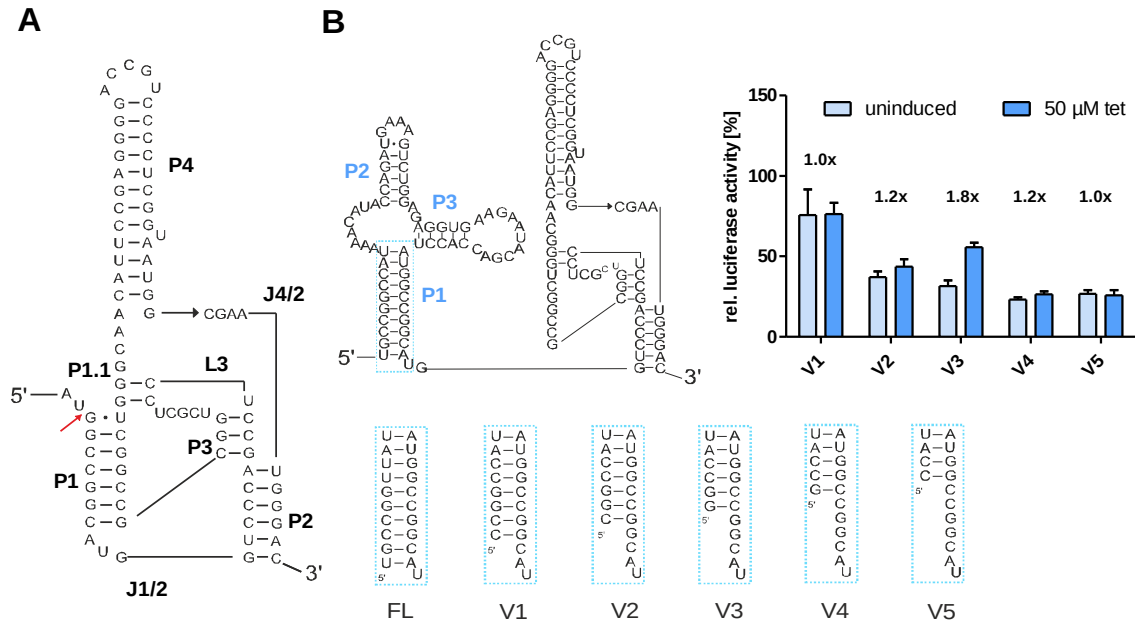

Figure 11: Tandem design. A) Nucleotide sequence of the HDV (shortened) ribozyme. Red arrow indicates the cleavage site and blue frame shows the point mutation (C to U) usable for inactivation. Stem regions, loops and junctions annotated as P, L and J, respectively. B) Nucleotide sequence of the aptazyme design in full length (FL) in the ligand-bound state (left). Aptamer sequence is derived from the cb28 minimer from [88].The variations with differing stem lengths of the aptameric P1 stem are labeled V1-V5. Dual luciferase assay (right) of Tet-dependent aptazyme constructs the 3'-UTR of the Renilla luciferase (hRLuc). The relative hRLuc activity is shown in absence and presence of 50 µM Tet, respectively. Shown are mean and standard deviation of two independent measurements, each performed in technical triplicates. The respective fold changes are indicated above the bars.

In the following, the V3 construct is referred to as 5' tandem construct. Additional optimization steps exchanging base pairs (G-C to G-U) or introducing mismatches within the P1 stem, did not increase the fold change (data not shown). Interestingly, the high background of the 5' tandem construct could be decreased using the shortened version of the HDV ribozyme (Figure 12), which was already introduced and described in 4.2.1. Although the switching activity was retained, the fold-change could not be improved. Known tandem designs of aptazymes contain the aptamer at the 5'-end of the ribozyme [101a]. The rationale behind this is that the aptamer can react to presence of the ligand first, before the ribozyme folds, otherwise it has no influence. However, for the HDV the P2 stem seems easier to tackle with a tandem design, as its GC-content is lower and it is formed later in the folding process [121], thus, easier controllable. The 3' tandem (Figure 10B) construct was indeed switching a bit (1.4-fold) but could not improve on the 5' analogue. Moreover, a combination of both, putting an aptamer at each end of the ribozyme, raised the background slightly, as expected, but did not surpass the fold change of the 5' tandem construct (Figure 12).

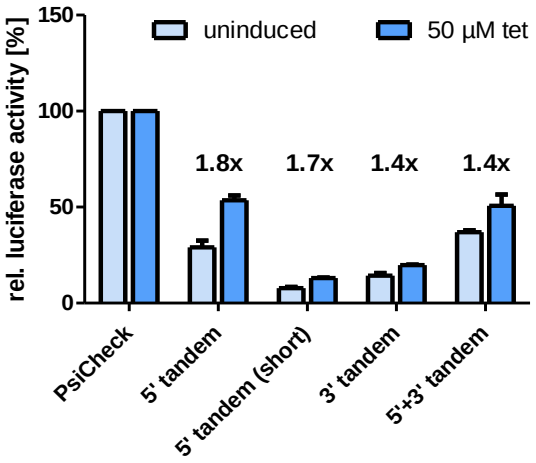

Figure 12: Best performing tandem designs. Dual luciferase assay of Tet-dependent aptazyme constructs in the 3'-UTR of the Renilla luciferase (hRLuc). The relative hRLuc activity is shown in absence and presence of 50 µM Tet, respectively. Shown are mean and standard deviation of three independent measurements, each performed in technical triplicates. The respective fold changes are indicated above the bars. Respective sequences are shown in Supplementary Table 2.

Comparing the WT ribozyme sequence to other members from that family, it is obvious that the structure is strongly conserved [110]. Furthermore, differences in sequence accumulate especially in less efficient relatives like the CPEB3 ribozyme (Figure 7). One could assume that the wild type sequence is highly optimized in nature and even minor changes to the sequence could severely reduce the cleavage activity. It is known that during the folding process the correct orientation of the P1 and P2-P3 helical segments is crucial for catalytic function [122]. This is in line with our aptazyme designs; when we vary the surrounding, stem strength and introduce mutations, the background directly increases. For that reason probably, tandem designs are not the most promising aptazyme strategy for this ribozyme.

In other natural HDV-like ribozymes, additional domains in the J1/2 region were discovered indicating that it can be altered while maintaining cleavage activity [122]. Within the crystal structure [109] the J1/2 and L3 region embrace the active cleavage site on the outside. In a next design, due to position of J1/2 and L3, the aptamer was tried to be inserted, respectively. Thereby, it is pointing directly outwards and is not interfering with the folding. A study from Kobori et al [99b] already used this strategy to create a set of well-performing OFF-switches. We used the same position, but in our case, upon ligand addition, the aptamer disrupts the structure interfering with surrounding stems (Figure 10C). However, we were not able to maintain proper ribozyme function after the aptamer was inserted and gene expression was full on (data not shown). This was an expected outcome for the insertion into L3, as we assume it to be too close to the catalytic center. And as a rather large structure the aptamer is interfering with the moderately weak pseudoknot formation in P1.1, which is crucial for the activity [123]. For insertion in J1/2 we assume that unspecific interaction with other parts of the ribozyme lead to the loss of activity. Since it is still too challenging to modulate reliable predictions of

tertiary structure, we cannot exclude this. However, as this was a successful strategy for the Gua aptamer, it could still be optimized further for our context.

Another strategy was to use the P4 stem of the HDV for aptamer insertion. It is less conserved compared to other parts of the catalytic core, and therefore it was tried to replace it by the Tet-aptamer. Besides, it was shown that the P4 stem can be drastically shortened or mutagenized while still maintaining ribozyme activity. There is the assumption that it does not directly participate in catalysis but stabilizes the active structure [109]. Hence, it provides suitable features to include the aptamer at this position. This was already shown to work in combination with the Gua-aptamer to create efficient OFF-switches. [96c, 99]. To construct an ON-switch we designed the aptamer to have a moderately stable P1 stem in order to prevent interference with the ribozyme folding in absence of the ligand. Upon Tet addition, the P1 stem of the aptamer is slipping to another conformation, partly masking the junction (J4/2) which is needed for catalytic activity (Figure 10D). Thereby, the ribozyme should be inactivated (Figure 13).

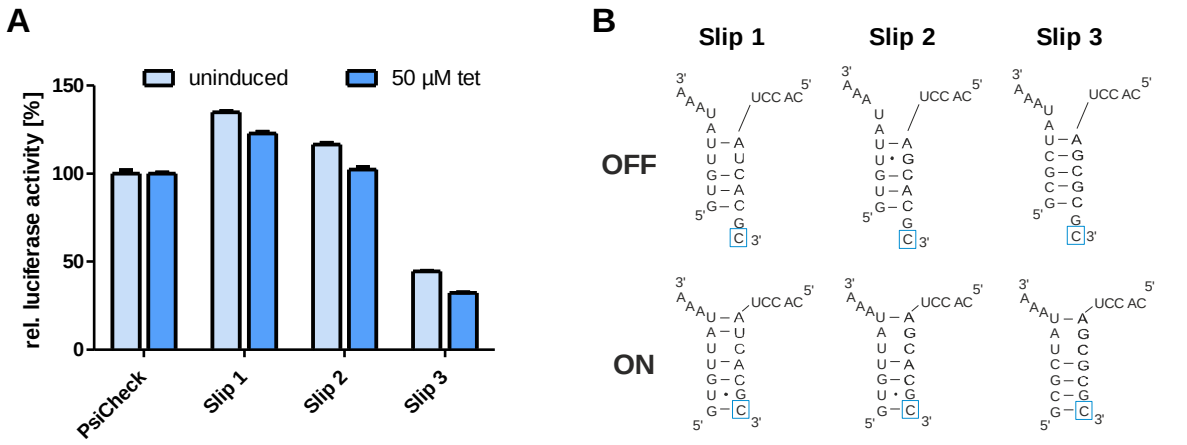

Figure 13: Slippage design. A) Dual luciferase assay of Tet-dependent aptazyme constructs in the 3'-UTR of the Renilla luciferase (hRLuc). The relative hRLuc activity is shown in absence and presence of 50 µM Tet, respectively. Shown are mean and standard deviation of three independent measurements, each performed in technical triplicates. B) Nucleotide sequences depicting the P4 stem of the slip aptazyme constructs shown in Figure 10D. Full sequences are listed in Supplementary Table 2. The Tet-binding causes the P4 stem to slip into another conformation masking the catalytic center of the HDV ribozyme (blue box). Therefore, in absence of the ligand, the ribozyme is still active and gene expression is OFF. Upon Tet addition, the gene expression is switched ON. Both conformations (On and OFF) of the P4 stem are depicted here, respectively.

In this context, we could observe that gene expression is not upregulated in presence of Tet. Indeed, stabilizing the OFF-state (Slip 1 to Slip 3) reduces the background overall, however, the tested designs show the tendency to rather reduce gene expression upon ligand binding. The aptamer as well as the HDV ribozyme exert stable structures. Hence, playing with the stability of connecting stem is challenging. Probably, this has to be conducted in a screening based approach randomizing the nucleotides to find the ideal communication module rather than via rational design.

As a last rational approach, we tried to control the tertiary structure of the ribozyme. In terms of the folding, it is known that the formation of the pseudoknot structure is a relatively slow process, as RNA typically forms local interactions before establishing long-range interactions [124]. Using that trait, we tried to interfere with the accessibility of the L3 segment forming the tertiary structure. Inserting a stem-loop sequence at the 3'-end of the ribozyme introduces an artificial loop that competes with L3 for the formation of the pseudoknot structure. The integrity of the stem can then be regulated using the aptamer as an "antistem" construct (Figure 10E). Indeed, a downstream stem-loop increased gene expression to 20 %. However, introducing the aptamer did not result in ligand-dependent change in hRLuc activity (data not shown). The increase in gene expression could be explained by the additional structure interfering with ribozyme activity in general and not only with the loop L3. Having additional nucleotides downstream of the HDV ribozyme, as in the longer version tested in the previous section 4.2.1, also increases the background. Considering the known influence of upstream regions on co-transcriptional folding [125], transferring the stem-loop motif to the 5'end of the HDV ribozyme is unlikely to have a beneficial effect. This approach is presumably not suitable for generating switches with a low background. Therefore, the project was discontinued and no further constructs were designed.

Overall, the HDV ribozyme is a very efficient candidate among catalytic RNAs within mammalian cells. However, due to the limitations in sequence variability and the strong structure conservation it is not a convenient candidate in designing Tet-dependent ON-switches. Indeed, for the tandem designs, a small set of switches was obtained. As they have a high background expression and limited dynamic range, they are not optimal for most applications. Nevertheless, the small size of aptazymes makes them suitable for combination with other riboswitches. In the need of a highly efficient riboswitch to control translation, the combination with aptazymes would be appealing, as the mechanism is independent from transcription and therefore advantageous. The HDV-based switches can be helpful to boost the performance in a riboswitch system. This strategy is further pursued in the following sections.

4.2.3 Alternative splicing-based design of riboswitches using uORFs

As already described in the previous chapters, there are multiple ways to regulate gene expression. One very efficient approach, which was further developed in our labs, is based on alternative splicing (Figure 4E). The system comprises two synthetic introns flanking an alternative exon that contains a premature stop codon, which downregulates gene expression when present in the mature mRNA [84b]. In this system, the 5'ss of the second intron was sequestered within the P1 stem of the Tet-aptamer upon ligand binding. This splice cassette

is inserted within the ORF. Conventional exons show sequence-conservation to increase splicing efficiency [126]. In target genes, which do not contain natural introns, the insertion of this system at random position into the ORF can cause improper splicing events and loss of function.

Within this work, we wanted to optimize this system to make it universally applicable. By placing the splice cassette of Finke et al. [84b] into the 5'-UTR the limitation of using only target genes naturally containing introns can be overcome. The advantages of the new approach include that any target gene can be chosen and only the 5'-UTR has to be adapted, the rather simple design and the combinability with other existing switches, which can improve the dynamic range. The first question, which had to be answered, was whether the splice cassette is also functional in the 5'-UTR. The second challenge was to find an element within the alternative exon, which downregulates gene expression when present in the 5'-UTR, since a stop codon would not have an effect in this context.

In the literature, two different systems are known to efficiently regulate gene expression and to contain splice elements within the 5'-UTR. The first was developed by Monteys et al. [127], employing a splice cassette containing drug-responsive pseudo exons to control reporter gene expression. This approach allowed them to achieve over 100-fold induction in the presence of the drug. The second system, published recently, called "pA regulator" is a combination of regulatory elements to ensure maximal control of gene expression combined with high sensitivity [128]. This Tet-dependent system uses an optimized Tet-aptamer to mask a PAS in presence of the ligand to prevent cleavage of the RNA. At the same time, to prevent interference of these highly structured elements in the 5'-UTR with the ribosome, an alternative splicing system is used to splice out these elements only in presence of the ligand to ensure proper translation. With this approach, they achieved induction of reporter gene expression up to 900-fold in presence of 2.25 µM Tet [128]. Therefore, they showed that it is feasible to develop riboswitches based on alternative splicing within the 5'-UTR.

In nature, the 5'-UTR contains a large set of regulators for translation [34]. One of them are small uORFs in close distance to the main open reading frame (mORF) [38]. They can have distinct effects on the mORF, stalling or distraction of the ribosome [38a], provoke mRNA decay [129] or they can even increase expression under stress conditions [130]. Their strength in repression depends on their number, length, distance to the mORF and the peptide charge [38a, 131]. Their efficiency in natural contexts and their short coding space make them a convenient tool to decrease protein levels by inhibiting translation [38a]. However, most uORF sequences in literature were mostly tested in their natural sequence context using the whole UTR [38a]. Thus, the surrounding sequence could add to the effect of the uORF. As uORFs appear to be efficient elements for gene regulations, we applied them in our splice context. For

reasons of simplicity in design, we first constructed an artificial sequence (Supplementary Table 3). Then we placed this sequence upstream of the *hRLuc* start codon to record its effect on gene expression (Figure 14B (2)).

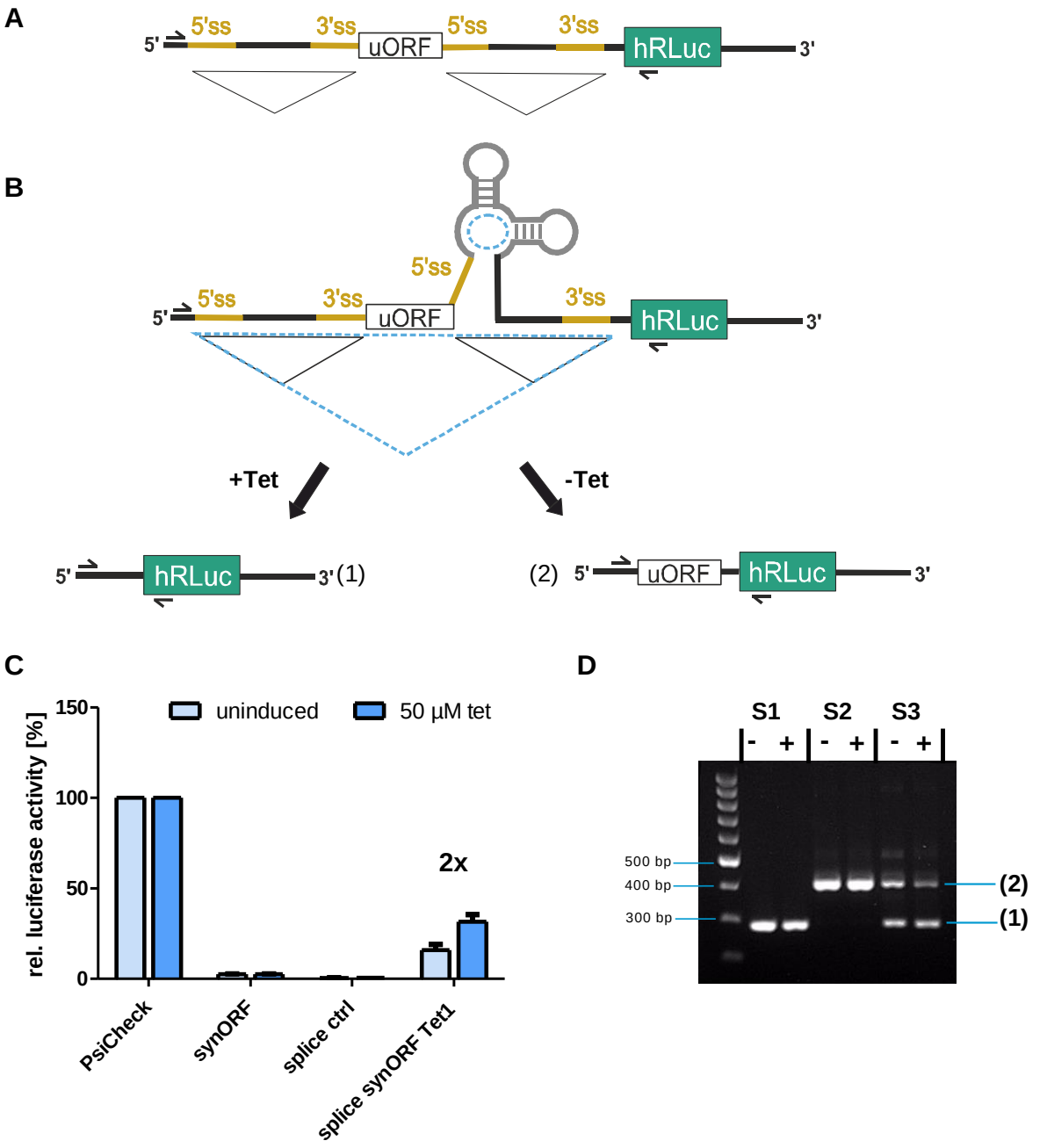

Figure 14: A) Schematic depiction of the uORF splice cassette control (splice ctrl) lacking the aptamer within the 5'-UTR of hRLuc. Introns are constitutively spliced. B) Alternative splicing regulated by the Tet-aptamer (grey) masking the 5'ss of the second intron. Upon ligand addition, the whole cassette is spliced out (blue dashed line), resulting in product (1) and high hRLuc activity. In absence of Tet both introns are spliced (black line) resulting in product (2) containing the uORF which downregulates gene expression. C) Dual luciferase assay of Tet-dependent splice switch and controls. The relative hRLuc activity is shown in absence and presence of 50 µM Tet, respectively. Shown are mean and standard deviation of three independent measurements, each performed in technical triplicates. The fold change of the switch is indicated above the bars. D) Transiently transfected HeLa cells were cultivated in the presence or absence of 50 µM Tet for 24 h. Total RNA was prepared and used for reverse-transcription-PCR. Small black arrows in A) and B) indicate primer binding sites used for RT-PCR. S1 corresponds to the PsiCheck empty vector (containing no splice cassette). S2 corresponds to the splice control lacking the aptamer for regulation and S3 corresponds to the splice synORF Tet1 switch depicted in B).

Indeed, introducing this synthetic uORF (synORF), hRLuc activity was reduced severely to about 2 % (Figure 14C). Next, we combined this synORF with the splice cassette to regulate its presence when the ligand is added. The splice cassette from our lab [84b] was placed directly upstream of the Kozak-sequence with the alternative exon replaced by the synORF (Figure 14B). As a control, the Tet aptamer masking the 5'ss was removed so that the synORF is spliced in constitutively (Figure 14A). In this case the synORF diminished gene expression again to <1 %. In the same step, we tested the construct containing the Tet aptamer in presence and absence of the ligand. Here, we observed a Tet-dependent increase in gene expression of about 2-fold, but with a much higher background in the 'OFF'-state than expected.

Prior to improve the system, we wanted to check if the data we obtained for the protein levels were also matching with the RNA levels. Using reverse transcription PCR (RT-PCR) we investigated the different splice products within the cell (Figure 14D). As a result, we obtained products matching the length of the fully spliced version (1) as well as the version were the uORF is spliced into the mature mRNA (2). The faint band above these products was checked by sequencing and contained a mix of fully spliced and synORF containing products. If they anneal together and bulge out non-complementary parts, it would also explain why they are running above the other bands. The empty vector control (PsiCheck), containing neither the splice cassette nor a uORF, only shows the short band, whereas the splice control lacking the aptamer shows only the constitutively spliced version containing the synORF. The switch contains both bands with a decreasing upper band upon ligand addition. This data matches our results for the protein levels and we assume that the splice cassette and the uORF are functional within this context.

Subsequently, we tried to optimize the system to obtain higher fold changes and a lower background. Splicing events in the 5'-UTR have already been described in the early 2000s [40a], however a lot of mechanisms are still not fully understood. One component in the splicing system that can influence gene expression is intron length. As relatively short introns in the 5'-UTR were observed to be associated with high gene expression [21], the two synthetic introns used in this system should be suitable as they are comparably small with <260 nt. Therefore, no adjustments were made in this respect. The first parameter for optimization would be to change the splice site strength to make regulation between the two states more efficient. Secondly, the masking of the 5' splice site by the aptamer can be improved, resulting in a lowered background. As a third strategy, the uORF was varied, since the current synORF was made by rational design and there are multiple natural sequences available.

The consensus sequence of the 5'ss in the 5'-UTR is similar to the conventional 5'ss in the ORF [40a]. To predict splice site strength, we used the SpliceRover tool [132]. We generated a

panel of constructs predicted to exhibit a weaker (W1-2) or stronger (S1-S3) 5'ss (Figure 15). Although the reliability is limited, we could observe a trend in mutating the splice site, respectively. Weakening the 5'ss resulted in an increased background activity of the hRLuc. This was expected, as the equilibrium would shift more to the fully spliced version not containing the uORF. In contrast, strengthening the 5'ss decreased the background to some extent. However, the fold change is getting worse in either direction, which was not expected. It can be assumed that this is due to the destabilisation of the P1 stem, when the splice site was mutated. However, restabilising the P1 stem did not improve the fold change compared to the initial construct (data not shown), indicating that changes in 5'ss strength do not benefit the system. Moreover, the overall fold changes are comparably low, so that conclusions should be drawn with caution.

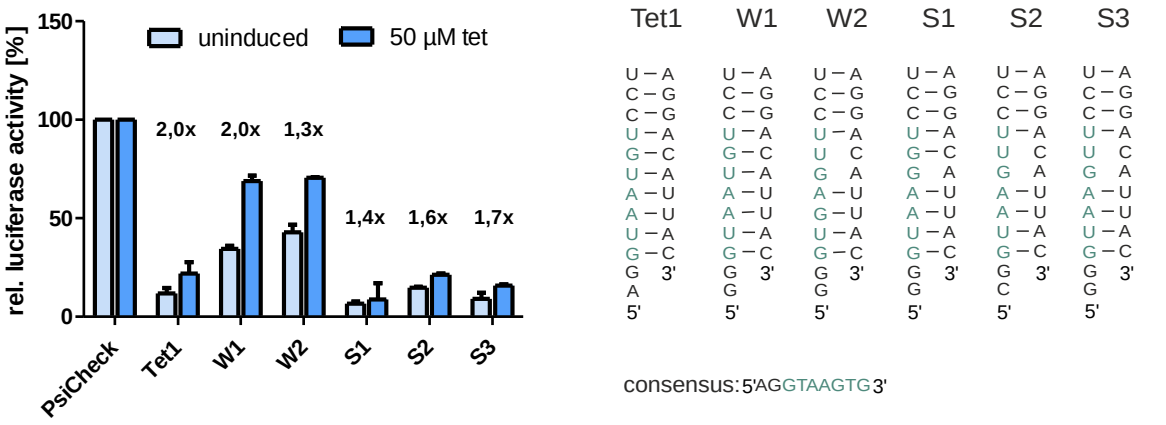

Figure 15: Dual luciferase assay of constructs with varied strengths of the 5'splice site masked by the Tet-aptamer (left). The relative hRLuc activity is shown in absence and presence of 50 µM Tet, respectively. Shown are mean and standard deviation of two independent measurements, each performed in technical triplicates. The respective fold changes are indicated above the bars. Corresponding sequences of the P1 stem containing the 5'ss are depicted on the right (W1,W2: weakened splice site, S1-S3: strengthened splice site according to SpliceRover [132]) .

In a next step, we varied the length of the P1 stem of the Tet-aptamer to influence the masking of the 5'ss. In the previous Tet1 construct, the stem length was 10 bp. We shortened it to 9 bp and also added another G-C pair for elongation (11 bp) (Figure 16). As expected, shortening the stem destabilizes it and makes the 5'ss more accessible, which could explain the lower background. At the same time, the stem is too short to mask the 5'ss efficiently even in presence of 50 µM Tet, causing the drop in the fold change. Since the spliceosome is associated with helicases [133], it takes highly stable stems in order to mask this site effectively. This can be observed for a stem length of 11 bp were the fold change increased to 2.6. However, further elongation raised the background and once again led to loss of the fold change (data not shown). This elongated stem is probably too stable and masks the 5'ss also in absence of Tet. In order to be applicable in therapeutic contexts, still, the background of the OFF-state has to be lowered, and the fold change must be increased.

Moreover, the Tet-aptamer itself also contains cryptic splice sites, which are rather weak according to SpliceRover [132]. Due to the structuring of the aptamer, they should not be very accessible for the spliceosome. When mutating the cryptic 3'ss in the P2 stem and the 5'ss in the P3 stem (Tet2 construct) the effect on gene expression was recorded again (Figure 16A). Indeed, these cryptic splice sites have been responsible for some of the background activity, resulting from other splice products. With the Tet2 construct, we could lower the switching levels from 10 % to almost 3 % in the OFF-state, while maintaining the same fold-change.

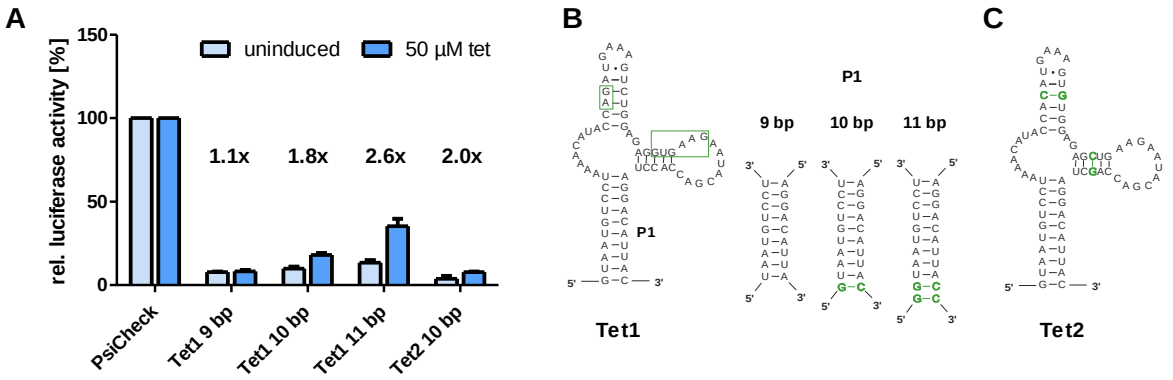

Figure 16: Dual luciferase assay of constructs with increasing stem lengths of the Tet-aptamer P1 stem. The relative hRLuc activity is shown in absence and presence of 50 µM Tet, respectively. Shown are mean and standard deviation of three independent measurements, each performed in technical triplicates. The respective fold changes are indicated above the bars. B) Nucleotide sequences of the Tet1 aptamer versions, varying in its P1 stem lengths. The different P1 stems are depicted on the right and additional nucleotides are marked in green. The green framed boxes indicate cryptic splice sites (3'ss and 5'ss) within the aptamer. C) Nucleotide sequences of the Tet2 aptamer with mutations to deactivate cryptic splice sites. Mutations marked in green. Secondary structures were predicted by mfold web server [134].

As a third way to optimize the system, we tested different uORF sequences on their efficiency to reduce the hRLuc activity. Therefore, we investigated several natural occurring sequences as well as synthetic designed motifs derived from the initial synORF construct (Figure 18). A recent study by Alghoul et al. [135] revealed two potent uORF sequences found in the context of Hox genes, Hox a3 and Hox a11 (Supplementary Table 3). They have the advantage, of obtaining a highly stable secondary structure due to the high G-C content. From this study, we picked the most efficient ones. Within the splicing context, introducing natural sequences always bears the risk that they contain cryptic splice sites, splicing enhancer or silencer sequences. Therefore, we aimed for rather short sequences to minimize the probability. A study from Clavo et al. [38a] identified a large set of natural uORFs, some of which are involved in diseases. From that pool, we picked two candidates with high potential, SRY and SPINK (Table 3). The 5'-UTRs in which they are found actually contain two small uORFs but only inactivation of the second one re-establishes gene expression completely [38a]. Consequently, we cloned a long and a short version, respectively; including either both or only the second uORF, to investigate which sequence is most efficient in our context. To test all these sequences on their efficiency within cells, the synORF sequence was replaced accordingly (Figure 17).

For the Hox a3 sequence, hRLuc activity was reduced to 11 %, but no difference was observed upon addition of Tet. As it is a comparably large motif, the presence of interfering motifs such as cryptic splice sites and splice regulators cannot be excluded. Due to the relatively high background we did not investigated this further. We assume that there is no potential for this motif in our context. In contrast, the Hox a11 motif was able to reduce the background expression significantly to a level that could make it interesting for therapeutic purposes (<3 %). However, it looses the fold change. This could not be elevated by a stronger masking of the 5'ss with an 11 bp P1 stem (data not shown).

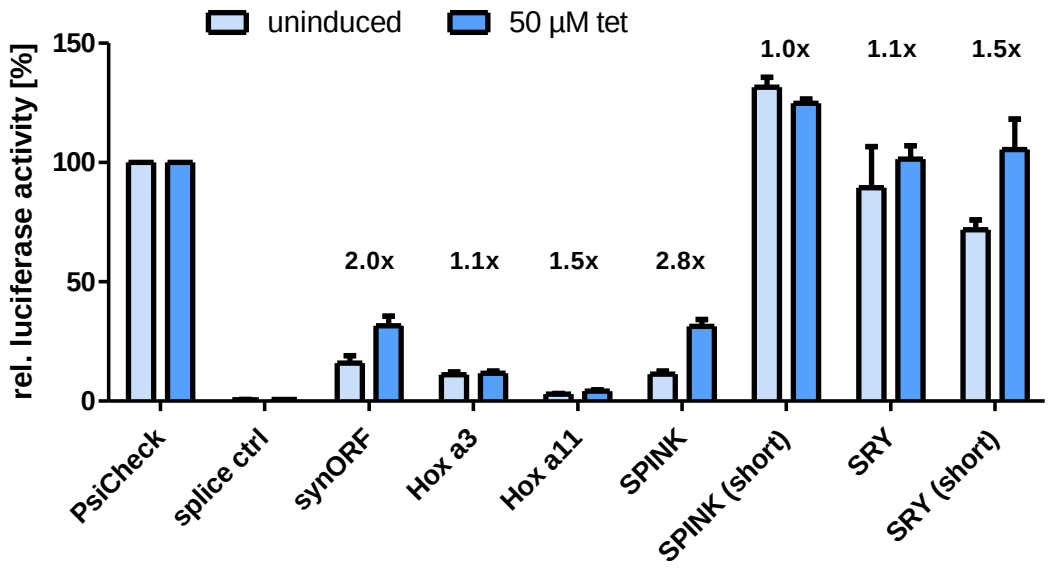

Figure 17: Dual luciferase assay of different natural uORF sequences in comparison with the synORF. The relative hRLuc activity is shown in absence and presence of 50 µM Tet, respectively. Shown are mean and standard deviation of three independent measurements, each performed in technical triplicates. The respective fold changes are indicated above the bars. Hox a11 and Hox a3 sequences are adapted from [135] and the SPINK and SRY motifs are taken from [38a]. The short versions of SPINK and SRY contain only the second uORF (and not both) residing in this sequence. Corresponding nucleotide sequences are listed in Supplementary Table 3.

For SRY we could only observe a prominent Tet-dependent effect in the shortened version. Although the alternative exon is rather small, splicing seems to work. Nevertheless, the OFF-state at about 70 % indicates that either the uORF is not efficient, which would oppose the results from Calvo et al.[38a], or that some unwanted splice products are formed. Indeed, according to predictions with SpliceRover [132] this sequence contains alternative splice sites. Weakening these did not improve the fold change nor the high background (data not shown). For this reason, we did not continue working on this.

With the long version of SPINK, we obtained a promising candidate with a background expression in the OFF-state of 11 % comparable to the synORF. But the fold change increased to 2.8. For the short version, the alternative exon was probably too short to be recognized as such. Exons with less than 50 nt are susceptible to exon skipping, yet micro exons below 25 nt are spliced efficiently [136]. However, with 9 nt the distance between the U1-binding site and the

3'ss is probably too short to be recognized. Therefore, we assume the whole cassette is spliced out constitutively in this case. Experimental results even suggest an optimal distance of >72 nt [137]. An extension of the longer SPINK version (from 40 to >70 nt) might decrease the background further, improving the dynamic range, as the exon recognition increases. Besides, luciferase activity slightly above 100 % is plausible, since splicing events can boost gene expression generally [21].

Although there are hundreds of natural uORF sequences available, we wanted to focus further on artificially designed motifs. However, among the synORF variants, no better candidate has been found in terms of low background and higher fold changes. We tried a lot of different designs of the alternative exons, varying the length, number and position of the uORF. Exemplary motifs (synORF1-3) are shown in Figure 18. As it is known that, reduction in gene expression is stronger, the closer the uORF ends to the mORF [131], for the initial construct (synORF1) we chose a small uORF directly at the end of the alternative exon (marked in green). Additionally, a start codon was introduced (brown) and set to be out of frame to the mORF, which can potentially result in a non-sense product of about 100 amino acids.

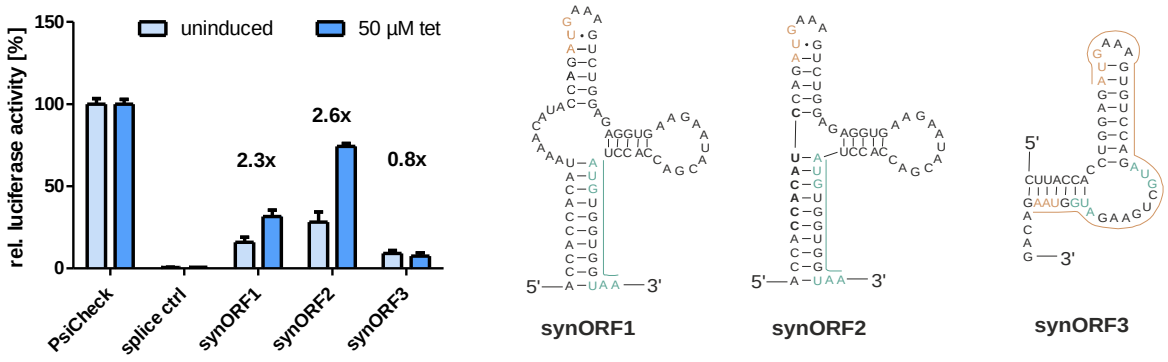

Figure 18: Dual luciferase assay of different alternative exons containing synthetic uORF sequences (synORF). The relative hRLuc activity is shown in absence and presence of 50 µM Tet, respectively (left). Shown are mean and standard deviation of three independent measurements, each performed in technical triplicates. The respective fold changes are indicated above the bars. On the right, the respective nucleotide sequences are depicted. In coloured lines (green and brown) the uORFs are indicated. Single start codons are highlighted but corresponding stop codons reside in the hRLuc ORF and are designed to be out of frame to the mAUG. Secondary structures were predicted by mfold web server [134].

When we deleted the junction between the two stems, the resulting sequence 5'-CCACATC-3' is a binding site for two splice factors, SRp40 and SRp55, according to a prediction tool for eukaryotic splicing enhancers [138]. These factors can promote translation [139]. Indeed, we were able to observe higher expression levels of our reporter gene (74 %). In addition, we observed a better fold-change of 2.6, but unfortunately, the OFF state was also higher compared to the initial construct. Changing the structure of the alternative exon even more led to the loss of switching activity. For the third construct, we designed a larger uORF compared to synORF 1 and 2 (brown). According to literature, longer uORFs are more effective [131]. Thereby, we could decrease the background to almost half compared to previous constructs. However, the correct splicing seems to be impaired, as no change upon ligand addition could be observed.

The data suggest that the choice of the alternative exon is a delicate thing and structural effects might also contribute to the efficiency of the system. In nature, the uORFs are mostly conserved, and probably optimized in their context [140]. Furthermore, when using rational design it is challenging to take all traits of uORFs into account. For example, we did not consider the peptide charge within our synORFs. Yet that could be an important feature to optimize the system. Moreover, we should consult more predictions of cryptic splice sites and splice factor binding sites. As current prediction tools might not be as reliable for the 5'-UTR, other bioinformatic pipelines should be used. However, our system seems to work in general, on protein level as well as on RNA level. In addition, since these switches are designed to be modular and easily applicable to other reporter genes, we created some combinations of switches.

Therefore, we tried to implement the splice switch into another context to prove its robustness. Furthermore, we combined it with an HDV-based aptazyme described in the previous chapter. Placing the splice cassette into the 5'-UTR of the Firefly Luciferase (hLuc+) analogous to the hRLuc construct, we checked its efficiency again in the DLA (Figure 19A). Although the promotor and the sequence environment differ, the splice switch performs similar to the Renilla context even with a slight increase in fold change (from 2-fold to 2.4-fold). This could be shown for the protein level (Figure 19A) as well as for the RNA level (Figure 19B). Therefore, it seems to be efficiently transferrable to another context.

It has to be mentioned that the background activity is slightly higher in the hLuc+ context, which can already be seen in the splice control. This could be advantageous as it suggests that by selecting different promotor strengths the system can also be optimized. To get further insights into the dynamic range of the system, we examined concentration dependent induction of the reporter gene testing a dilution series of the ligand (Figure 19C). Despite having a higher OFF-state, we observed a slight increase in sensitivity within the hLuc+ context, where the switch reacts better to the ligand already in low concentrations. Since higher concentrations of Tet (>200 µM) interfere with cell viability no reliable data could be obtained in this range. Consequently, as the saturation for the upper induction level is not reached corresponding EC_{50} values could not be determined. Depending on the context (hRluc or hLuc+), the out of frame start codon in synORF1 results in different peptides, which are formed during translation because the ORF and the position of the stop codon differs. The higher background could result from a less efficient recognition of this start codon. However, since it is only a minor difference, we did not follow up on this.

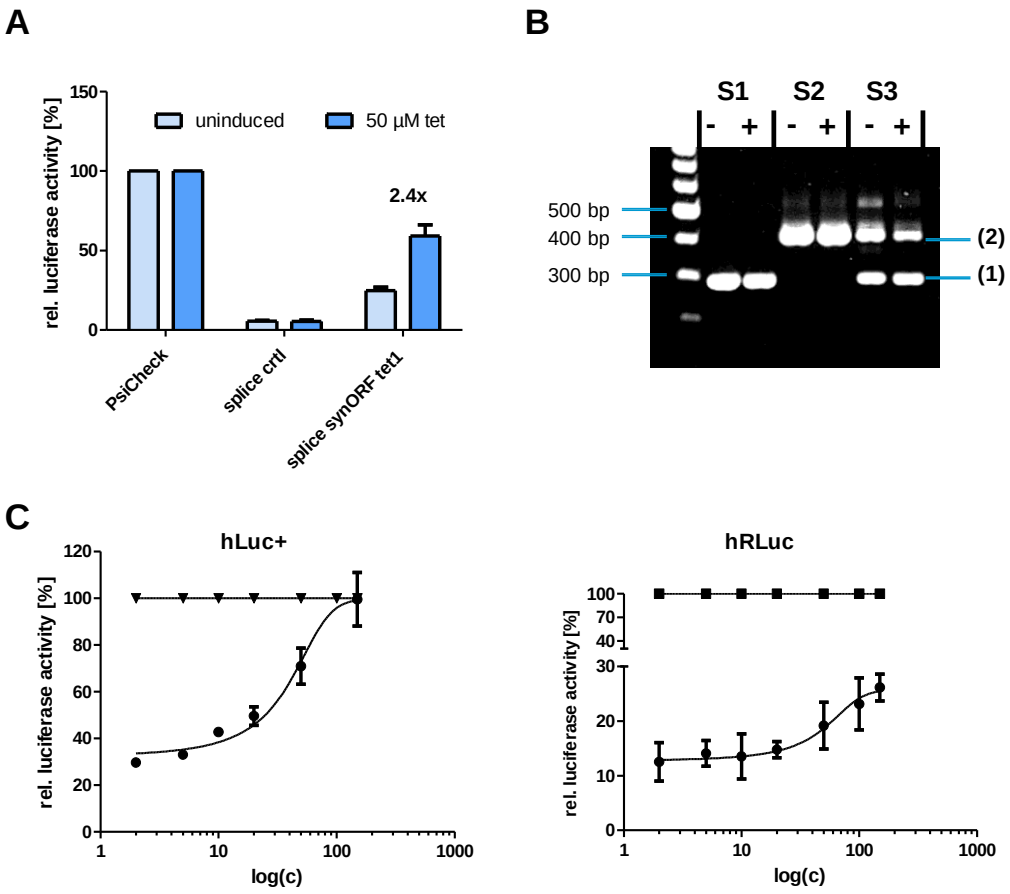

Figure 19: A) Dual luciferase assay of the splice cassette switch containing the synthetic uORF sequence (synORF) within the 5'-UTR of the Firefly luciferase (hLuc+). The relative hLuc+ activity is shown in absence and presence of 50 µM Tet, respectively. Shown are mean and standard deviation of three independent measurements, each performed in technical triplicates. The respective fold change is indicated above the bars. B) Transiently transfected HeLa cells were cultivated in the presence or absence of 50 µM Tet for 24 h. Total RNA was prepared and used for reverse-transcription-PCR. S1 corresponds to the PsiCheck empty vector (containing no splice cassette). S2 corresponds to the splice control lacking the aptamer for regulation and S3 corresponds to the splice synORF Tet1 switch. Primer sequences are listed in the Methods section. C) Dose-dependent luciferase activity (c = µM Tet) of the synORF switch in the hLuc+ and hRLuc, respectively. Error bars represent the standard deviation of the mean values of two independent measurements, each done in technical triplicates.

Moreover, to evaluate the combinability of these switches, the synORF-containing splice cassette in the 5'-UTR was combined with the two best switching tandem-designed aptazymes in the 3'-UTR (Figure 20). Combination 1 showed an elevated fold change (up to almost 5-fold) and at the same time a reduced background activity of 3 % in the OFF-state. For Combination 2 the decrease in background was even greater (<1 %) but the ON-state was reduced as well and switches only to about 2.5 %.

In addition, the sensitivity of Combination 1 was slightly increased compared to the single synORF construct (Figure 19C). Recording the dose-dependency of the reporter activity, with Tet concentrations of only 20 µM, the hRLuc activity almost doubled compared to the OFF-state (Figure 20B). To verify if the effects only add up or if they have a synergistic effect of boosting their efficiency, we tried another aptazyme for combination, which exerts a higher fold change. We combined an HHR-based Tet-dependent aptazyme from a co-worker in our lab (Vera Hedwig, unpublished) with two versions of our splice cassette containing the synORF.

With an 8-fold induction when tested alone, in combination we could achieve up to 18-fold switch (Figure 20C). This suggest that the efficiency multiplies in combination, making the splice cassette as well as the aptazymes a strong modular tool to regulate gene expression.

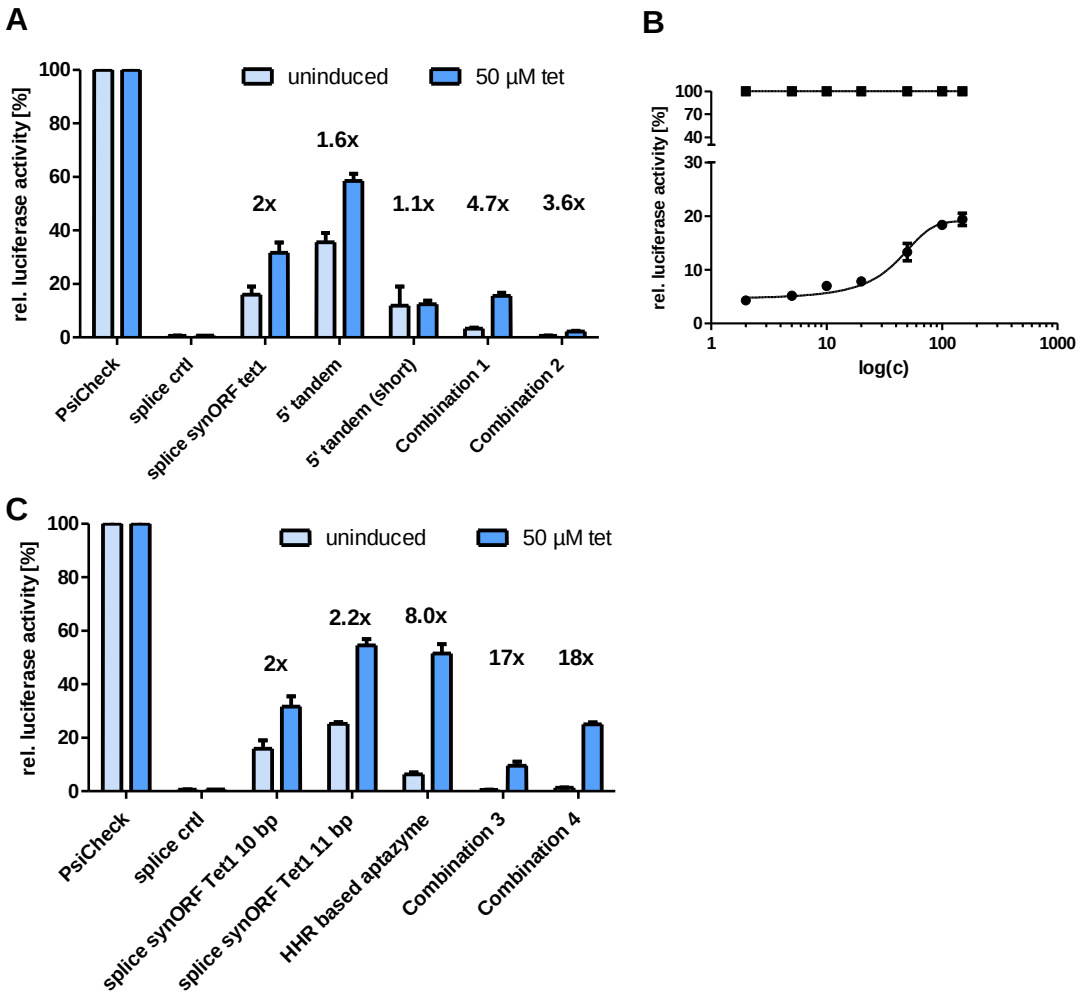

Figure 20: A) and C) Dual luciferase assay of riboswitch combinations controlling Renilla luciferase (hRLuc). The relative hRLuc activity is shown in absence and presence of 50 µM Tet, respectively. Shown are mean and standard deviation of three independent measurements. The respective fold change is indicated above the bars. B) Dose-dependent luciferase activity (c = µM Tet) exemplary of Combination 1. Error bars represent the standard deviation of the mean values of two independent measurements.

In summary, within this section we were able to generate a functional riboswitch based on alternative splicing that resides in the 5'-UTR of the target gene. We followed different optimization strategies and found ways to achieve minor improvements to the system. However, for therapeutic applications the fold change as well as the high background activity in the OFF-state might not be sufficient. Furthermore, we could show this system can be easily transferred to another context, while maintaining its switching activity. In addition, we combined the splice-based switches with aptazymes, to show the potential of combinability. Thereby, we obtained a system that shows induction levels of almost 5-fold while exerting a low OFF-state. The improvements found within the process, could be used for further combinations to develop a set of better-performing switches.

4.2.4 Alternative splicing-based design of riboswitches using self-cleaving ribozymes

We successfully demonstrated that the splice cassette functions within the 5' UTR when regulating the presence of a uORF within the mRNA. As choosing suitable uORF sequences revealed to be challenging, we did not want to limit this system to the use of only this element. To expand the toolset we exchanged the alternative exon with another promising downregulator of gene expression – a self-cleaving ribozyme. They have already been proven to be highly active elements within the 3'-UTR as described in the previous chapters. Additionally, they are suitable for the use in the 5'-UTR to cleave mRNA, which has already been shown for a Tet-dependent HHR construct [141]. Consequently, we inserted potent candidates from the most efficient ribozyme classes (the HDV, HHR t3, TS-2 and twister) into the splice cassette as alternative exons (Figure 21). On the protein level, only the HHR constructs showed a ligand induced switching activity (>2-fold). For the other ribozymes, no significant induction effect could be observed. Interestingly, the expression levels increased with decreasing ribozyme efficiency. Observing this trend suggests that the ribozyme cleavage is functional in this context. For the HDV ribozyme, we would have expected better performance as it could almost suppress gene expression in the 3'-UTR context. However, according to SpliceRover [132] it contains another weak cryptic splice site. From previous experiments, we further conclude that even minor changes in the sequence can reduce its efficiency. Therefore, the HDV ribozyme is not convenient in this splicing context. Furthermore, the TS2-p5 motif and the twister ribozyme were unable to reduce gene expression efficiently (Figure 21B). Summarizing, the HHR is the only promising candidate, which we used to further optimize this expression platform.

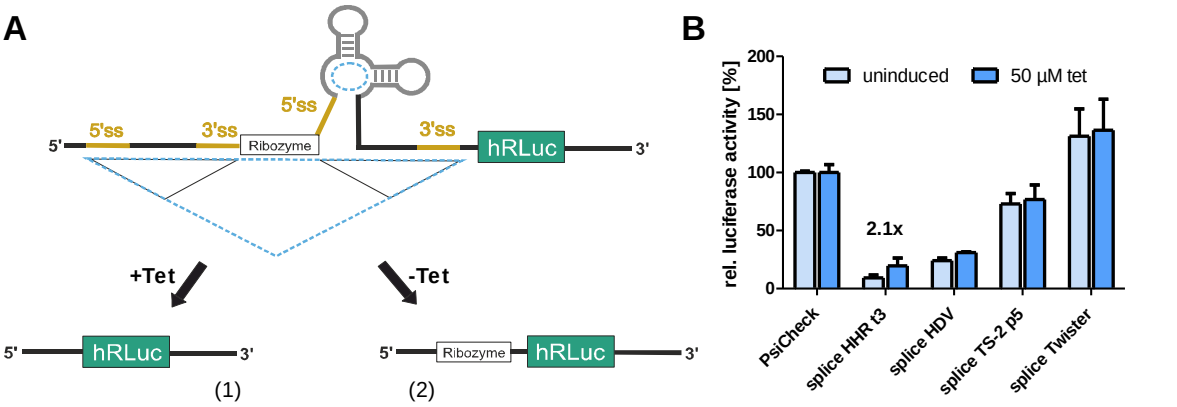

Figure 21: A) Alternative splicing regulated by Tet-aptamer (grey) masking the 5'ss of the second intron. Upon ligand addition, the whole cassette is spliced out (blue dashed line), resulting in product (1) and *hRluc* expression is on. In absence of Tet both introns are spliced (black line) resulting in product (2) containing a ribozyme which downregulates gene expression. C) Dual luciferase assay of Tet-dependent splice switch and controls. The relative hRLuc activity is shown in absence and presence of 50 µM Tet, respectively. Shown are mean and standard deviation of two independent measurements, each performed in technical triplicates. The fold change of the switches is indicated above the bars.

Concerning the splice HHR construct, the background activity in the OFF-state was again very high with 9 %. The spliceosome, as a very large ribonucleoprotein, creates a very crowded environment. The splicing process as well as ribozyme folding is known to happen co-transcriptionally. Although the folding of the HDV ribozyme and HHR happens fast, it could be impaired due to the crowded environment. Subsequent reduction of ribozyme activity could explain the background expression of hRLuc in absence of the ligand. At the same time, if the ribozyme would already cleave the RNA before the splicing could occur, the mRNA pool would be strongly degraded. This could reduce the induction levels severely in presence of the ligand. For these reasons, we wanted to separate the two processes by ensuring the ribozyme would only cleave after correct splicing. Thus, the idea was to split the ribozyme and insert the pieces flanking the first intron of the splice cassette (Figure 22). In absence of Tet, after splicing, the pieces are united again and the ribozyme can cleave the mRNA. In presence of the ligand, part of the ribozyme within the alternative exon is removed from the mRNA and gene expression is on. For this strategy, the ribozyme needs to fulfil two requirements. First, no start codons are allowed within the sequence upstream of the intron, as they would remain in the RNA after splicing. This would downregulate gene expression in the ON-state. Secondly, the ribozyme has to be split after an AG to ensure integrity of the 5'ss requiring an upstream AG for proper recognition by the spliceosome. Considering this, we designed different construct containing the HHR (Table 5).

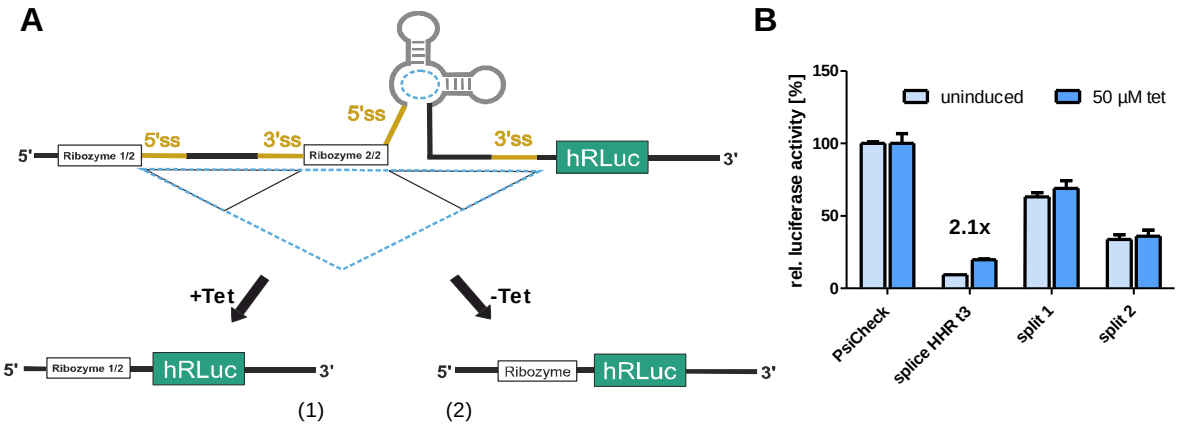

Figure 22: A) Alternative splicing regulated by Tet-aptamer (grey) masking the 5'ss of the second intron. Upon ligand addition, the whole cassette is spliced out (blue dashed line), resulting in product (1) containing only one part of the ribozyme which is not functional and *hRLuc* expression is on. In absence of Tet both introns are spliced (black line) resulting in product (2) containing the full functional ribozyme which downregulates gene expression. C) Dual luciferase assay of Tet-dependent splice switch and controls. The relative hRLuc activity is shown in absence and presence of 50 µM Tet, respectively. Shown are mean and standard deviation of two independent measurements, each performed in technical triplicates. The fold change of the switches is indicated above the bars.

Unfortunately, no ligand dependent induction of hRLuc activity could be observed. We know from previous experiments that the splice cassette is functional and the ribozyme does not contain any cryptic splice sites. Therefore, the data indicates that the ribozyme cannot fold correctly. During the folding process, different intermediates are formed in order to build up the native structure [142]. The splitting of the ribozyme could prevent the formation of some intermediates, which are crucial to adopt the correct structure. Since folding is a very conserved mechanism, this approach seems to be not convenient for ribozymes. The reduction in gene expression could also result from interference of the first part of the ribozyme with the translation process. It seemed like a straightforward strategy, but as this expression platform was not functional, we discarded the idea.

Instead, we wanted to work on reducing the background activity in the OFF-state. From literature we know, splicing events >50 nt downstream of the stop codon cause the mRNA to be degraded via NMD [44]. However, we could use this to decrease the background activity, by placing the splice cassette into the 3'-UTR of the hRLuc (Figure 23).

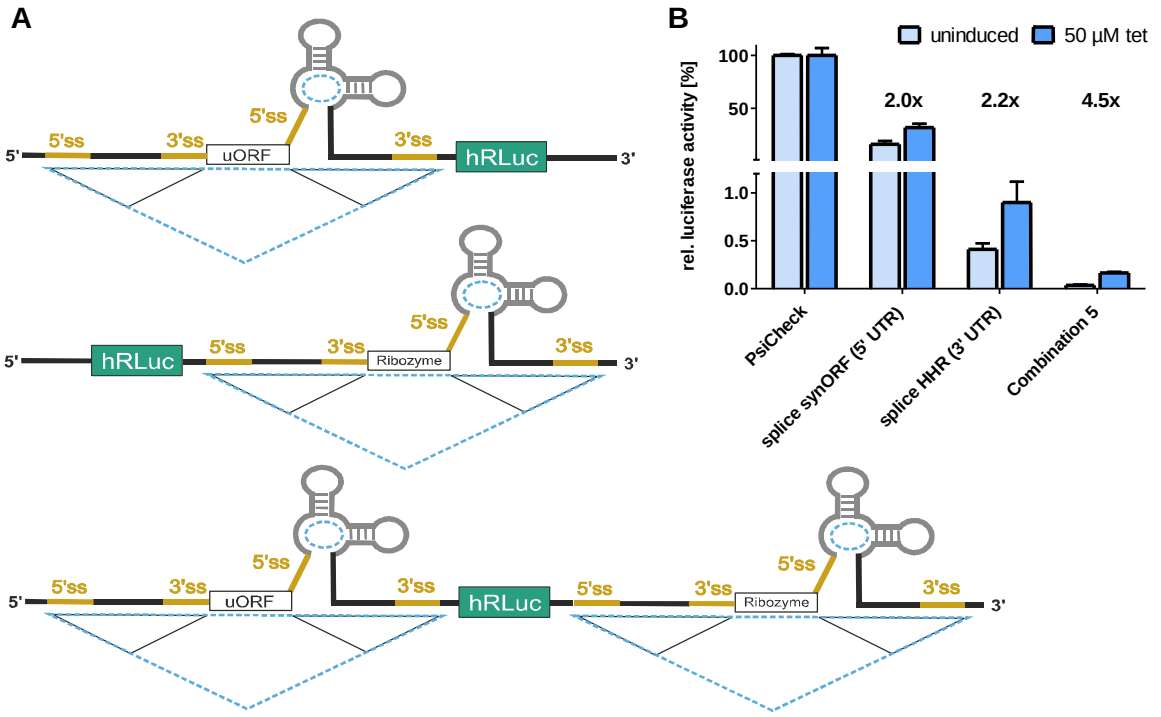

Figure 23: A) Different expression platforms using the splice cassette, regulating the presence of uORFs (at the top) or ribozymes (middle). Additionally, the combination of both riboswitches is shown in the bottom. Alternative splicing regulated by Tet-aptamer (grey) masking the 5'ss of the second intron. C) Dual luciferase assay of Tet-dependent splice switch and controls. The relative hRLuc activity is shown in absence and presence of 50 µM Tet, respectively. Shown are mean and standard deviation of three independent measurements, each performed in technical triplicates. The fold change of the switches is indicated above the bars.

Furthermore, we wanted to test the combination of the uORF splice cassette and this ribozyme design here. Placing the splice cassette containing the HHR into the 3'-UTR indeed reduced the background from 9 % to 0.5 %. The fold change, when adding 50 µM Tet, was maintained and even slightly increased. Although this is a major improvement concerning the different applications, for a good switch the fold change must be increased further. Using the modularity of the system again, we could achieve 4.5-fold induction of gene expression in combination with the uORF splice cassette in the 5'-UTR. Here, the OFF-state was only 0.04 %.

With our data, we could show that the splice cassette is a robust expression platform, which is easily transferrable between the chosen contexts. It can be assumed that it can be used even beyond that. Moreover, we could highlight the modularity of our system, making it easily combinable with other riboswitches. In summary, the splice cassette in the UTR may not be the best switch on its own, but it can enhance and improve other systems through synergistic effects.

4.3 Conclusion

In this chapter, we first conducted a comparative survey, employing a dual luciferase assay (DLA) and an eGFP/mCherry-based assay, evaluating the self-cleaving activity of various ribozyme classes in HeLa cells. Notably, the hepatitis delta virus (HDV) ribozyme emerged as a standout performer, demonstrating remarkable efficiency, especially when the catalytic core was reduced to the essential elements (2 %). Comparative analysis with the closely-related CPEB3 ribozyme highlighted the HDV ribozyme's structural optimization in nature.

The newly discovered hovlinc ribozyme and the hatchet motif did not lead to reduction of gene expression in our context within mammalian cells. The other classes, including hairpin, pistol, twister and TS ribozyme showed moderate activity with our reporters. However, concerning aptazyme design, due to their structural properties they provide suitable tools for aptamer insertions. In literature well-performing aptazymes for the twister and pistol ribozyme have already been developed for different organisms [100a, 101b]. Moreover, the commonly used HHR was also observed to reduce the reporter gene expression efficiently in both contexts, which is in line with previous studies [81a, 96c]. The influence of the ribozyme position within the 3'-UTR on gene expression revealed a consistent trend: proximity to the stop codon correlated with increased ON/OFF-ratios, emphasizing the importance of strategic placement for optimal performance.

Indeed, the HDV ribozyme consistently displayed robust cleavage activity, overshadowing other ribozyme classes. However, challenges arose in the design of Tet-dependent ON-switches using HDV-based aptazymes, with tandem designs exhibiting high background

expression. Exploring alternative strategies involved the insertion of the Tet-aptamer within loop regions, exploiting a “slippage” mechanism, and manipulating the tertiary structure. While certain designs showed promise in reducing background expression, achieving a reliable ON-switch proved challenging due to the structural limitations the HDV ribozyme exerts to maintain its activity. The findings provide valuable insights for future efforts in developing efficient aptazymes for diverse applications, emphasizing the need for innovative design strategies and context-dependent optimization.

Additionally in this chapter, the development and optimization of a riboswitch, which is based on alternative splicing was described, presenting a tool for the precise control of gene expression. The initial design, which was optimized in our lab [84b], involving synthetic introns flanking an alternative exon with a premature stop codon, was refined and adapted for universal applicability by relocating the splice cassette to the 5’-UTR of the gene of interest. This enables flexibility in choosing target genes and enhancing combinability with other regulatory switches, thereby improving the dynamic range of the system. The exploration of small upstream open reading frames (uORFs) within the 5’-UTR as an alternative exon confirmed their potential as effective elements for reducing protein levels by inhibiting translation [38a]. Through systematic examination of different uORF sequences, we identified promising candidates that significantly interfere with gene expression, contributing to the fine-tuning of the riboswitch performance. Optimization efforts focused on enhancing the efficiency of the splicing system involved strategies such as adjusting splice site strength and modifying the Tet-aptamer structure. However, remaining challenges include the need to increase the dynamic range and minimize background activity to be applicable for therapeutic applications.

Notably, the newly designed splice cassette was successfully transferred to another gene context, containing a different promotor, sequence context and another reporter gene, while maintaining its switching activity. This highlights the riboswitch's adaptability. Furthermore, the combinability of the splice-based switches with aptazymes demonstrated the potential for creating more sophisticated and efficient regulatory systems. The resulting approach exhibited robust induction levels (~5-fold) and reduced background activity (3 % and <1 %), paving the way for the development of a set of better-performing switches.

As a last step in this chapter, due to challenges in selecting suitable uORF sequences, we expanded the toolset by replacing the alternative exon with self-cleaving ribozymes (HDV, HHR t3, TS-2, and twister). Only the HHR constructs exhibited ligand-induced switching activity on the protein level, while the other ribozymes did not show significant induction effects. To address the high background activity of the HHR construct in the OFF-state, we attempted to split the ribozyme and insert its parts flanking the first intron of the splice cassette. Unfortunately, ligand-dependent induction was not observed, suggesting the ribozyme might

not fold correctly after splicing. As an additional approach to drop the background activity, we explored placing the splice cassette into the 3'-UTR, successfully reducing background from 9 % to 0.5 %. Combining this design with the uORF splice cassette in the 5'-UTR yielded a 4.5-fold induction of gene expression, demonstrating improved switch performance.

Our findings emphasize the robustness and modularity of the splice cassette as an expression platform, easily transferrable between different contexts. While it may not be the optimal switch independently, its synergistic effects enhance and improve other systems. In summary, the splice cassette in the UTR proves to be a versatile tool with potential applications beyond the studied contexts.

5. Chapter III: A self-cleaving ribozyme as a target for antibiotic compounds

5.1 Introduction

The emergence of drug-resistant pathogens and the constant need for innovative therapeutics have spurred a search for unconventional drug targets. In particular, antibiotics that target unexploited areas of bacterial metabolism are promising candidates to combat drug-resistant bacteria [143]. In the previous chapters, only a few aspects of functional RNAs were pointed out which make them a potent tool for therapeutic strategies. Additional to riboswitches, also simple ribozymes are used. The HHR as well as the hairpin ribozyme already have been exploited to overcome viral disease in immune cells [144]. Thereby, the ribozymes are designed to be partly complementary to essential viral elements, such as the TAT region, which is crucial for viral replication. The ribozyme cleavage site resides within the target sequence and by *trans*-cleavage the target mRNA is selectively degraded [144c]. Using similar approaches, HIV infection could be successfully slowed down [145] or even a resistance could be induced in human cell culture [144a]. Moreover, the effect of artificially generated *trans*-cleaving HHR on selective reduction of mRNA levels was already examined in animal model systems over 20 years ago [146]. However, catalytic RNAs are not only serving as a tool for drug development. They provide a suitable target for the development of new antibiotics, because especially ribozymes are mostly found in pathogens like bacteria and fungi, but are extremely rare in humans [147]. Thus, a specific antibiotic targeting such a catalytic RNA should allow interference with the viability of the pathogen without adverse effects for the patient. As an example, group I introns are examined on their potential as a target for antifungal compounds [148]. Over the past years, multiple small molecules were found to interact with such ribozymes impairing their function [67, 149]. It could be demonstrated that aminoglycosides selectively inhibit the self-splicing of group I introns [67]. Furthermore, the class of tetracyclines was shown to reduce HHR activity severely in higher concentrations [149].

Because ribozymes and riboswitches enable a fine-tuned control over gene expression, bacteria employ them to regulate their metabolism. One example would be *glmS* ribozyme, residing in the 5'-UTR of the mRNA, which is controlling the gene encoding for the enzyme glucosamine-6-phosphate-synthase (GlmS) [150]. This enzyme uses glutamine and fructose-6-phosphate (Fru6P) to synthesize glucosamine-6-phosphate (GlcN6P). GlcN6P is essential for the cell wall synthesis of bacteria, which makes the *glmS* ribozyme a convenient target for antibiotic drug development (Figure 24) [150a, 151]. The *glmS* ribozyme uses GlcN6P to catalyse its self-cleavage, as described in more detail later in this chapter. After cleavage, the *glmS* mRNA is prone to degradation by RNase J1. [66b] Therefore, the bacteria creates a negative feedback loop to react to variations in GlcN6P concentrations. Interfering with cell wall

biosynthesis by activating the *glmS* ribozyme with a drug, is desirable. As this mechanism is unique to gram-positive bacteria, side effects in humans are expected to be low. A GlcN6P mimic that acts as a *glmS* ribozyme activator and interferes with bacterial cell wall synthesis would be a promising candidate for a future antibiotic drug [66a, 151a].

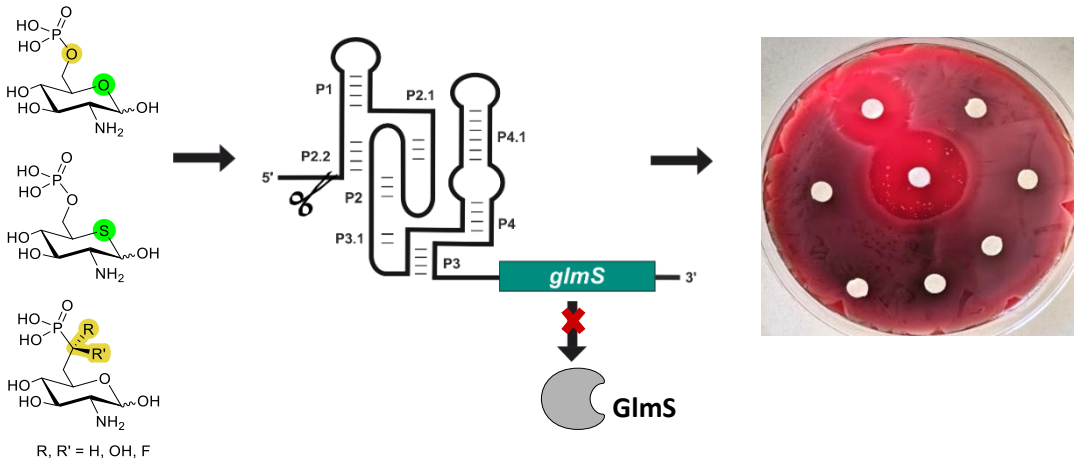

Figure 24. GlcN6P, and derived mimics (left) activate the *glmS* ribozyme (middle). The mRNA containing the *glmS* gene is cleaved and prone for degradation. The encoded enzyme glucosamine-6-phosphate-synthase (GlmS) is essential for bacterial cell wall biosynthesis. Reduction in expression would cause severe growth inhibition of the Bacteria which can be visualized by filter disk assays (right).

The structural requirements for GlcN6P mimics to catalyse the self-cleavage reaction of the *glmS* ribozyme have been thoroughly investigated in the past [150a, 152]. The self-cleavage ability of the *glmS* ribozyme relies entirely on the presence of amine-containing ligands, indicating that the RNA alone lacks a functional catalytic site [152a]. The ligand-activated catalysis is dependent on the pK_a of the amine functionality, and derivatives lacking the N lone pair are ineffective [153]. RNA structures exert a more limited chemical diversity than proteins. Therefore, RNAs exploit functional groups from other molecules to enhance their biological functionality, which supports the theory of an old complex RNA world metabolism [154]. The data indicate that GlcN6P acts as a coenzyme for *glmS* ribozyme self-cleavage rather than an allosteric effector modulating catalytic activity [66b, 152a, 153].

Additionally, specific sugar hydroxyl groups play a crucial role in binding and catalysis, as the 4-hydroxy group which acts as a hydrogen-bond donor [153]. The ribozyme selectively binds to the *α*-anomer of GlcN6P and removal or inversion of such hydroxy groups results in significant loss or total absence of activity [153]. Interestingly, a carba-sugar analogue of GlcN6P demonstrates comparable activity to the natural ligand, indicating that the ring oxygen can be replaced without affecting activity [66c]. Moreover, the phosphate group is proposed to be important for correct positioning of GlcN6P in the active site of the ribozyme through chelation to Mg^{2+} [153]. However, phosphatase-inert *glmS* ribozyme activators would be promising as they would not be metabolized and could trigger the self-cleavage permanently. Therefore, previous

attempts be the Ye [155] and Soukup [153] group were made to develop suitable phosphatase-inert GlcN6P mimics. The *in vitro* data showed only minor activation of the self-cleavage of the *glmS* ribozyme in presence with these compounds, which they explained by different electrical properties of hydroxyphosphonates and steric problems [155] or lower acidity of the phosphonate compared to the GlcN6P, affecting its ability to bind Mg^{2+} ions [153]. However, to our knowledge, there has been no systematic examination of GlcN6P derived phosphonate analogues exerting diverse pK_a values on their efficiency to activate the *glmS* ribozyme.

Here, we demonstrate the biological activity of two classes of newly synthesized GlcN6P mimics (Figure 25) [66b]. A set of C7 phosphonate derivatives with difluoro (**1**), hydroxy ((*R*)-**2** and (*S*)-**2**), and monofluoro substitution ((*R*)-**3** and (*S*)-**3**), which differ in their acidity compared to GlcN6P, as well as a thia-GlcN6P **4** that contains a sulfur atom instead of the ring oxygen were tested on their efficiency to trigger the *glmS* ribozyme *in vitro*. Whereas the phosphonates regardless of their acidity, turned out to be less efficient riboswitch activators, thia-GlcN6P **4** activated self-cleavage of the *glmS* ribozyme with the same efficiency as the natural metabolite GlcN6P. A detailed look at the published X-ray structure of GlcN6P provided an explanation of the reduced activity of the phosphonates and allowed to draw conclusions for the design of future riboswitch activators [66b]. Due to the impressive performance of the thia-GlcN6P **4**, we conducted *in vivo* experiments to investigate its effect on bacterial cells. We tested the influence of thia-GlcN6P **4** on the growth of gram-positive bacteria that contain the *glmS* ribozyme, such as two *Bacillus* strains and *Staphylococcus aureus (S. aureus)*.

Bacillus subtilis (*B. subtilis*), a soil dwelling and non-pathogenic bacterium, which is major model organism usually used to study e.g. biofilm formation. It has served as the primary model organism for understanding gram-positive bacteria for many years [156]. Additionally, *B. subtilis* is able to grow on a variety of carbohydrates as single carbon sources, respectively [157]. The catabolite control protein A (CcpA) is the major transcription factor to control carbon metabolism. If glucose is present, CcpA binds to target sites upstream of catabolic operons, resulting in downregulation or activation of certain target genes. This process is called catabolite repression. [158] Several carbohydrates, such as glucosamine (GlcN), N-acetylglucosamine (GlcNAc) or glucose, are taken up via phosphotransferase system (PTS), which phosphorylates the sugars upon uptake [159]. These mechanisms are highly conserved among related species [158b]. In order to investigate the biological activity of the compounds tested in this work, they have to be taken up by the bacteria efficiently. For polar and charged compounds, such as the phosphonates and phosphates described here, we cannot expect that they would passively diffuse into the cells and have to exploit a natural uptake system.

We also included *Bacillus thuringiensis* (*B. thuringiensis*), another member of the *Bacillus* genus, in our studies. It can produce a variety of highly potent insecticidal proteins, which are

mostly not harmful to humans. However, it is closely related to *B. anthracis* causing the acute fatal disease anthrax and is highly toxic [160]. Consequently, finding an effective antibiotic against *B. thuringiensis* could be advantageous to fight off relatives that are more dangerous.

Moreover, we examined the effect on different strains of *S. aureus*. The species contains several strains being pathogenic to humans. Among them, the methicillin-resistant *Staphylococcus aureus* (MRSA), which is a major cause of hospital and community-acquired infection [161]. These strains have acquired a Staphylococcal Cassette Chromosome mec carrying the *mecA* gene that confers resistance to all β-lactam antibiotics [162]. Also the methicillin-susceptible strains are responsible for severe invasive *S. aureus* infection [161]. Therefore, there is an urgent need for new strategies to develop selective antibiotic substances to contain the spread of these bacteria.

5.2 Results and discussion

5.2.1 Activation of *glmS* ribozyme self-cleavage by phosphonate and thia-sugar analogues of GlcN6P

To assess the capability of newly synthesized compounds in stimulating the cleavage activity of the *glmS* ribozyme, we conducted ligand-dependent self-cleavage assays [66c]. Therefore, we used a 5'-^{32}P labelled ribozyme sequence from *B. subtilis*, incubated it with the respective ligand and analysed the RNA fragments by analytical PAGE. Initially, the compounds **1**, (*R*)-**2**, (*S*)-**2**, (*R*)-**3**, (*S*)-**3**, or **4** were incubated with the glmS ribozyme in the presence of 10 mM $MgCl_2$. We observed that compounds (*R*)-**2**, (*S*)-**2**, and **4** prompted efficient cleavage of the ribozyme at a concentration of 1 mM (Figure 25).

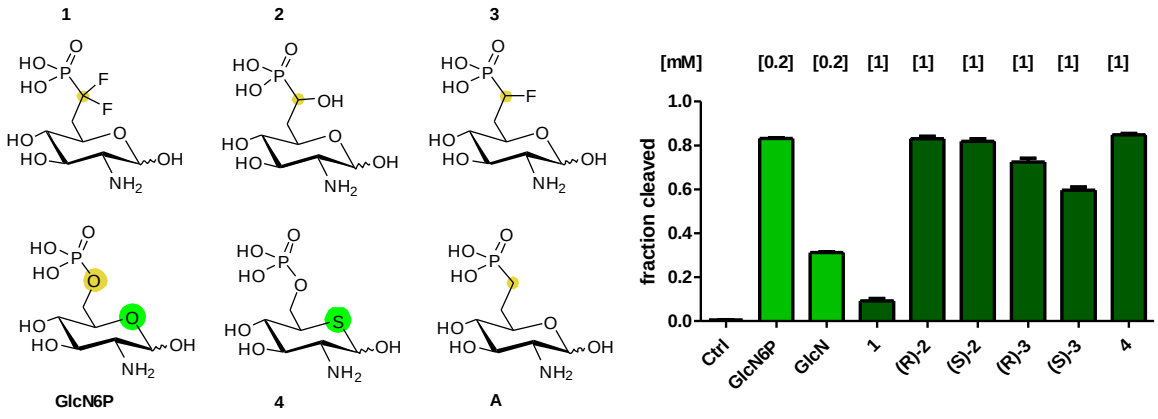

Figure 25. Left: Natural ligand of the *glmS* ribozyme, GlcN6P, and derived mimics (1-4) synthesized by Silkenath et al [66b]. C-7 methylene phosphonate (A) mimic synthesized by Soukup [153]. Right: Initial assessment of the activity to activate self-cleavage of the *glmS* ribozyme from *B. subtilis* by the newly synthesized compounds 1, (*R*)-2, (*S*)-2, (*R*)-3, (*S*)-3, and 4. As a control, the RNA was incubated in presence of 10 mM Mg^{2+} without any compound (Ctrl). GlcN6P and GlcN were used for comparison at a concentration of 0.2 mM. All new compounds were tested at a concentration of 1 mM and incubated for 30 min. The error bars display the standard deviation of triplicates.

In contrast, compounds (*R*)-**3** and (*S*)-**3** displayed slightly reduced activity, while difluorophosphonate **1** exhibited only minor induction of the self-cleavage reaction.

To better assess the efficiency of cleavage activation for the most promising compounds, we conducted kinetic measurements involving (*R*)-**2**, (*S*)-**2**, (*R*)-**3**, (*S*)-**3**, and **4**. As a control, the natural metabolite GlcN6P was used and we included the methylene phosphonate **A** from existing literature [152a]. 5'-^{32}P-labeled *B. subtilis* ribozyme was incubated with varying activator concentrations, followed by measuring the cleaved fraction over time (Figure 26). Our observations revealed that the induction of self-cleavage by phosphonates **A**, (*R*)-**2**, (*S*)-**2**, (*R*)-**3**, and (*S*)-**3** was less efficient compared to GlcN6P. Hence, time-resolved measurements were performed using activator concentrations spanning from 200 µM to 1 mM. For each concentration we determined the corresponding rate constants k_{obs} (Table 1). Although all phosphonates were found to activate the riboswitch, their efficiency was notably lower than that of the natural metabolite GlcN6P. For instance, **A** exhibited a k_{obs} (0.332 min^{-1} at 500 µM) that was 7.5 times slower compared to GlcN6P (2.49 min^{-1}), which is similar to what was reported by Soukup [153] when they investigated the *glmS* ribozyme from *Bacillus cereus*.

Interestingly, the hydroxy- and fluorophosphonates (*R*)-**2**, (*S*)-**2**, (*R*)-**3**, and (*S*)-**3** displayed even lower activity. Although fluorophosphonates (*R*)-**3** and (*S*)-**3** show almost identical pK_a values as the natural ligand [66b], their k_{obs} values were smaller than those of hydroxyphosphonates (*R*)-**2** and (*S*)-**2** (Table 1). This suggests that the pK_a value of phosphonate derivatives is not the sole determining factor for their ability to induce riboswitch self-cleavage. Based on the crystal structure of the *glmS* ribozyme from *B. anthracis* [163], it can be inferred that both the phosphate and sugar components of GlcN6P are recognized. The three non-bridging oxygens of the phosphate make contacts with the hydrated Mg^{2+} ions.[163]. Furthermore, it was proposed that the bridging oxygen (O6) is involved in two hydrogen bonds to G1, one to N1 and one to the NH_2 group at C2, which is not possible with the phosphonates. The disruption of these hydrogen bonds could result in weaker binding of the compounds that could explain the reduced activity in triggering the cleavage [66b]. Therefore, the presence of the oxygen at the 6-position seems to be more important than initially thought.

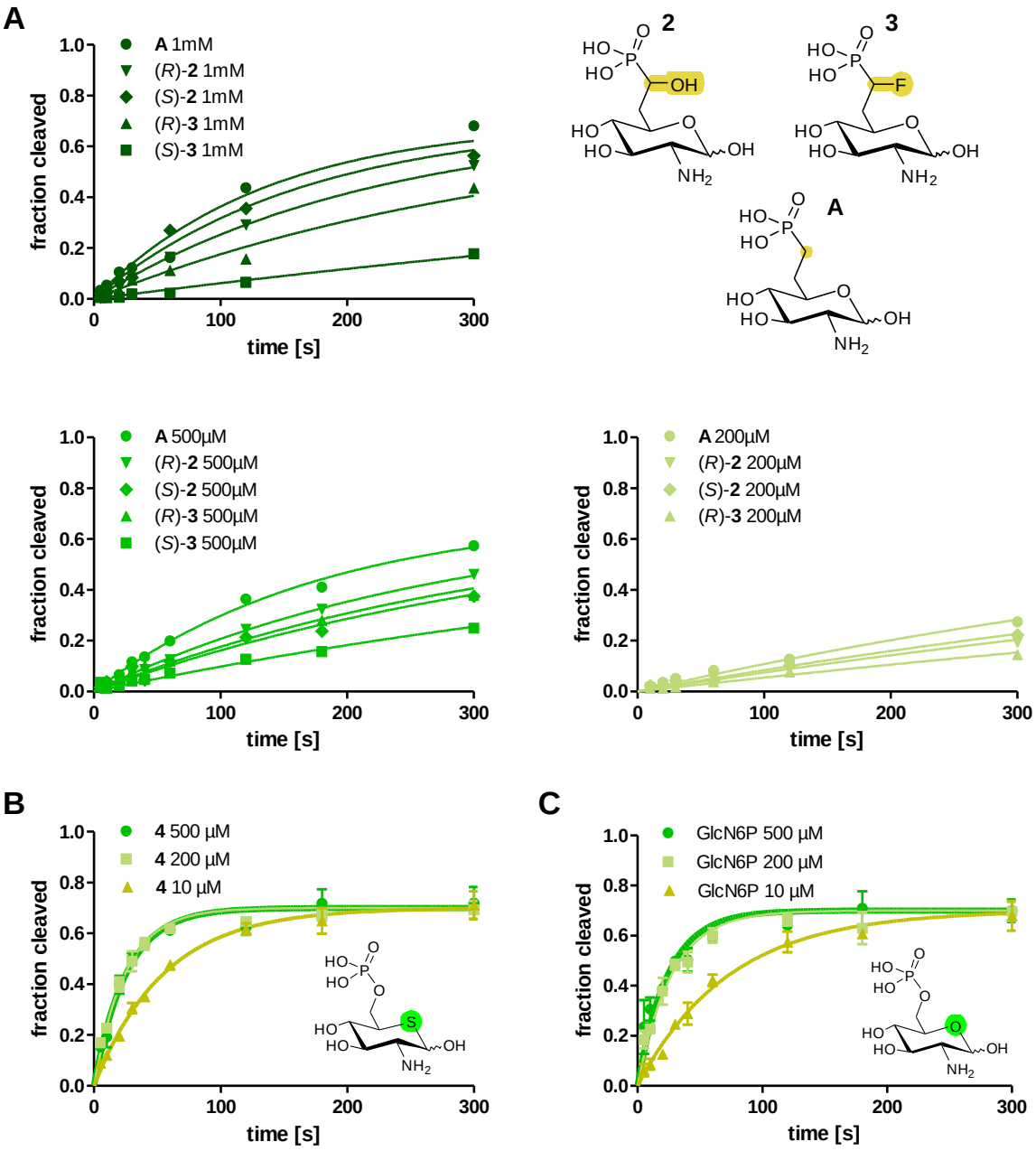

Figure 26: Kinetic measurements of the self-cleavage of 5'-^{32}P-labeled *B. subtilis glmS* ribozyme induced by (A) hydroxyphosphonates (*R*)-2 and (*S*)-2, fluorophosphonates (*R*)-3 and (*S*)-3, and methylene phosphonate A (schematic structure; top right), in decreasing concentrations from 1 mM (top left) over 500 µM (bottom left) to 200 µM (bottom right), respectively. (B) Kinetic measurements using thia-GlcN6P 4 and (C) GlcN6P as activators. All measurements performed at the same concentration are represented in the same colour. The error bars in (B), (C) represent the standard deviation of three independent measurements. Exemplary radiographs of the experiments can be found in the appendix.

Table 1. Rate constants k_{obs} of *B. subtilis glmS* ribozyme cleavage induced by compounds (*R*)-2, (*S*)-2, (*R*)-3, (*S*)-3, methylene phosphonate A, thia-GlcN6P 4, and GlcN6P.

compound	k_{obs} [min^{-1}]			
	10 µM	200 µM	500 µM	1 mM
GlcN6P	0.820 ± 0.04	2.21 ± 0.18	2.49 ± 0.28	n.d.
A	n.d.	0.103 ± 0.004	0.332 ± 0.01	0.439 ± 0.05
(*R*)-**2**	n.d.	0.069 ± 0.004	0.211 ± 0.01	0.270 ± 0.01
(*S*)-**2**	n.d.	0.078 ± 0.004	0.157 ± 0.01	0.362 ± 0.03
(*R*)-**3**	n.d.	0.049 ± 0.002	0.174 ± 0.01	0.173 ± 0.01
(*S*)-**3**	n.d.	n.d.	0.091 ± 0.004	0.055 ± 0.003
4	1.09 ± 0.15	2.44 ± 0.12	2.36 ± 0.04	n.d.

We proceeded to determine the rate constants (k_{obs}) for the self-cleavage reaction triggered by thia-GlcN6P **4** at concentrations of 10 µM, 200 µM, and 500 µM (Figure 26B, Table 1). Remarkably, we found nearly identical rate constants to those observed with the natural ligand GlcN6P (Figure 26C, Table 1), suggesting the thia-GlcN6P **4** as a highly potent mimic of GlcN6P. The same efficiency could be observed with *glmS* ribozymes obtained from *Listeria monocytogenes* (*L. monocytogenes*) and *Clostridium difficile* (*C. difficile*) (Figure 27), confirming that multiple *glmS* ribozyme can use thia-GlcN6P **4** as a ligand. We could successfully identify a new artificial ligand for the *glmS* ribozyme, which possesses the ability to activate the self-cleaving reaction *on par* with the natural ligand.

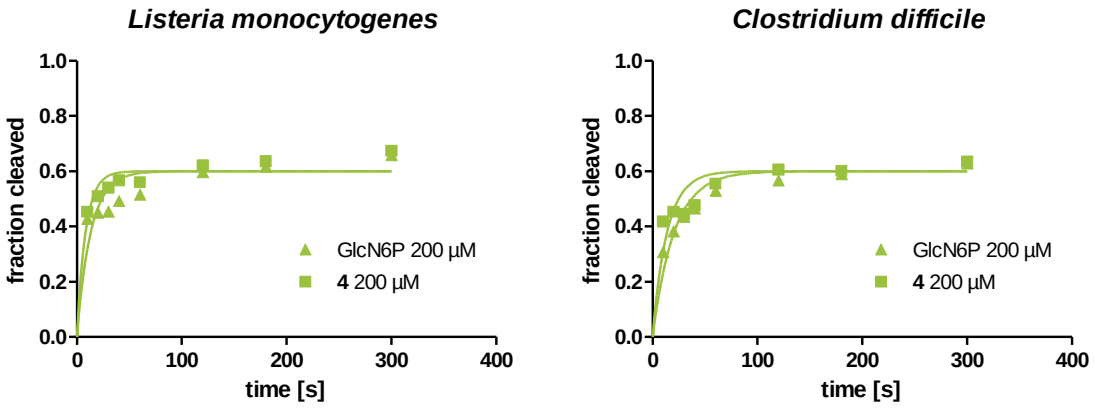

Figure 27: Kinetic measurements of the self-cleavage of 5'-^{32}P-labeled *glmS* ribozyme from *Listeria monocytogenes* (left) and *Clostridium difficile* (right) induced by GlcN6P and thia-GlcN6P 4 in a concentration of 200 µM, respectively.

5.2.2 Antimicrobial activity of *glmS* ribozyme ligand analogues

The potential of GlcN6P mimics to trigger self-cleavage of the *glmS* ribozyme very efficiently, particularly thia-GlcN6P **4**, gave us the opportunity to continue and investigate the antimicrobial effects. First, we conducted growth-inhibition tests on two *Bacillus* strains, *B. subtilis* and *B. thuringiensis*. The *in vitro* cleavage assays showed that their *glmS* ribozyme accept the thia-GlcN6P **4** as a ligand. Concerning the uptake into the bacteria we expected the thia-GlcN6P **4** to exploit the PTS as it is known for closely related compounds [159]. Thereby, the 6-hydroxy group is phosphorylated, which is not feasible in case the phosphate group is already there. Hence, we included the unphosphorylated thia-sugar (thia-GlcN **5**) which is converted into the active thia-GlcN6P **4** upon uptake. This approach already proved to be successful in examining the antimicrobial traits of carba-GlcN [151a]. However, for the non-natural phosphonates **1**, **2**, and **3**, this strategy was not feasible. Despite this, we investigated unprotected phosphonates, although we expect the uptake to be hindered.

Initially, filter disk assays were used to assess the antimicrobial potential of the synthesized compounds (Figure 28). Therein, we used chloramphenicol (Cm) as a known antibiotic for comparison and GlcN, which is converted to the natural ligand GlcN6P by the PTS system. GlcN was anticipated to have no impact on bacterial growth. Chloramphenicol showed a distinct inhibition zone (2.3 cm), validating its effectiveness. As expected, hydroxyphosphonate (R)-**2**, fluorophosphonate (S)-**3**, thia-GlcN6P **4**, and GlcN demonstrated no growth inhibition on the tested bacterial strains.

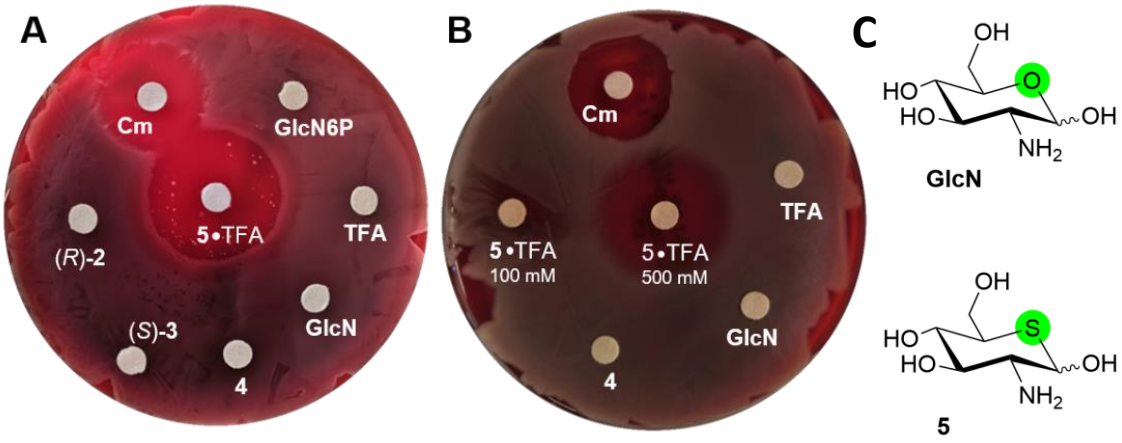

Figure 28. Filter disk assay on Mueller Hinton agar plates. A) *B. subtilis* wt 168 plated out and respective compounds were applied on a filter disc (10 µL) at a concentration of 100 mM. Hydroxyphosphonates (*R*)-2 and (*S*)-2, fluorophosphonates (*R*)-3 and (*S*)-3, thia-GlcN6P 4, Cm: chloramphenicol at a concentration of 9.3 mM. TFA (trifluoroacetic acid) was also tested since thia-GlcN 5 was employed as TFA salt. B) *B. thuringiensis* plated out and respective compounds were applied on a filter disc (10 µL) at a concentration of 100 mM. Additionally, thia-GlcN 5 was also tested with 500 mM. Cm: chloramphenicol at a concentration of 9.3 mM. TFA (trifluoroacetic acid) was also tested since thia-GlcN 5 was employed as TFA salt. C) Chemical structure of glucosamine (GlcN) and thia-glucosamine (5).

For thia-GlcN **5**, we observed a clear growth inhibition (2.8 cm) for both strains. To clarify if this is an unspecific effect, we repeated the experiment for *Escherichia coli* (*E. coli*), which does not contain any *glmS* ribozyme as a member of gram-negative bacteria (Figure 29A). No

growth inhibition was observed, suggesting that it either is not taken up or does not have any effect on the viability. From the literature it is known that the uptake of GlcN and GlcNAc is also mediated by the PTS [164]. We expect that the closely related thia-GlcN **5** is also efficiently taken up by *E. coli* via this route. Therefore, we would assume that the thia-GlcN **5** is specifically affecting the viability of the tested *Bacillus* species.

Since filter disc assays represent a convenient but rather qualitative characterization, we quantified the antibiotic activity and determined the minimal inhibitory concentration (MIC) for *B. subtilis* and *B. thuringiensis* in a liquid culture (Supplementary Figure 2). These experiments revealed a MIC of thia-GlcN **5** of 460 µg mL^{-1} towards *B. subtilis* and 1.15 mg mL^{-1} towards *B. thuringiensis* corresponding to 2 mM and 5 mM, respectively. Additionally, we were searching in the literature for known thia-sugars that cause toxic effects within cells to derive a probable mode of action for thia-GlcN **5**. The only report we could find was thia-glucose, which is an efficient inhibitor for the hexokinases *in vivo* and it is known to mark an effect on the energy metabolism of Schistosoma mansoni *in vitro* [165]. However, the conversion of thia-GlcN6P **4** to thia-glucose would take several steps via thia-fructose-6-phosphate and thia-Glucose-6-phosphate [166] and, furthermore, it is not known if the respective enzymes would accept the thia-sugar also as a substrate. Moreover, in the growth experiments even high concentrations, up to 20 mM (Supplementary Figure 2), could not show an effect on bacterial growth. Therefore, we excluded the theory of thia-GlcN **5** being converted into thia-glucose to induce the antimicrobial effect and investigated other strategies.

Furthermore, we wanted to investigate if the antimicrobial effect of thia-GlcN **5** is limitied to *Bacillus* strains. We expanded the tests and repeated the filter disk assays with other gram-positive bacteria, such as *Deinococcus radiodurans* (Figure 29B) and different *S. aureus* strains (Figure 29C-D). Moreover, we included *Staphylococcus cohnii, Enterococcus hirae* and *Enterococcus feacalis* but could not observe any effect of the thia-GlcN **5** (Supplementary Figure 3).

Deinococcus radiodurans showed a small zone of inhibition (1.1 cm) applying a concentration of 500 mM of thia-GlcN **5**. In contrast to Cm, here the border to the not affected growing bacteria was diffuse. Therefore, the effect of thia-GlcN **5** on *Deinococcus radiodurans* is rather small which could be due to different uptake efficiencies between the species. More interestingly, different strains of *S. aureus* reacted differently to our compound. Whereas, we observed a clear zone of growth inhibition with Oxford H (Figure 29C, List of strains) already for an applied concentration of 100 mM, for *S. aureus* NRL05/507 (Figure 29D, List of strains) the effect was not as clear. In case of *S. aureus* NRL05/507, the zone around the filter disk was completely covered by a very thin layer of bacteria. Nevertheless, the presence of thia-GlcN **5** noticeably reduced bacterial growth in the area of the filter disk compared to the entire

plate. Within *S. aureus* the catabolite repression is not as pronounced as in *B. subtilis* and it has multiple redundant mechanisms for sugar uptake [167]. This could explain why the growth of *S. aureus* is not completely impaired.

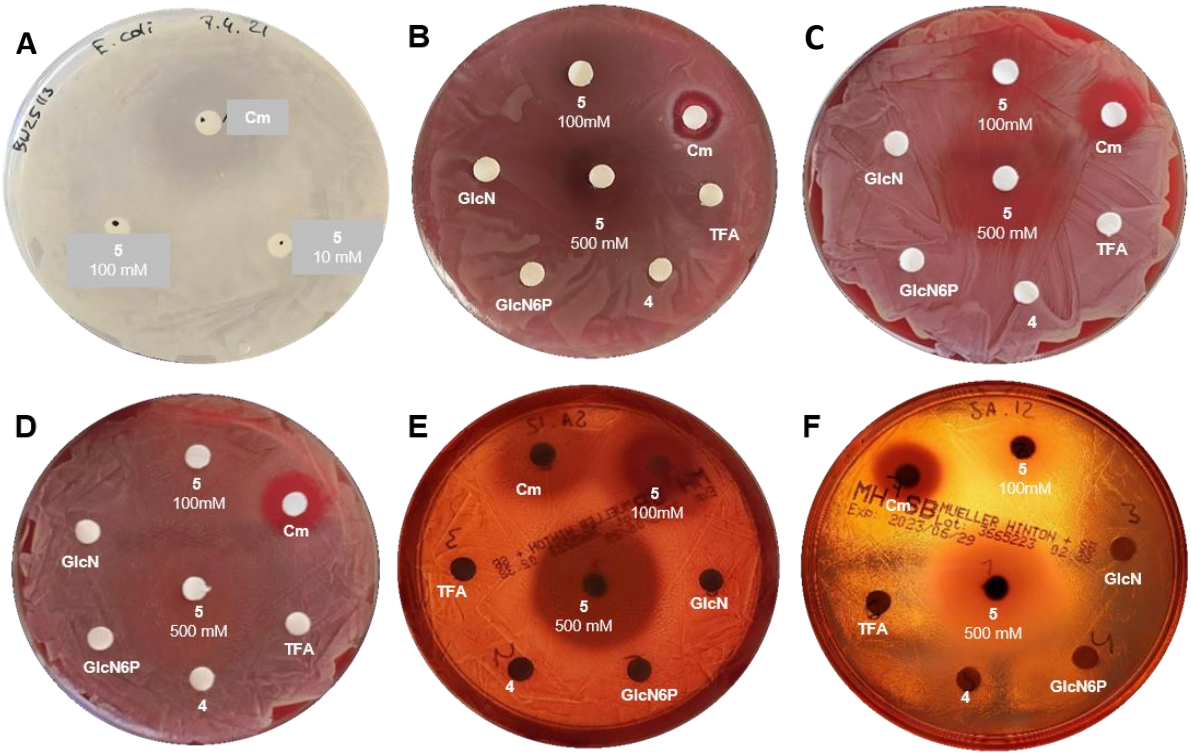

Figure 29. Filter disk assay on Mueller Hinton agar plates. A) *E. coli* BW25113 plated out on LB agar plate and respective compounds tested on a filter disc (10 µL) at a concentration of 100 mM. B) *Deinococcus radiodurans*, C) *S. aureus* Oxford H and D) *S. aureus* NRL05/507 plated out on Mueller Hinton blood agar plates and respective compounds tested on a filter disc (10 µL). thia-GlcN 5 at a concentration of 100 mM and 500 mM, respectively. Cm: chloramphenicol at a concentration of 9.3 mM. Other compounds at 100 mM. E) Same plate as in (C) but image was taken from the bottom to visualize hemolysis of *S. aureus* (strain 2) after 48 h and (F) after 96 h of incubation.

Interestingly, for *S. aureus* another effect became visible after 48h of incubation. Since the *S. aureus* NRL05/507 is known to be haemolytic, releasing specific toxins [168], the blood from the agar plate was slowly decomposed. This resulted in a colour change making the plate increasingly transparent. Looking at the bottom of the plate, beneath the bacterial layer the plate indeed became more transparent, however in the area where the antibiotic compounds (Cm and thia-GlcN **5**) were applied, it remained red and turbid. This indicates that the thia-GlcN **5** seems to affect the *S. aureus* severely as they cannot produce their haemolytic toxins. After 96 h (Figure 29F) this effect is still observed. However, compared to Cm, the thia-GlcN **5** containing areas start slowly to be haemolysed. The potential of the thia-GlcN **5** to strongly reduce cell growth of pathogenic bacteria is promising for the development of new effective antibiotics or to study their pathogenicity further.

In order to shed more light on the cause and effect of the antibiotic activity of thia-GlcN **5** we aimed at the generation of a strain that shows increased resistance to the thia-GlcN **5**. First,

we tested the resistant *B. subtilis* colonies, which were growing in the zone of inhibition (Figure 28A). We checked them on mutations within the *glmS* ribozyme and *glmS* gene by amplifying the area and sending the PCR product for sequencing. However, no mutation within this area could be detected. As a next step, we directly generated a strain, which exerts a resistance to thia-GlcN **5**. For this purpose, *B. subtilis* wt 168 was grown in presence of increasing concentrations of thia-GlcN **5**. We started with a concentration of 1.5 mM that is below the observed MIC for this strain. After four rounds of growth in increasing concentrations, a resistant *B. subtilis* culture (designated as *B. subtilis* **5**-res) was obtained that grew efficiently in 50 mM thia-GlcN **5** in liquid culture. Bacteria were streaked on a plate and a single clone was isolated. The genome of the resistant clone was sequenced and compared to the original *B. subtilis* strain in order to identify a mechanism of resistance to thia-GlcN **5**.

B. subtilis **5**-res has accumulated a single mutation in comparison to the parental strain that causes a frameshift within the open reading frame and hence an inactivation of the *ptsH* gene product. *ptsH* encodes for a protein HPr that is an important component of the PTS system. It is crucial for the uptake of sugars like glucose and fructose. HPr acts as a cargo-independent phosphocarrier protein in this mechanism, hence the mutation should affect all kinds of PTS systems [169]. This finding suggests that the likely mechanism how strain *B. subtilis* **5**-res tolerates increased concentrations of thia-GlcN **5** is an impaired uptake into the bacterial cell. In accordance with our findings, a previous study already observed increased resistance to the related compound carba-α-D-glucosamine in a *ptsH* deletion strain [151a].

In order to confirm that carbohydrate uptake systems are indeed impaired in the raised strain *B. subtilis* **5**-res, we cultivated it in minimal medium with glucose as a sole carbon source. As expected, opposed to the wild type strain, *B. subtilis* **5**-res was not able to grow under these conditions (Figure 30).

Taken together, these results explain the resistance towards thia-GlcN **5**. However, they do not provide evidence that the *glmS* ribozyme is a main target of the antimicrobial effect of thia-GlcN **5**. A study from Schüller et al [151a] could show applying the carba-GlcN to the bacteria intracellular levels of *glmS* mRNA are decreasing significantly. They conclude that also *in vivo* the ribozyme is triggered by this mimic. Therefore, we would expect the same effect for our thia-GlcN **5** as the efficiency to activate the riboswitch is even increased compared to the carba-GlcN [66c]. Further studies, e.g. transcriptome analysis, need to be conducted to elucidate the thia-GlcN **5** mode of action.

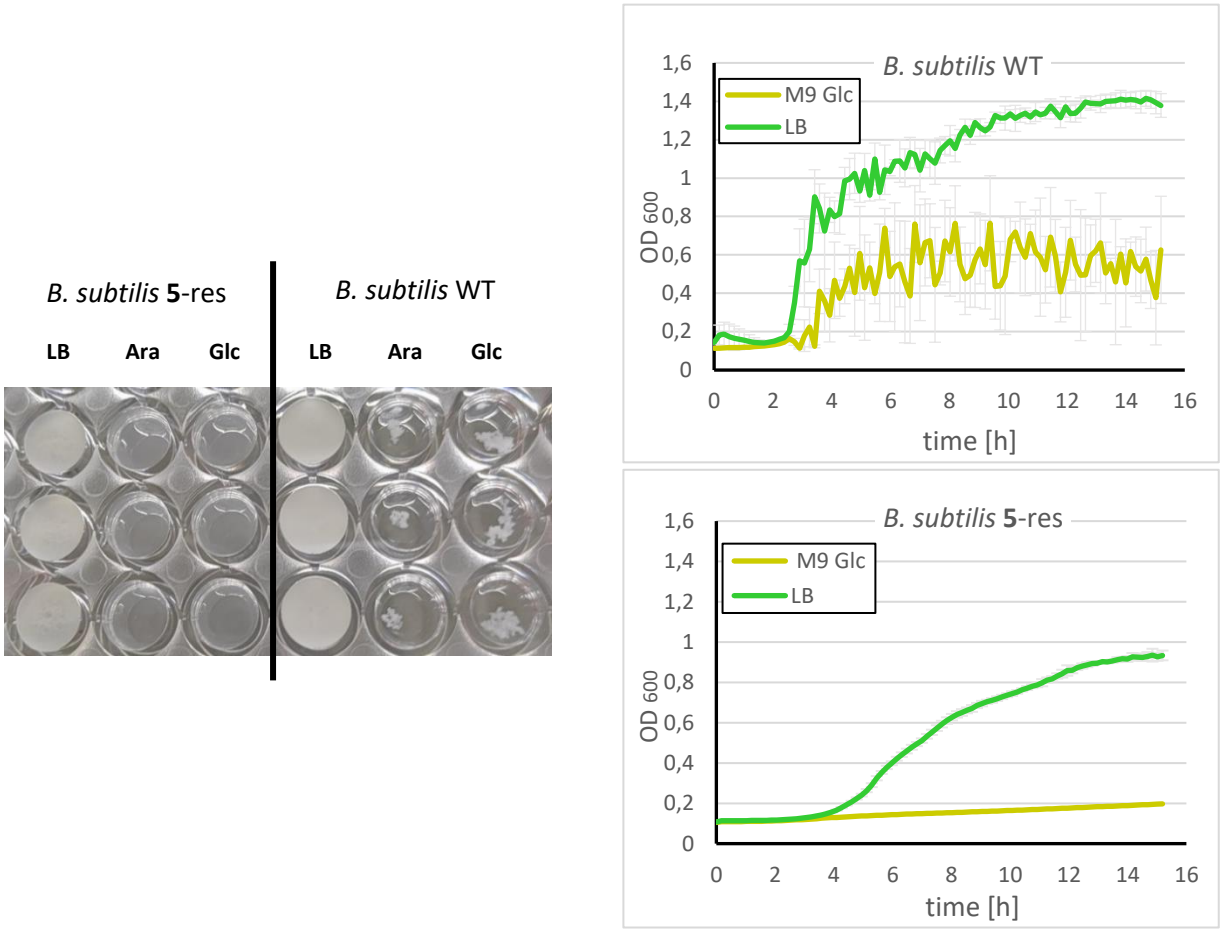

Figure 30: Growth experiments monitoring the OD_{600} of *B. subtilis* wild type (WT) and *B. subtilis* 5 res over time at 30°C. Measurements were done in triplicates. Respective growth curves for growth on LB (green) and minimal medium (M9 + 0.4 % Glucose (Glc)) (yellow) are depicted right. Left, the growth was also monitored with Arabinose (Ara) as a carbon source. *B. subtilis* wild type was forming biofilms during growth, which made measurements of OD values difficult. The respective error bars represent the standard deviation of three replicates. *B. subtilis* 5 res was not able to grow on glucose as sole carbon source.

Furthermore, Mund et al. [170] proposed that the carba-glucosamine is also efficiently converted to carbocyclic peptidoglycan nucleotides *in vivo*, such as UDP-carba-D-N-acetylglucosamine and UDP-carba-D-N-acetylmuramic acid-pentapeptide, which are interfering with biosynthetic enzyme functions. This adds another layer to the antibiotic effect. If that is also the case for our thia-GlcN6P **4** must be tested and further studies would be necessary in order to clarify the exact mode of action of the observed antibiotic activity.

5.3 Conclusion

Within this chapter, we investigated the ligand-dependent self-cleavage of a 5'-^{32}P-labeled *glmS* ribozyme from *B. subtilis* by newly synthesized compounds by the Wittmann group [66b]. The results demonstrated that *(R)*-**2**, *(S)*-**2**, and **4** efficiently prompted ribozyme cleavage at a concentration of 1 mM. Further kinetic measurements were conducted to assess the efficiency of cleavage activation. Interestingly, the hydroxy- and fluorophosphonates *(R)*-**2**, *(S)*-**2**, *(R)*-**3**,

and *(S)*-**3** all exhibited lower activity compared to the natural ligand GlcN6P, suggesting that the pK_a value of phosphonate derivatives is not as critical as previously assumed for inducing riboswitch self-cleavage. Thia-GlcN6P **4**, however, demonstrated nearly identical rate constants to GlcN6P, establishing it as a highly potent mimic of the natural ligand *in vitro*. The same efficiency could also be shown for other *glmS* ribozyme originating from *L. monocytogenes* and *C difficile*.

Moreover, also the antimicrobial activity of these GlcN6P mimics was investigated using their unphosphorylated derivatives, which are required for efficient uptake by the bacteria. Thia-GlcN **5** displayed growth inhibition of almost every *glmS* ribozyme containing strain tested, indicating its effectiveness against various gram-positive bacteria (MIC of 2 mM towards *B. subtilis* and 5 mM towards *B. thuringiensis*), including human pathogens as *S. aureus*. To gain further insights into the mode of action of this compound, we evolved a thia-GlcN **5** resistant strain (*B. subtilis* 5-res). Due to a deletion in the *ptsH* gene, causing a frameshift, the PTS responsible for sugar uptake was affected. This also prevents the *B. subtilis* 5-res bacteria from growing on glucose as a sole carbon source. Although this finding does not reveal the exact mechanism how the thia-GlcN **5** is interfering with the bacterial metabolism, this data confirms the uptake of thia-GlcN **5** and unveil a starting point for further investigations.

Taken together, the observed antimicrobial effects, especially the promising activity of thia-GlcN6P **4**, suggest its potential to study the pathogenicity of various bacteria. However, future studies, including transcriptome analysis and investigations into the exact mode of action, are required to understand and further harness the antimicrobial properties of these compounds.

6. Conclusion and future prospects

This thesis contributes to the diversification of self-cleaving ribozymes for aptazyme design, focusing on small (<100 nt) and independently self-cleaving ribozymes. Generally, it is evident that employing artificial riboswitches, as simple aptamers controlling the accessibility of regulatory sequences or within more intricate systems such as allosteric ribozymes, provides a flexible and widely applicable mechanism for regulating gene expression at the level of RNA. This can be useful for basic research as specific knockdown or overexpression of a gene can lead to severe side effects interfering with cell viability. Artificial riboswitches offer a way to exert precise temporal and spatial control over gene expression. This can also be exploited for therapeutic applications where dose-dependent expression of transgenes enables a fine-tuned regulation.

Within this work, we could provide an overview to expand the repertoire of self-cleaving ribozymes suitable for aptazyme design, with the HDV ribozyme standing out as a potent candidate. This serves as a starting point for further studies to investigate more parameters than positioning in the 3'-UTR to integrate self-cleaving RNAs into the mammalian cell context. Moreover, the different ribozyme classes have to be screened for optimized structures that prove to be more efficient in human cells, as they provide suitable properties for aptazyme design, such as the TS-ribozyme class. However, as for the HDV ribozyme, challenges in achieving robust ON-switches highlight the complexity of designing aptazymes within the constraints of stable ribozyme structures. Using screening-based methods, as done by Strobel et al. [96c], the obtained switches could be further improved. Nevertheless, the findings within Chapter II provide valuable insights for future efforts in developing efficient aptazymes for diverse applications, emphasizing the need for innovative design strategies.

The primary objective of further development of synthetic riboswitches should not only be the achievement of higher dynamic ranges. Rather, the next step is the implementation of the switches in functional contexts, controlling therapeutically relevant genes such as interleukins and test their transferability. The reporter assays used in this work provide a highly sensitive way to monitor gene expression levels. In nature, by employing weaker promotors or other regulation factors, already slight induction of gene expression can be sufficient to induce a distinct change in phenotype and a minor leaky basal expression could be negligible.

The herein, newly adapted splice cassette poses a convenient strategy for integration in a variety of genetic contexts. Although the generated switches do not yet have a wide dynamic range, the use of these for different genes is a first indication of the adaptability of this design. Since splicing efficiency varies between different organisms and is known to be even tissue-specific [171], it has to be further investigated if this system is also functional in other cell types.

However, the basic principle of the switch should be applicable in all mammalian cells. As we were able to show, it can be used to control two different elements (uORFs and ribozymes) and there is plenty of potential for adaptation and improvement. In addition, our knowledge of splicing events in the 5' UTR is constantly increasing. New insights could make the switches developed here even more efficient. Thus, these switches represent a foundation for universal and robust splice designs.

Besides, one obstacle to synthetic riboswitches is the lack of suitable aptamer-ligand pairs. The choice of efficient ligands is very limited. Many of them are toxic in high concentrations, are directly metabolised by the cell or even occur naturally *in vivo* in significant amounts. This can cause unwanted side effects. Therefore, the development of new aptamer-ligand pairs that can be used efficiently in the areas presented here must be a concern in the future. This could further diversify the switches developed in this thesis.

Overall, artificial riboswitches continue to develop from fundamental proof-of-principle studies to more applied research within humans and other higher organisms. In conclusion, engineered catalytic RNAs will serve as universally applicable tools and specific targets for gene regulation in future applications.

7. Materials and methods

7.1 Methods

Plasmid construction

Sequences up to 80 nt were introduced via PCR with overhang primers containing a phosphorylated 5'-end into a psiCHECK-2 vector (Promega) carrying two luciferase genes, the Renilla (hRLuc) and Firefly luciferase (hluc+). Larger sequences were introduced via Gibson Assembly®. The Phusion Plus DNA Polymerase protocol (Thermo Fischer) was used for PCR. The PCR product was digested with DpnI (NEB) to get rid of the template plasmid and purified by gel electrophoresis. Recovery was done with the Zymoclean Gel DNA Recovery Kit. After ligation with Quick Ligase (NEB), or a Gibson assembly (NEB), the product was transformed into the XL10-Gold Escherichia coli strain (Stratagene). Individual colonies were verified to contain the correct sequence by Sanger sequencing at Eurofins Genomics/GATC Biotech or Azenta Genewiz. Sequences used are listed in Supplementary Table 1-3 and Supplementary Figure 4.

Agarose gel electrophoresis

Agarose gel electrophoresis was used for PCR products either for monitoring or DNA-purification. Depending on the size of the DNA fragments agarose concentrations ranged from 0.8 to 2.0 % in 0.5x TBE buffer (40 mL gel). 1 µL of Midori Green Advanced (NIPPON Genetics) was added to visualize the bands under UV light. Samples were loaded with agarose loading dye and a DNA ladder of a corresponding size was included. Gels were run in 0.5x TBE buffer at 140 V for 35 minutes. The gel was analyzed using the Gel documentation device Biometra GelDoc under UV light.

Cell cultivation and transfection

HeLa cells (ATCC, cat. no. ATCC-CCL-2) were cultured in Dulbecco's modified Eagle's medium (DMEM) + GlutaMAX-I + 10 % foetal calf serum (Gibco/Thermo Fisher Scientific). The medium was supplemented with 1 % Penicillin/Streptomycin. The cells were cultivated at 37°C and with 5 % CO2. Prior to transfection, within a 96-well plate the HeLa cells were seeded out to 8.000 cells/well to achieve a confluency of ~ 70 % after 24 h. Transfection was conducted using Lipofectamine 3000 (Invitrogen) according to the manufacturer's protocol. After 4 h at 37°C, the medium was exchanged with medium containing the respective ligand concentrations, and after 20 h, the Dual-Luciferase Reporter Assay (Promega) was performed. Since the ribozymes and riboswitches only interfere with hRLuc expression and consequently its activity, the hLuc+ is used as an internal control. For each construct, the ratio of hLuc+ and hRLuc is calculated and normalized to the respective activity of the empty psiCHECK-2 plasmid (without any ribozyme or riboswitch) with full expression of both luciferases. For

constructs affecting the hLuc+ the procedure is conducted *vice versa*. Measurements were performed with Spark® multimode microplate reader (Tecan) with a settle time of 0 ms and an integration time of 2000 ms. If not stated otherwise, all constructs were measured in technical triplicates in at least three independent experiments.

Concerning the eGFP-based screen, the cells were treated as described above, before and during transfection. After exchanging the medium the cells were kept at 37°C for 48 h prior to the measurement. After washing with 1× PBS the fluorescence was measured with Spark® multimode microplate reader (Tecan) using the Top reading. The eGFP (478 nm/524 nm) fluorescence was normalized on mCherry (568 nm/620 nm) fluorescence. Thereby the relative eGFP levels were obtained. All constructs were measured in technical triplicates in at least three independent experiments.

Reverse transcription-PCR

HeLa cells (ATCC, cat. no. ATCC-CCL-2) were cultured in Dulbecco's modified Eagle's medium (DMEM) + GlutaMAX-I + 10 % foetal calf serum (Gibco/Thermo Fisher Scientific). The medium was supplemented with 1 % Penicillin/Streptomycin. The cells were cultivated at 37°C and with 5 % CO2. Prior to transfection, within a 12-well plate the HeLa cells were seeded out to 80.000 cells/well to achieve a confluency of ~ 70 % after 24 h. Transfection was conducted using Lipofectamine 3000 (Invitrogen) according to the manufacturer's protocol. After 4 h at 37°C, the medium was exchanged with medium containing the respective ligand concentration, and after 20 h the cells were harvested and lysed. Using the Quick-RNA™ Miniprep Kit (Zymo Research) according to manufacturer's protocol the RNA from the cell of each sample was isolated and eluted in 56 µL of ultra purified H_2O. Afterward the RNA concentrations were measured to check if RNA was eluted efficiently. As a next step, remaining DNA was digested using the DNase I (RNase-free) (NEB) in rCutSmart™ Buffer (NEB) inserting the whole RNA sample. After 1 h incubation at 37°C the RNA was purified using RNA Clean & Concentrator Kit (Zymo Research) according to manufacturer's protocols. The pure RNA was eluted in 25 µL of ultra purified H_2O and RNA concentration were measured. For reverse transcription the High-Capacity cDNA Reverse Transcription Kit (Thermo Fischer Scientific) was used according to manufacturer's protocols, inserting 2 µg of inserted RNA in each sample. For construct affecting the hRLuc the following primers were used: (fw: 5'-CTGACACAACAGTCTCGAACTTAAG -3') and (rv: 5'-TCGGCGTGCTTCTCGGAATC-3') For construct affecting the hLuc+ the following primers were used: (fw: 5'-GCTTGGCATTCCGGTACTG-3') and (rv: 5'-GTTCTCAGAGCACACCACGA-3').

Preparation of *glmS* RNA

The *glmS*-ribozyme was amplified from genomic DNA of B. subtilis by PCR using Phusion Plus DNA-Polymerase (Thermo Fischer). A T7 Promotor was introduced upstream using the following primers for amplification (fw: 5'-TAATACGACTCACTATAGGCCTATAATT-ATAGCGCC-3') and (rv: 5'-AAGATCATGTGATTTCTC-3'). The PCR product was purified by DNA Clean & Concentrator kit (Zymo) according to manufacturers protocol. For *in vitro* transcription (37 °C, 3 h) with T7 RNA-polymerase 1 µg of DNA was used in 80 mM HEPES, 4 mM spermidine, 40 mM dithiothreitol (DTT), 24 mM $MgCl_2$ (pH7.5). The resulting RNA product was purified by denaturing polyacrylamide gel electrophoresis (PAGE). After gel extraction in 10 mM HEPES 200 NaCl, 1 mM EDTA (pH7.5) and filtering through glass whool, the RNA was precipitated adding 3 volumes ice cold EtOH (100 %) (-80 °C, o/n). After centrifugation the pellet was washed with ice cold EtOH (70 %). The purified RNA was dephosphorylated using recombinant shrimp alkaline phosphatase (rSAP, NEB) in 50 mM KOAc, 20 mM HEPES, 10 mM Mg(OAc)2, 100 µg mL-1 BSA (pH 7.9). After heat inactivation of the enzyme (3 min, 75°C), the RNA was radioactively labelled with γ-^{32}P-ATP (10 mCi mL^{-1}, Hartmann Analytics) at the 5'-end using the T4 polynucleotide kinase (PNK, NEB) in 70 mM HEPES, 10 mM MgCl2 and 5 mM DTT (pH 7.6). All mixtures were prepared on ice, and incubated at 37 °C for 45 min. The product was again purified by Urea-PAGE followed by gel extraction and precipitation (-80 °C, 1h). For *C. difficile* and *L. monocytogenes* the experiments were conducted the same. For them, a T7 Promotor was introduced upstream using the following primers for amplification *C. difficile*: (fw: 5'-TCGTAATACGACTCACTATAGGTTTAA-AGGGTATTCTC-3') and (rv: 5'-TAGGTCATATAAGTTTACTTTGGCTTCCC-3') and *L. monocytogenes:* (fw: 5'-TCGTAATACGACTCACTATAGGTCAGCTCGCTCCTTTTTGTATC-3') and (rv: 5'-AGTAAAACTCCT-CCAATAATTAACTTGAGGGC-3'), respectively.

Kinetic self-cleavage assay

The purified radioactively labelled RNA was dissolved in ultrapurified H_2O. From here, all steps were conducted on ice. The reaction buffer (50 mM HEPES (pH 7.5), 200 mM KCl and 10 mM $MgCl_2$) was mixed with the respective compounds to result in different concentrations (10 µM, 200 µM, 500 µM, 1 mM). After RNA addition the reaction was incubated at 37 °C. The cleavage reaction was stopped at different time points (5-300 s) adding PAGE loading dye (9 M Urea, 20 % w/v Sucrose, 0.1 % w/v SDS, 0.05 % w/v bromophenol blue, 0.05 % w/v xylene cyanol, 90 mM Tris-HCl, 90 mM Borate, 1 mM EDTA). Samples were stored at -20 °C until they were analysed on a 10 % Urea-PAGE (40 W, 30 min). The respective bands were detected using Typhoon FLA 7000 phosphorimager (GE Healthcare Bio-Sciences AB). Data analysis was done using ImageJ and the Prism (GraphPad) software. The rate constants (k_{obs}) were determined by plotting the fraction cleaved in dependence of time and the resulting curves were obtained using a pseudo-first order association kinetic fit. The compound taken

for testing were synthesized by the Wittmann group [66b], a set of C7 phosphonate derivatives: difluoro (**1**) (Mw: 327 g/mol) (2x NH_3 salt), hydroxy ((R)-**2** and (S)-**2**) (Mw: 475 g/mol) (2x NEt_3 salt), and monofluoro substitution ((R)-**3** and (S)-**3**) (Mw: 309 g/mol) (2x NH_3 salt) and the thia-GlcN6P (**4**) (Mw: 525 g/mol) (2x NEt_3 salt).

Filter disk assay and MIC determination

B. subtilis wt168 and *B. thuringiensis* were plated out from an overnight culture on Mueller-Hinton Agar plates containing 5 % sheep blood. Filters were saturated with 10 µL of different compound solutions. As a positive control, chloramphenicol (1 mg/mL) was used. The respective compounds were tested in concentrations of either 100 mM for *B. subtilis* or 500 mM for *B. thuringiensis*. Filters were left to dry for 10 min at RT before placing them on the plates. Incubation was done at 37 °C overnight. Subsequently, the diameter of the inhibition zones was measured and compared. For MIC determination a single colony from an LB agar plate (grown at 37°C o/n) was used to inoculate 5 mL of LB medium and incubated o/n. This culture was used to inoculate LB medium to an OD_{600} of 0.05 containing a dilution series of the potential antibiotic in a 96-deep-well plate format. A sterile control was included adding only medium as well as a growth control without any antibiotic. As a positive control, a dilution series of chloramphenicol was prepared. After incubation o/n at 37 °C, the MIC was determined as lowest concentration of the respectively added compounds, inhibiting bacterial growth. Lack of growth was checked by turbidity of the medium by eye.

Genome sequencing

A liquid culture in LB-medium of the wild type *B. subtilis* was set to an OD600 of 0.05. The medium also contained 1.5 mM thia-GlcN6P 4**.** After growth for 24 h at 37 °C the liquid culture was diluted again to an OD600 of 0.05, simultaneously the thia-GlcN6P **4** concentration was slightly increased. After several days of subsequent increase, the medium containing 50 mM of thia-GlcN6P **4** was plated out on an LB agar plate. A single colony was picked, cultivated and the genomic DNA was isolated using DNeasy Blood & Tissue Kit (Quiagen) according to manufacturer's protocol. Samples were send for genome sequencing (Novogene).

Cultivation of bacteria and growth experiments

A single colony of the wild type strain and *B. subtilis* 11-res was used respectively to inoculate fresh LB medium. The liquid culture was grown over night. In a 96-deep well plate within 1 mL of M9 minimal medium containing glucose (22 mM) as a sole carbon source and 1 % LB medium, the OD600 was set to 0.1. The growth in minimal medium and full medium (LB) was recorded for 18 h at 30°C using the TECAN. Each condition was tested in triplicates.

7.2 Materials

Additional buffers, solutions and media

Table 2: List of additional buffers, solutions and media used in this project.

Name	Composition
1x PBS (pH 7.4)	137 mM NaCl, 2.7 mM KCl, 4.3 mM Na_2HPO_4* $2H_2O$, 1.47 mM KH_2PO_4
5x TBE buffer (pH 8.3)	54 g/L Tris base, 27.5 g/L boric acid, 10 mM EDTA
LB medium	5 g/L NaCl, 5 g/L yeast extract, 10 g/L tryptone, pH 7.0
LB-Carb	LB medium, 100 µg/mL carbenicilline
Brain Heart Infusion (BHI) medium	(Sigma Aldrich/Merck) 37.5 g/L
M9 minimal medium	8.5 g/L $NaHPO_4$*$2H_2O$, 3 g/L KH_2PO_4, 0.5 g/L NaCl, 1 g/L NH_4Cl, 1 mM $MgSO_4$*$7H_2O$, 100 µM $CaCl_2$, 1 mL/L Vitamin solution
SOC (super optimal broth with catabolite repression) medium	2 % (w/v) tryptone, 0.5 % yeast extract, 0.05 % (w/v) NaCl, 10 mM $MgCl_2$, 10 mM $MgSO_4$ x 7 H2O, 20 mM glucose

Chemicals

Table 3: List of used chemicals

Name	Company
Carbenicillin	Roth
Streptomycin/Penicillin (10000 U/mL)	Fisher Scientific
Tetracycline	Merck
dNTPs	Fermentas
Oligonucleotides	Merck
Lipofectamine™ 3000/P3000™	Fisher Scientific
Gibco Dulbecco's Modified Eagle Medium (DMEM)	Fisher Scientific
Fetal calf serum (FCS)	Fisher Scientific
Opti-Mem®	Fisher Scientific
Midori Green Advanced	Nippon Genetics Europe
6x Gel Loading Dye	New England Biolabs
Gene RulerDNA ladder (100bp, 1kb)	Fisher Scientific
Agarose Standard	Roth
Glucosamine-6-phosphate	Merck
Glucosamine	Merck
5-Thioglucose	Merck
Blood-agar plates (sheep-blood)	Fisher Scientific

Gadgets and equipment

Table 4: List of gadgets and equipment

Name	Company
Inkubator 1000 Titramax 1000	Heidolph
Thermocylcer	Biometra
Agarose gel electrophoresis systems	BioRad
Gel documentation device Biometra GelDoc	Biometra
Spark® multimode microplate reader	Tecan
Nanodrop plate Tecan NanoQuant	Tecan
P-87 micropipette Puller	Sutter Instrument Co.
Laboratory Pipettes	Eppendorf
Table top centrifuge mini spin	Eppendorf
Bright-field microscope	Olympus SZ51
Electroporation 2510device	Eppendorf
Thermomixer comfort	Eppendorf
Eppendorf Centrifuge 5810R, refrigerated	Eppendorf
Eppendorf Centrifuge 5417R, refrigerated tabletop	Eppendorf
RNA gel electrophoresis system	Biometra
Gel dryer	Bio Rad
Typhoon FLA 7000 phosphorimager	GE Healthcare Bio-Sciences

Disposables

Table 5: List of disposables

Name	Company
Reaction tubes (1.5, 2 mL)	Sarstedt
PCR tubes	Thermo Scientific
Falcon tubes (15, 50 mL)	BD Biosciences
96-well plates flat bottom transparent polystyrene	BD Biosciences
96- well micro-titer plates, half-area, black polystyrene	Costar
96 deep well plates	Sarstedt
Pipette tips (10, 200, 1000 µL)	Sarstedt
Electroporation cuvettes 1 mm	Roth
Sterilizing filters	Sarstedt

List of strains

Escherichia coli XL 10 Gold (Stratagene) strain was used for plasmid expression;

Genotype: Tet^rΔ(mcrA)183;Δ(mcrCB-hsdSMR-mrr)173; endA1;supE44; thi-1 recA1; gyrA96; relA1; lac; Hte [F′; proAB; $lacI^q$ZΔM15;Tn10;(Tet^r); Amy; Cam^r].

H. sapiens HeLa cells were used for cell culture experiments

Used for filter disk assays:

Escherichia coli K12 MG1655 strain

Genotype: F- λ- ilvG- rfb-50 rph-1

Bacillus subtilis wt 168 strain (generated AG Chr. Mayer, Uni Tübingen)

B. subtilis **5**-res: derived from *Bacillus subtilis* wt 168 strain

Genotype: *ptsH* p. Asn43fs

Bacillus thuringiensis subsp. finitimus YBT-020 (BGSC)

Staphylococcus aureus Oxford H (Rosenbach 1884) DSM No.: 683

Staphylococcus aureus NRL05/507 (Rosenbach 1884) DSM No.: 19041

Staphylococcus cohnii GH 137 (Schleifer and Kloos 1975) DSM No.: 20260

Deinococcus radiodurans R_1 (Brooks and Murray 1981) DSM No.: 20539

Enterococcus faecalis Tissier NCTC 775 (ATCC) DSM No.: 20478

Enterococcus hirae (Farrow and Collins 1985) DSM No.:20160

8. List of Abbreviations

°C	degree Celsius
bp	base pair
CPEB3	cytoplasmic polyadenylation element binding protein
DNA	deoxyribonucleic acid
dNTP	deoxynucleotide
EC50	half maximal effective concentration
eGFP	enhanced green fluorescent protein
K_D	dissociation constant
L	litre
LB	lysogeny broth
M	molar
mCi	millicurie
Mg	magnesium
mg	milligram
min	minute
mL	millilitre
mM	millimolar
Mn	manganese
ng	nanogram
nm	nanometer
nt	nucleotides
NTP	ribonucleotide
OD600	optical density measured at 600 nm
PBS	phosphate-buffered saline
PCR	polymerase chain reaction
pre-mRNA	precursor messenger RNA
RNA	ribonucleic acid
RNase	ribonuclease
rpm	rotations per minute
S	Svedberg unit
s	seconds
t	time
TBE	Tris-borate-EDTA-buffer
Tet	tetracycline
U	units
V	volt
w/v	weight per volume
wt	wild type
µg	microgram
µL	microlitre
µm	micrometre

9. References

[1] D. Kläge, E. Müller, J. S. Hartig, *RNA biology* **2024**, *21*, 1-11.

[2] M. S. Marek, A. Johnson-Buck, N. G. Walter, *Physical Chemistry Chemical Physics* **2011**, *13*, 11524-11537.

[3] M. Cobb, *PLOS Biology* **2017**, *15*, e2003243.

[4] A. Rich, D. R. Davies, *Journal of the American Chemical Society* **1956**, *78*, 3548-3549.

[5] P. Cramer, D. A. Bushnell, R. D. Kornberg, *Science* **2001**, *292*, 1863-1876.

[6] T. R. Cech, A. J. Zaug, P. J. Grabowski, *Cell* **1981**, *27*, 487-496.

[7] J. K. Wickiser, W. C. Winkler, R. R. Breaker, D. M. Crothers, *Molecular Cell* **2005**, *18*, 49-60.

[8] D. M. Lilley, *Philosophical transactions of the Royal Society of London. Series B, Biological sciences* **2011**, *366*, 2910-2917.

[9] N. Sanchez de Groot, A. Armaos, R. Graña-Montes, M. Alriquet, G. Calloni, R. M. Vabulas, G. G. Tartaglia, *Nature Communications* **2019**, *10*, 3246.

[10] S. V. Solomatin, M. Greenfeld, S. Chu, D. Herschlag, *Nature* **2010**, *463*, 681-684.

[11] Y. T. Vandenhoogen, C. Erkelens, E. Devroom, G. A. Vandermarel, J. H. Vanboom, C. Altona, *Eur J Biochem* **1988**, *173*, 295-303.

[12] J. Houseley, D. Tollervey, *Cell* **2009**, *136*, 763-776.

[13] T. Maniatis, R. Reed, *Nature* **1987**, *325*, 673-678.

[14] W.-Y. Zhou, Z.-R. Cai, J. Liu, D.-S. Wang, H.-Q. Ju, R.-H. Xu, *Molecular Cancer* **2020**, *19*, 172.

[15] E. C. Merkhofer, P. Hu, T. L. Johnson, *Methods in molecular biology (Clifton, N.J.)* **2014**, *1126*, 83-96.

[16] Y. Lee, D. C. Rio, *Annu Rev Biochem* **2015**, *84*, 291-323.

[17] N. H. Gehring, J.-Y. Roignant, *Trends in Genetics* **2021**, *37*, 355-372.

[18] X. Roca, R. Sachidanandam, A. R. Krainer, *RNA* **2005**, *11*, 683-698.

[19] Z. Wang, C. B. Burge, *RNA* **2008**, *14*, 802-813.

[20] Q. Pan, O. Shai, L. J. Lee, B. J. Frey, B. J. Blencowe, *Nature Genetics* **2008**, *40*, 1413-1415.

[21] C. Cenik, A. Derti, J. C. Mellor, G. F. Berriz, F. P. Roth, *Genome Biology* **2010**, *11*, R29.

[22] aB. Raj, D. O'Hanlon, J. P. Vessey, Q. Pan, D. Ray, N. J. Buckley, F. D. Miller, B. J. Blencowe, *Mol Cell* **2011**, *43*, 843-850; bM. Quesnel-Vallières, M. Irimia, S. P. Cordes, B. J. Blencowe, *Genes & development* **2015**, *29*, 746-759.

[23] aY. Mayshar, E. Rom, I. Chumakov, A. Kronman, A. Yayon, N. Benvenisty, *Stem cells (Dayton, Ohio)* **2008**, *26*, 767-774; bT. Zhang, Y. Lin, J. Liu, Z. G. Zhang, W. Fu, L. Y. Guo, L. Pan, X. Kong, M. K. Zhang, Y. H. Lu, Z. R. Huang, Q. Xie, W. H. Li, X. Q. Xu, *Stem cells (Dayton, Ohio)* **2016**, *34*, 1776-1789.

[24] J. Tazi, N. Bakkour, S. Stamm, *Biochimica et Biophysica Acta (BBA) - Molecular Basis of Disease* **2009**, *1792*, 14-26.

[25] J. Sperling, M. Azubel, R. Sperling, *Structure* **2008**, *16*, 1605-1615.

[26] A. Ramanathan, G. B. Robb, S.-H. Chan, *Nucleic acids research* **2016**, *44*, 7511-7526.

[27] M. Pabis, N. Neufeld, M. C. Steiner, T. Bojic, Y. Shav-Tal, K. M. Neugebauer, *RNA* **2013**, *19*, 1054-1063.

[28] S. M. Flaherty, P. Fortes, E. Izaurralde, I. W. Mattaj, G. M. Gilmartin, *Proceedings of the National Academy of Sciences of the United States of America* **1997**, *94*, 11893-11898.

[29] P. R. Andersen, M. Domanski, M. S. Kristiansen, H. Storvall, E. Ntini, C. Verheggen, A. Schein, J. Bunkenborg, I. Poser, M. Hallais, R. Sandberg, A. Hyman, J. LaCava, M. P. Rout, J. S. Andersen, E. Bertrand, T. H. Jensen, *Nature structural & molecular biology* **2013**, *20*, 1367-1376.

[30] L. A. Passmore, J. Coller, *Nature reviews. Molecular cell biology* **2022**, *23*, 93-106.

[31] Y. Xie, Y. Ren, *Traffic (Copenhagen, Denmark)* **2019**, *20*, 829-840.

[32] T. V. Pestova, V. G. Kolupaeva, I. B. Lomakin, E. V. Pilipenko, I. N. Shatsky, V. I. Agol, C. U. T. Hellen, *Proceedings of the National Academy of Sciences* **2001**, *98*, 7029-7036.

[33] F. Mignone, C. Gissi, S. Liuni, G. Pesole, *Genome Biology* **2002**, *3*, reviews0004.0001.

[34] K. Leppek, R. Das, M. Barna, *Nature reviews. Molecular cell biology* **2018**, *19*, 158-174.

[35] J. R. Babendure, J. L. Babendure, J. H. Ding, R. Y. Tsien, *RNA* **2006**, *12*, 851-861.
[36] R. Hänsel-Hertsch, M. Di Antonio, S. Balasubramanian, *Nature reviews. Molecular cell biology* **2017**, *18*, 279-284.
[37] R. Marques, R. Lacerda, L. Romão, *Biomedicines* **2022**, *10*.
[38] aS. E. Calvo, D. J. Pagliarini, V. K. Mootha, *Proceedings of the National Academy of Sciences of the United States of America* **2009**, *106*, 7507-7512; bC. Barbosa, I. Peixeiro, L. Romão, *PLoS genetics* **2013**, *9*, e1003529.
[39] C.-Y. A. Chen, A.-B. Shyu, *Trends in Biochemical Sciences* **1995**, *20*, 465-470.
[40] aE. Eden, S. Brunak, *Nucleic acids research* **2004**, *32*, 1131-1142; bG. M. Wilson, Y. Sun, J. Sellers, H. Lu, N. Penkar, G. Dillard, G. Brewer, *Molecular and cellular biology* **1999**, *19*, 4056-4064.
[41] aS. N. Floor, J. A. Doudna, *eLife* **2016**, *5*, e10921; bA. Zhiwei, E. H. Katharina, D. Manuel Torres, S. Carolin, Z. Sisi, X. Feng, D. F. Catherine, P. L. Joseph, Y. Y. Scarlet, A. Mukta, P. Vinodh, C. Emeline, M. L. Marilyn, K. T. Sarah, B. Yoseph, J. S. Stephen, T.-T. Andrei, *bioRxiv* **2023**, 2023.2002.2019.529123.
[42] D. Hong, S. Jeong, *Molecules and cells* **2023**, *46*, 48-56.
[43] aD. G. Scofield, X. Hong, M. Lynch, *Molecular Biology and Evolution* **2007**, *24*, 896-899; bY.-F. Chang, J. S. Imam, M. F. Wilkinson, *Annual Review of Biochemistry* **2007**, *76*, 51-74.
[44] M. Preussner, Q. Gao, E. Morrison, O. Herdt, F. Finkernagel, M. Schumann, E. Krause, C. Freund, W. Chen, F. Heyd, *Genome Biology* **2020**, *21*, 186.
[45] C. E. Weinberg, Z. Weinberg, C. Hammann, *Nucleic Acids Res* **2019**, *47*, 9480-9494.
[46] aR. M. Jimenez, J. A. Polanco, A. Lupták, *Trends in Biochemical Sciences* **2015**, *40*, 648-661; bH. Peng, B. Latifi, S. Müller, A. Lupták, I. A. Chen, *RSC Chemical Biology* **2021**, *2*, 1370-1383; cY. Chen, F. Qi, F. Gao, H. F. Cao, D. Y. Xu, K. Salehi-Ashtiani, P. Kapranov, *Nature Chemical Biology* **2021**, *17*, 601-607.
[47] aG. A. Prody, J. T. Bakos, J. M. Buzayan, I. R. Schneider, G. Bruening, *Science* **1986**, *231*, 1577-1580; bA. C. Forster, R. H. Symons, **1987**, *50*, 9-16.
[48] J. M. Buzayan, W. L. Gerlach, G. Bruening, *Proceedings of the National Academy of Sciences* **1986**, *83*, 8859-8862.
[49] L. Sharmeen, M. Y. Kuo, G. Dinter-Gottlieb, J. Taylor, *Journal of Virology* **1988**, *62*, 2674-2679.
[50] B. J. Saville, R. A. Collins, *Cell* **1990**, *61*, 685-696.
[51] J. E. Barrick, K. A. Corbino, W. C. Winkler, A. Nahvi, M. Mandal, J. Collins, M. Lee, A. Roth, N. Sudarsan, I. Jona, J. K. Wickiser, R. R. Breaker, *Proceedings of the National Academy of Sciences* **2004**, *101*, 6421-6426.
[52] N. G. Kolev, E. I. Hartland, P. W. Huber, *Nucleic Acids Res* **2008**, *36*, 5530-5539.
[53] A. Roth, Z. Weinberg, A. G. Y. Chen, P. B. Kim, T. D. Ames, R. R. Breaker, *Nature Chemical Biology* **2014**, *10*, 56-60.
[54] aZ. Weinberg, P. B. Kim, T. H. Chen, S. Li, K. A. Harris, C. E. Lünse, R. R. Breaker, *Nature Chemical Biology* **2015**, *11*, 606-610; bK. Beilstein, A. Wittmann, M. Grez, B. Suess, *ACS Synthetic Biology* **2015**, *4*, 526-534; cK. A. Harris, C. E. Lunse, S. Li, K. I. Brewer, R. R. Breaker, *Rna* **2015**, *21*, 1852-1858.
[55] A. J. Hernandez, A. Zovoilis, C. Cifuentes-Rojas, L. Han, B. Bujisic, J. T. Lee, *P Natl Acad Sci USA* **2020**, *117*, 415-425.
[56] aJ. Tang, R. R. Breaker, *Proc Natl Acad Sci U S A* **2000**, *97*, 5784-5789; bK. P. Williams, S. Ciafré, G. P. Tocchini-Valentini, *The EMBO Journal* **1995**, *14*, 4551-4557.
[57] M. D. Canny, F. M. Jucker, E. Kellogg, A. Khvorova, S. D. Jayasena, A. Pardi, *Journal of the American Chemical Society* **2004**, *126*, 10848-10849.
[58] M. Martick, W. G. Scott, *Cell* **2006**, *126*, 309-320.
[59] A. Ren, R. Micura, D. J. Patel, *Curr Opin Chem Biol* **2017**, *41*, 71-83.
[60] G. M. Emilsson, S. Nakamura, A. Roth, R. R. Breaker, *Rna* **2003**, *9*, 907-918.
[61] M. De La Peña, R. Ceprián, J. L. Casey, A. Cervera, *Virus Evolution* **2021**, *7*.
[62] aI. García-Robles, J. Sánchez-Navarro, M. De La Peña, **2012**, *393*; bK. Salehi-Ashtiani, A. Lupták, A. Litovchick, J. W. Szostak, *Science* **2006**, *313*, 1788-1792.

[63] aW. C. Winkler, A. Nahvi, A. Roth, J. A. Collins, R. R. Breaker, *Nature* **2004**, *428*, 281-286; bJ. A. Collins, I. Irnov, S. Baker, W. C. Winkler, *Genes & Development* **2007**, *21*, 3356-3368; cD. D. Seith, J. L. Bingaman, A. J. Veenis, A. C. Button, P. C. Bevilacqua, *ACS Catal* **2018**, *8*, 314-327.
[64] N. Pavlova, D. Kaloudas, R. Penchovsky, *Gene* **2019**, *708*, 38-48.
[65] aP. J. McCown, W. C. Winkler, R. R. Breaker, *Methods in molecular biology (Clifton, N.J.)* **2012**, *848*, 113-129; bP. J. McCown, A. Roth, R. R. Breaker, *RNA* **2011**, *17*, 728-736.
[66] aD. Matzner, A. Schuller, T. Seitz, V. Wittmann, G. Mayer, *Chem. Eur. J.* **2017**, *23*, 12604-12612; bB. Silkenath, D. Kläge, H. Altwein, N. Schmidhäuser, G. Mayer, J. S. Hartig, V. Wittmann, *ACS Chemical Biology* **2023**, *18*, 2324-2334; cC. E. Lünse, M. S. Schmidt, V. Wittmann, G. Mayer, *ACS Chem. Biol.* **2011**, *6*, 675-678.
[67] U. von Ahsen, J. Davies, R. Schroeder, *Nature* **1991**, *353*, 368-370.
[68] D. Alonso, A. Mondragón, *Biochemical Society transactions* **2021**, *49*, 1529-1535.
[69] W. Hong, J. Zeng, J. Xie, *Acta Pharmaceutica Sinica B* **2014**, *4*, 258-265.
[70] J. O'Neill, *Tackling Drug-Resistant Infections Globally: final report and recommendations*, The Review on Antimicrobial Resistance, http://amr-review.org, **2016**.
[71] aA. Ariza-Mateos, A. Nuthanakanti, A. Serganov, *Biochemistry (Moscow)* **2021**, *86*, 962-975; bS. Lotz Thea, B. Suess, *Microbiology Spectrum* **2018**, *6*, 10.1128/microbiolspec.rwr-0025-2018; cR. R. Breaker, *Cold Spring Harbor perspectives in biology* **2018**, *10*.
[72] aM. T. Cheah, A. Wachter, N. Sudarsan, R. R. Breaker, *Nature* **2007**, *447*, 497-500; bA. Wachter, M. Tunc-Ozdemir, B. C. Grove, P. J. Green, D. K. Shintani, R. R. Breaker, *The Plant cell* **2007**, *19*, 3437-3450.
[73] aA. V. Sherwood, T. M. Henkin, *Annual Review of Microbiology* **2016**, *70*, 361-374; bK. Kavita, R. R. Breaker, *Trends in Biochemical Sciences* **2023**, *48*, 119-141.
[74] aH. B. White, 3rd, *Journal of molecular evolution* **1976**, *7*, 101-104; bS. A. Benner, A. D. Ellington, A. Tauer, *Proceedings of the National Academy of Sciences of the United States of America* **1989**, *86*, 7054-7058.
[75] aW. Winkler, A. Nahvi, R. R. Breaker, *Nature* **2002**, *419*, 952-956; bA. Nahvi, N. Sudarsan, M. S. Ebert, X. Zou, K. L. Brown, R. R. Breaker, *Chemistry & Biology* **2002**, *9*, 1043-1049; cA. S. Mironov, I. Gusarov, R. Rafikov, L. E. Lopez, K. Shatalin, R. A. Kreneva, D. A. Perumov, E. Nudler, *Cell* **2002**, *111*, 747-756.
[76] A. D. Ellington, J. W. Szostak, *Nature* **1990**, *346*, 818-822.
[77] G. Werstuck, M. R. Green, *Science* **1998**, *282*, 296-298.
[78] aC. M. Connelly, T. Numata, R. E. Boer, M. H. Moon, R. S. Sinniah, J. J. Barchi, A. R. Ferré-D'Amaré, J. S. Schneekloth, *Nature Communications* **2019**, *10*, 1501; bL. A. Wurmthaler, M. Sack, K. Gense, J. S. Hartig, M. Gamerdinger, *Nature Communications* **2019**, *10*, 491; cB. Suess, K. D. Entian, P. Kötter, J. E. Weigand, *Methods in molecular biology (Clifton, N.J.)* **2012**, *824*, 381-391; dJ. A. Howe, L. Xiao, T. O. Fischmann, H. Wang, H. Tang, A. Villafania, R. Zhang, C. M. Barbieri, T. Roemer, *RNA biology* **2016**, *13*, 946-954.
[79] aH. G. Hwang, A. Milito, J. S. Yang, S. Jang, G. Y. Jung, *Metabolic engineering* **2023**, *75*, 143-152; bL.-B. Zhou, A.-P. Zeng, *ACS Synthetic Biology* **2015**, *4*, 1335-1340.
[80] aA. S. Khalil, J. J. Collins, *Nature reviews. Genetics* **2010**, *11*, 367-379; bG. E. Vezeau, L. R. Gadila, H. M. Salis, *Nature Communications* **2023**, *14*, 2416.
[81] aG. C. Zhong, H. M. Wang, W. H. He, Y. J. Li, H. H. Mou, Z. J. Tickner, M. H. Tran, T. L. Ou, Y. M. Yin, H. T. Diao, M. Farzan, *Nature Biotechnology* **2020**, *38*, 169-+; bZ. J. Tickner, M. Farzan, *Pharmaceuticals (Basel, Switzerland)* **2021**, *14*; cB. Strobel, M. J. Düchs, D. Blazevic, P. Rechtsteiner, C. Braun, K. S. Baum-Kroker, B. Schmid, T. Ciossek, D. Gottschling, J. S. Hartig, S. Kreuz, *ACS Synthetic Biology* **2020**, *9*, 1292-1305.
[82] aM. Spöring, R. Boneberg, J. S. Hartig, *ACS Synthetic Biology* **2020**, *9*, 3008-3018; bH. Mou, G. Zhong, M. R. Gardner, H. Wang, Y. W. Wang, D. Cheng, M. Farzan, *Molecular therapy : the journal of the American Society of Gene Therapy* **2018**, *26*, 1277-1286.
[83] aM. Y. Chou, S. C. Lin, K. Y. Chang, *RNA* **2010**, *16*, 1236-1244; bC. H. Yu, J. Luo, D. Iwata-Reuyl, R. C. Olsthoorn, *ACS Chem Biol* **2013**, *8*, 733-740.

[84] aJ. E. Weigand, B. Suess, *Nucleic acids research* **2007**, *35*, 4179-4185; bM. Finke, D. Brecht, J. Stifel, K. Gense, M. Gamerdinger, J. S. Hartig, *Nucleic acids research* **2021**, *49*, e71.
[85] J. E. Weigand, M. Sanchez, E. B. Gunnesch, S. Zeiher, R. Schroeder, B. Suess, *RNA* **2008**, *14*, 89-97.
[86] C. Lyu, I. M. Khan, Z. Wang, *Talanta* **2021**, *229*, 122274.
[87] F. Groher, C. Bofill-Bosch, C. Schneider, J. Braun, S. Jager, K. Geißler, K. Hamacher, B. Suess, *Nucleic acids research* **2018**, *46*, 2121-2132.
[88] C. Berens, A. Thain, R. Schroeder, *Bioorganic & Medicinal Chemistry* **2001**, *9*, 2549-2556.
[89] M. Müller, J. E. Weigand, O. Weichenrieder, B. Suess, *Nucleic acids research* **2006**, *34*, 2607-2617.
[90] M. Finke, **2021**.
[91] B. Suess, J. E. Weigand, *RNA biology* **2008**, *5*, 24-29.
[92] L. Yen, J. Svendsen, J.-S. Lee, J. T. Gray, M. Magnier, T. Baba, R. J. D'Amato, R. C. Mulligan, *Nature* **2004**, *431*, 471-476.
[93] Z. J. Tickner, M. Farzan, *Pharmaceuticals* **2021**, *14*, 554.
[94] J. Tang, R. R. Breaker, **1997**, *4*, 453-459.
[95] M. Wieland, J. S. Hartig, *Angew Chem Int Ed Engl* **2008**, *47*, 2604-2607.
[96] aP. Ceres, A. D. Garst, J. G. Marcano-Velázquez, R. T. Batey, *ACS Synthetic Biology* **2013**, *2*, 463-472; bJ. Stifel, M. Sporing, J. S. Hartig, *Synth Biol (Oxf)* **2019**, *4*, ysy022; cB. Strobel, M. Spöring, H. Klein, D. Blazevic, W. Rust, S. Sayols, J. S. Hartig, S. Kreuz, *Nature Communications* **2020**, *11*.
[97] aG. C. Zhong, H. M. Wang, C. C. Bailey, G. P. Gao, M. Farzan, *Elife* **2016**, *5*; bS. Ausländer, P. Ketzer, J. S. Hartig, *Molecular BioSystems* **2010**, *6*, 807-814.
[98] aJ. S. Xiang, M. Kaplan, P. Dykstra, M. Hinks, M. McKeague, C. D. Smolke, *Nature Communications* **2019**, *10*, 4327; bY. Y. Chen, M. C. Jensen, C. D. Smolke, *Proceedings of the National Academy of Sciences* **2010**, *107*, 8531-8536.
[99] aY. Nomura, L. Zhou, A. Miu, Y. Yokobayashi, **2013**, *2*, 684-689; bS. Kobori, Y. Nomura, A. Miu, Y. Yokobayashi, *Nucleic acids research* **2015**, *43*, e85-e85.
[100] aK. Mustafina, Y. Nomura, R. Rotrattanadumrong, Y. Yokobayashi, *Acs Synthetic Biology* **2021**, *10*, 2040-2048; bK. Fukunaga, V. Dhamodharan, N. Miyahira, Y. Nomura, K. Mustafina, Y. Oosumi, K. Takayama, A. Kanai, Y. Yokobayashi, *J Am Chem Soc* **2023**, *145*, 7820-7828.
[101] aK. Mustafina, K. Fukunaga, Y. Yokobayashi, *ACS Synthetic Biology* **2020**, *9*, 19-25; bM. Felletti, J. Stifel, L. A. Wurmthaler, S. Geiger, J. S. Hartig, *Nature Communications* **2016**, *7*.
[102] aP. Ketzer, S. F. Haas, S. Engelhardt, J. S. Hartig, D. M. Nettelbeck, *Nucleic Acids Res* **2012**, *40*, e167; bB. Strobel, B. Klauser, J. S. Hartig, T. Lamla, F. Gantner, S. Kreuz, *Mol Ther* **2015**, *23*, 1582-1591; cC. A. Reid, E. R. Nettesheim, T. B. Connor, D. M. Lipinski, *Sci Rep* **2018**, *8*, 11763.
[103] P. Ketzer, J. K. Kaufmann, S. Engelhardt, S. Bossow, C. von Kalle, J. S. Hartig, G. Ungerechts, D. M. Nettelbeck, *Proc Natl Acad Sci U S A* **2014**, *111*, E554-562.
[104] aE. R. Lee, J. L. Baker, Z. Weinberg, N. Sudarsan, R. R. Breaker, *Science* **2010**, *329*, 845-848; bS. S. S. Panchapakesan, R. R. Breaker, *Nature Chemical Biology* **2021**, *17*, 375-382.
[105] A. R. Ferre-D'Amare, *Q Rev Biophys* **2010**, *43*, 423-447.
[106] P. Y. Watson, M. J. Fedor, *Nature Structural & Molecular Biology* **2011**, *18*, 359-363.
[107] C. Mayr, *Annu Rev Genet* **2017**, *51*, 171-194.
[108] J. V. Coumans, D. Gau, A. Poljak, V. Wasinger, P. Roy, P. Moens, *Exp Cell Res* **2014**, *320*, 33-45.
[109] A. R. Ferre-D'Amare, K. Zhou, J. A. Doudna, *Nature* **1998**, *395*, 567-574.
[110] D. M. Chadalavada, A. L. Cerrone-Szakal, P. C. Bevilacqua, *Rna* **2007**, *13*, 2189-2201.
[111] Y. Lian, M. B. De Young, A. Siwkowski, A. Hampel, J. Rappaport, *Gene Ther* **1999**, *6*, 1114-1119.
[112] S. A. Kazakov, S. V. Balatskaya, B. H. Johnston, *Rna* **2006**, *12*, 446-456.
[113] M. J. Fedor, *Biochemistry* **1999**, *38*, 11040-11050.
[114] M. DeYoung, A. M. Siwkowski, Y. Lian, A. Hampel, *Biochemistry* **1995**, *34*, 15785-15791.
[115] S. Li, C. E. Lunse, K. A. Harris, R. R. Breaker, *Rna* **2015**, *21*, 1845-1851.

[116] L. Zheng, C. Falschlunger, K. Huang, E. Mairhofer, S. Yuan, J. Wang, D. J. Patel, R. Micura, A. Ren, *Proc Natl Acad Sci U S A* **2019**, *116*, 10783-10791.
[117] Y. Nomura, H. C. Chien, Y. Yokobayashi, *Chem Commun (Camb)* **2017**, *53*, 12540-12543.
[118] D. Eiler, J. Wang, T. A. Steitz, *Proc Natl Acad Sci U S A* **2014**, *111*, 13028-13033.
[119] C. Hammann, A. Luptak, J. Perreault, M. De La Pena, *Rna* **2012**, *18*, 871-885.
[120] R. L. Tanguay, D. R. Gallie, *Molecular and Cellular Biology* **1996**, *16*, 146-156.
[121] C. Reymond, J.-D. Beaudoin, J.-P. Perreault, *Cellular and Molecular Life Sciences* **2009**, *66*, 3937-3950.
[122] C.-H. T. Webb, D. Nguyen, M. Myszka, A. Lupták, *Scientific Reports* **2016**, *6*, 28179.
[123] T. S. Wadkins, A. T. Perrotta, A. R. Ferré-D'Amaré, J. A. Doudna, M. D. Been, *RNA* **1999**, *5*, 720-727.
[124] D. M. Chadalavada, S. E. Senchak, P. C. Bevilacqua, *Journal of Molecular Biology* **2002**, *317*, 559-575.
[125] Y. Wang, Z. Wang, T. Liu, S. Gong, W. Zhang, *RNA* **2018**, *24*, 1229-1240.
[126] M. Movassat, E. Forouzmand, F. Reese, K. J. Hertel, *RNA* **2019**, *25*, 1793-1805.
[127] A. M. Monteys, A. A. Hundley, P. T. Ranum, L. Tecedor, A. Muehlmatt, E. Lim, D. Lukashev, R. Sivasankaran, B. L. Davidson, *Nature* **2021**, *596*, 291-295.
[128] L. Luo, J. D.-Y. Jea, Y. Wang, P.-W. Chao, L. Yen, *Nature Biotechnology* **2024**.
[129] J. T. Mendell, N. A. Sharifi, J. L. Meyers, F. Martinez-Murillo, H. C. Dietz, *Nat Genet* **2004**, *36*, 1073-1078.
[130] K. A. Spriggs, M. Bushell, A. E. Willis, *Mol Cell* **2010**, *40*, 228-237.
[131] G. E. May, C. Akirtava, M. Agar-Johnson, J. Micic, J. Woolford, J. McManus, *eLife* **2023**, *12*, e69611.
[132] J. Zuallaert, F. Godin, M. Kim, A. Soete, Y. Saeys, W. De Neve, *Bioinformatics* **2018**, *34*, 4180-4188.
[133] O. Cordin, J. D. Beggs, *RNA biology* **2013**, *10*, 83-95.
[134] M. Zuker, *Nucleic acids research* **2003**, *31*, 3406-3415.
[135] F. Alghoul, S. Laure, G. Eriani, F. Martin, *Elife* **2021**, *10*.
[136] L. Guo, C.-M. Liu, *Scientific Reports* **2015**, *5*, 18087.
[137] D.-Y. Hwang, J. B. Cohen, *Molecular and cellular biology* **1997**, *17*, 7099-7107.
[138] L. Cartegni, J. Wang, Z. Zhu, M. Q. Zhang, A. R. Krainer, *Nucleic acids research* **2003**, *31*, 3568-3571.
[139] C. M. Swanson, N. M. Sherer, M. H. Malim, *Journal of virology* **2010**, *84*, 6748-6759.
[140] T. E. Dever, I. P. Ivanov, M. S. Sachs, *Annual review of genetics* **2020**, *54*, 237-264.
[141] D. Kelvin, B. Suess, *RNA biology* **2023**, *20*, 457-468.
[142] X. W. Fang, P. Thiyagarajan, T. R. Sosnick, T. Pan, *Proceedings of the National Academy of Sciences* **2002**, *99*, 8518-8523.
[143] G. Dougan, C. Dowson, J. Overington, *Drug Discov. Today* **2019**, *24*, 452-461.
[144] aM. Weerasinghe, S. E. Liem, S. Asad, S. E. Read, S. Joshi, *Journal of virology* **1991**, *65*, 5531-5534; bO. Yamada, M. Yu, J. K. Yee, G. Kraus, D. Looney, F. Wong-Staal, *Gene therapy* **1994**, *1*, 38-45; cC. Zhou, I. C. Bahner, G. P. Larson, J. A. Zaia, J. J. Rossi, E. B. Kohn, *Gene* **1994**, *149*, 33-39.
[145] M. C. Leavitt, M. Yu, F. Wong-Staal, D. J. Looney, *Gene therapy* **1996**, *3*, 599-606.
[146] S. Larsson, G. Hotchkiss, M. Andäng, T. Nyholm, J. Inzunza, I. Jansson, L. Ahrlund-Richter, *Nucleic acids research* **1994**, *22*, 2242-2248.
[147] N. K. Tanner, *FEMS Microbiology Reviews* **1999**, *23*, 257-275.
[148] B. Malbert, V. Labaurie, C. Dorme, E. Paget, *Molecules (Basel, Switzerland)* **2023**, *28*.
[149] J. B. Murray, J. R. Arnold, *Biochem J* **1996**, *317 (Pt 3)*, 855-860.
[150] aW. C. Winkler, A. Nahvi, A. Roth, J. A. Collins, R. R. Breaker, *Nature* **2004**, *428*, 281-286; bA. R. Ferre-D'Amare, *Q. Rev. Biophys.* **2010**, *43*, 423-447.
[151] aA. Schüller, D. Matzner, C. E. Lünse, V. Wittmann, C. Schumacher, S. Unsleber, H. Brötz-Oesterhelt, C. Mayer, G. Bierbaum, G. Mayer, *ChemBioChem* **2017**, *18*, 435-440; bV. Panchal, R. Brenk, *Antibiotics* **2021**, *10*.

[152] aT. J. McCarthy, M. A. Plog, S. A. Floy, J. A. Jansen, J. K. Soukup, G. A. Soukup, *Chem. Biol.* **2005**, *12*, 1221-1226; bJ. Lim, B. C. Grove, A. Roth, R. R. Breaker, *Angew. Chem.* **2006**, *118*, 6841-6845.
[153] X. Fei, T. Holmes, J. Diddle, L. Hintz, D. Delaney, A. Stock, D. Renner, M. McDevitt, D. B. Berkowitz, J. K. Soukup, *ACS Chemical Biology* **2014**, *9*, 2875-2882.
[154] V. R. Jadhav, M. Yarus, *Biochimie* **2002**, *84*, 877-888.
[155] G.-N. Wang, P. S. Lau, Y. Li, X.-S. Ye, *Tetrahedron* **2012**, *68*, 9405-9412.
[156] S. Arnaouteli, N. C. Bamford, N. R. Stanley-Wall, Á. T. Kovács, *Nature Reviews Microbiology* **2021**, *19*, 600-614.
[157] H. Ludwig, N. Rebhan, H.-M. Blencke, M. Merzbacher, J. Stülke, *Molecular Microbiology* **2002**, *45*, 543-553.
[158] aT. M. Henkin, *FEMS microbiology letters* **1996**, *135*, 9-15; bJ. Stülke, W. Hillen, *Annu Rev Microbiol* **2000**, *54*, 849-880.
[159] K. Morabbi Heravi, J. Altenbuchner, *Journal of bacteriology* **2018**, *200*.
[160] E. Helgason, O. A. Okstad, D. A. Caugant, H. A. Johansen, A. Fouet, M. Mock, I. Hegna, A. B. Kolstø, *Applied and environmental microbiology* **2000**, *66*, 2627-2630.
[161] H. Grundmann, D. M. Aanensen, C. C. van den Wijngaard, B. G. Spratt, D. Harmsen, A. W. Friedrich, *PLoS medicine* **2010**, *7*, e1000215.
[162] M. U. Okwu, M. Olley, A. O. Akpoka, O. E. Izevbuwa, *AIMS microbiology* **2019**, *5*, 117-137.
[163] J. C. Cochrane, S. V. Lipchock, S. A. Strobel, *Chem. Biol.* **2007**, *14*, 97-105.
[164] L. I. Alvarez-Añorve, M. L. Calcagno, J. Plumbridge, *Journal of bacteriology* **2005**, *187*, 2974-2982.
[165] A. G. M. Tielens, M. Houweling, S. G. Van Den Bergh, *Biochemical Pharmacology* **1985**, *34*, 3369-3373.
[166] F. Vincent, G. J. Davies, J. A. Brannigan, *Journal of Biological Chemistry* **2005**, *280*, 19649-19655.
[167] N. P. Vitko, M. R. Grosser, D. Khatri, T. R. Lance, A. R. Richardson, *mBio* **2016**, *7*.
[168] Z. Moraveji, M. Tabatabaei, H. Shirzad Aski, R. Khoshbakht, *Iranian journal of veterinary research* **2014**, *15*, 326-330.
[169] G. Gonzy-Tréboul, M. Steinmetz, *Journal of bacteriology* **1987**, *169*, 2287-2290.
[170] M. Milena, F. Simon, E. Anna, M. Daniel, B. Alexander, M. Dirk, B.-O. Heike, M. Christoph, M. Günter, *bioRxiv* **2023**, 2023.2002.2008.527593.
[171] E. Badr, M. ElHefnawi, L. S. Heath, *PLOS ONE* **2016**, *11*, e0166978.

10. Appendix

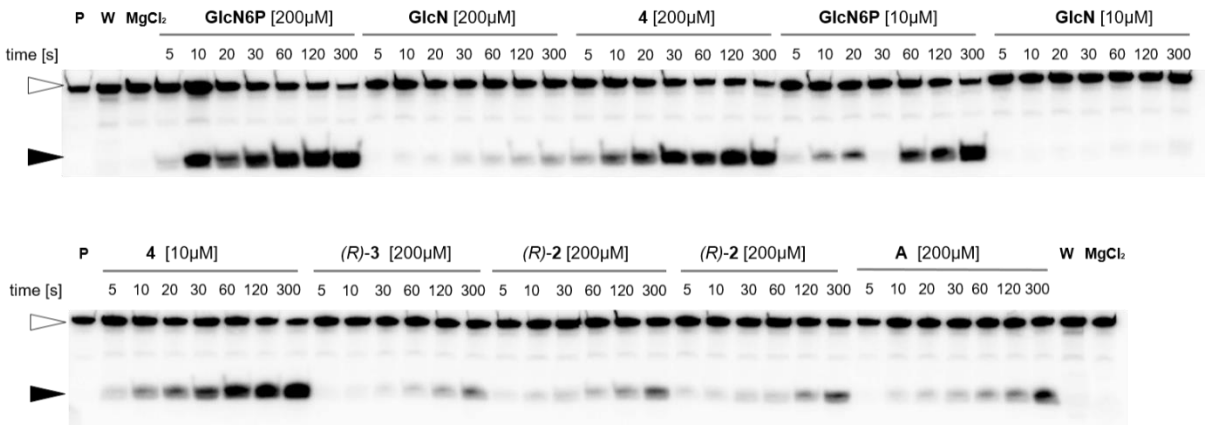

Supplementary Figure 1: Exemplary radiographs of the self-cleavage reaction of 5'-^{32}P-labeled *glmS* ribozyme from *B. subtilis* in presence of different coenzymes. The precursor lane (P) shows the untreated ribozyme RNA without any compounds. Another control (W) shows the ribozyme incubated for 300 s at 37 °C only in ultra-purified water. We also incubated the *glmS* ribozyme for 300 s at 37 °C in presence of 10 mM $MgCl_2$. Time-dependent cleavage was recorded for GlcN6P, GlcN, thia-GlcN6P (4), fluorophosphonate *(R)*-3, hydroxyphosphonates *(R)*-2 and *(S)*-2 and the methylene phosphonate A. The respective coenzyme concentrations are depicted in brackets. The white arrow indicates the full-length band, whereas cleavage band is indicated by the black arrow. The fluorophosphonate *(S)*-3 and difluorophosphonate 1 are not shown here as they were tested only in higher concentrations on another gel and for reasons of clarity.

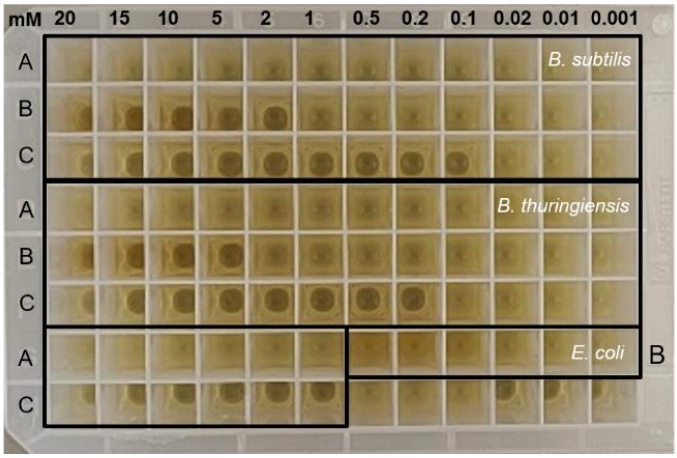

Supplementary Figure 2: Minimal inhibitory concentration of A) thia-glucose, B) thia-glucosamine 5, C) chloramphenicol determined in liquid culture. Different compound concentrations are tested for *B. subtilis* and *B. thuringiensis*, as well as *E. coli* as a negative control. For *E. coli* only the six highest concentrations were tested for each compound (1-20 mM) Additionally growth in absence of the respective compound and sterile control was added (bottom right).Cell growth was determined by eye and dark spots are the bottom of the well, which can be seen if the medium is still clear.

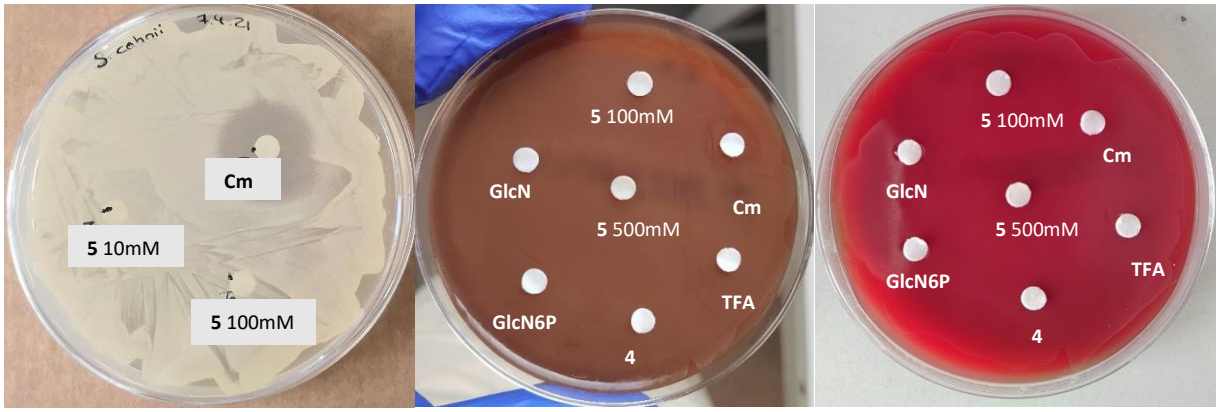

Supplementary Figure 3: Filter disk assay on Mueller Hinton agar plates. Left: *Staphylococcus cohnii* plated out on LB agar plate and respective compounds tested on a filter disc (10 µL). Middle: *Enterococcus hirae*, Right: *Enterococcus feacalis* plated out on Mueller Hinton blood agar plates and respective compounds tested on a filter disc (10 µL). thia-GlcN 5 at a concentration of 100 mM and 500 mM, respectively. Cm: chloramphenicol at a concentration of 9.3 mM. Other compounds at 100 mM. No effect on bacterial growth of the synthetic compound could be observed.

Supplementary Table 1: Nucleotide sequences of used ribozyme motifs. Inactivation mutation is highlighted in red. For the short hepatitis delta virus (HDV) ribozyme and short human RECK HHR version the blue sequence is deleted.

Class	Sequence 5'-3'
HDV	caaacaaacaaaTGGCCGGCATGGTCCCAGCCTCCTCGCTGGCGCCGGCTGGGCAACATTC CGAGGGGACCGTCCCCTCGGTAATGG(C/T)GAATGGGACGCACAAATCTCTCTAGcaaa caaacaaa
HHR t1 (N107)	caaacaaacaaaTGAGGTGCAGGTACATCCAGCTGACGAGTCCCAAATAGGACGA(A/G)ACG CGCTTCGGTGCGTCCTGGATTCCACTGCTATCCAcaaacaaacaaa
HHR t3	caaacaaacaaaGCGCGTCCTGGATTCCACGGTACATCCAGCTGATGAGTCCCAAATAGGAC GA(A/G)ACGCGCcaaacaaacaaa
Twister p3	caaacaaacaaaCTCCTTTAAAGCG(GT/TG)TACAAGCCCGCAAAAATAGCAGAGTAATGGGA AACCATTAATGCAGCTTTAAAGGAGAcaaacaaacaaa
TS-1 p1	caaacaaacaaaACCCGCAAGGCCGACGGCATCCGCCGCCGCTGGTGCAAGTCCAGCCGCC CCGAAAGGGGCGGGCGCTCATGGGTcaaacaaacaaa
TS-1 p5	caaacaaacaaaGGGGCGGGCGCTCATGGGTGAAAACCCGCAAGGCCGACGGCATCCGCC GCCGCTGGTGCAAGTCCAGCCGCCCCcaaacaaacaaa
TS-2 p1	caaacaaacaaaGCAGGGCAAGGCCCAGTCCCGTGAAAGCCGGGACCGCCCCGAAAGGGG CGCGGCGCTCATGCCTGCcaaacaaacaaa
TS-2 p5	caaacaaacaaaGGGGCGCGGCGCTCATGCCTGCGAAAGCAGGGCAAGGCCCAGTCCCGT GAAAGCCGGGACCGCCCCcaaacaaacaaa
TS-3 p1	caaacaaacaaaGACCCGCAAGGCCGACGGCATCCCGCCGCCGCTGGTGCAAGCCCAGCC GCCCCGAAAGGGGCGGGCGCTCATGGGTCcaaacaaacaaa
TS-3 p5	caaacaaacaaaGGGGCGGGCGCTCATGGGTCGAAAGACCCGCAAGGCCGACGGCATCCC GCCGCCGCTGGTGCAAGCCCAGCCGCCCCcaaacaaacaaa
TS-4 p1	caaacaaacaaaTTTGGCAGGGCAAGGCCCAGTCCC(GT/TG)GCAAGCCGGGACCGCCCCT TCGGAAAGAGGGGGCGCGGCGCTCATTCCTGCcaaacaaacaaa
TS-4 p5	caaacaaacaaaGAGGGGGCGCGGCGCTCATTCCTGCCAAAGAAATTTTGGCAGGGCAAGG CCCAGTCCCGTGCAAGCCGGGACCGCCCCTTCcaaacaaacaaa
Pistol	caaacaaacaaaGGAGCCGTTCGGGCGGCTATAAACAGACCTCAGGCCCGAA(GC/TA)GTG GCGGCGAAAGCCGCCGGTGGTAcaaacaaacaaa
Hairpin	caaacaaacaaaGCGCA(G/C)TACTGTTTCCTCCAAACAGCGAAGCGCGCCAGGGAAACAC ACCATGTGTGGTATATTATCTGGCAcaaacaaacaaa
Hovlinc	caaacaaacaaaGCTAATGAGCCACATACCTACCCATCTCTCGCAATGTGTAACTTCCCCCT GGTTGGAGAGATCCGGACTAG(G/C)AGCCAGGGGGCcaaacaaacaaa
Ht-2	caaacaaacaaaCATTCCTCAGAAAATGACAAACCTGTGGGGCGTAAGTAGATATGTGAAA ACATATCTATGATCGT(GC/AA)AGACGTTAAAATCAGGTcaaacaaacaaa
glmS (*B. subtilis*)	caaacaaaCCTATAATTATAGCGCCCGAACTAAGCGCCCGGAAAAAGGCTTAGTTGACGA GGATGGAGGTTATCGAATTTTCGGCGGATGCCTCCCGGCTGAGTGTGCAGATCACAGC CGTAAGGATTTCTTCAAACCAAGGGGGTGACTCCTTGAACAAAGAGAAATCcaaacaaa
CPEB3	caaacaaacaaaGGATAA(A/C)AGGGGGCCACAGCAGAAGCGTTCACGTCGCAGCCCCTGTCA GATTCTGGTGAATCTGCGAATTCTGCTGcaaacaaacaaa

Supplementary Table 2: Nucleotide sequences of used aptazyme constructs. The Tet-aptamer is highlighted in blue. For the 5' tandem (short) the orange sequence is deleted. Green is an additional stem structure.

Aptazymes	Sequence 5'-3'
5' tandem	caaacaaacaaaGGCCATAAAACATACCAGATGAAAGTCTGGAGAGGTGAAGAATACGACCAC CTATGGCCGGCATGGTCCCAGCCTCCTCGCTGGCGCCGGCTGGGCAACATTCCGAGGGG ACCGTCCCCTCGGTAATGGCGAATGGGACGCACAAATCTCTCTAGcaaacaaacaaa
3' tandem	caaacaaacaaaATGGCCGGCATGGTCCCAGCCTCCTCGCTGGCGCCGGCTGGGCAACATTC CGAGGGGACCGTCCCCTCGGTAATGGCGAATGGGACTAAAACATACCAGATGAAAGTCTG GAGAGGTGAAGAATACGACCACCTAGTCCCATTCGcaaacaaacaaa
Insertion in J1/2	caaacaaacaaaTGGCCGGCCATAAAACATACCAGATGAAAATCTGGAGAGGTGAAGAATTCG ACCACCTAGGTCCCAGCCTCCTCGCTGGCGCCGGCTGGGCAACATTCCGAGGGGACCGT CCCCTCGGTAATGGCGAATGGGACcaaacaaacaaa
Insertion in L3	caaacaaacaaaATGGCCGGCATGGTCCCACGCTCCTCGCTAAAACATACCAGATGAAAATCT GGAGAGGTGAAGAATTCGACCACCTAGCGGCCGGCTGGGCAACATTCCGAGGGGACCGT CCCCTCGGTAATGGCGAATGGGACcaaacaaacaaa
Slip 1	caaacaaacaaaATGGCCGGCATGGTCCCAGCCTCCTCGCTGGCGCCGGCTGGGCAAGTGTT ATAAAACATACCAGATGAAAGTCTGGAGAGGTGAAGAATACGACCACCTAGCACGCGAATG GGACcaaacaaacaaa
Slip 2	caaacaaacaaaATGGCCGGCATGGTCCCAGCCTCCTCGCTGGCGCCGGCTGGGCAAGTGTT ATAAAACATACCAGATGAAAGTCTGGAGAGGTGAAGAATACGACCACCTATCACGCGAATG GGACcaaacaaacaaa
Slip 3	caaacaaacaaaATGGCCGGCATGGTCCCAGCCTCCTCGCTGGCGCCGGCTGGGCAAGCGCT ATAAAACATACCAGATGAAAGTCTGGAGAGGTGAAGAATACGACCACCTAGCGCGCGAATG GGACcaaacaaacaaa
Pseudoknot 1	caaacaaacaaaATGGCCGGCATGGTCCCAGCCTCCTCGCTGGCGCCGGCTGGGCAACATTC CGAGGGGACCGTCCCCTCGGTAATGGCGAATGGGACGAAAGGCCGATGGGAGCGACATC GGCCcaaacaaacaaa
Pseudoknot 2	caaacaaacaaaATGGCCGGCATGGTCCCAGCCTCCTCGCTGGCGCCGGCTGGGCAACATTC CGAGGGGACCGTCCCCTCGGTAATGGCGAATGGGACGAAAGGCCGATGGGCGAGGCATC GGCCTAAAACATACCAGATGAAAGTCTGGAGAGGTGAAGAATACGACCACCTAGGCCGATG Caaacaaacaaa

Supplementary Table 3: Nucleotide sequences of uORF motifs. Flanking splice sites are highlighted in orange.

Aptazymes	Sequence 5'-3'
SynORF 1	agACCACCACATAAAACATACCAGATGAAAGTCTGGAGAGGTGAAGAATACGACCACCAT GTGGTGGTAAGgtaatg
SynORF 2	agACCACCACATCCAGATGAAAGTCTGGAGAGGTGAAGAATACGACCACCATGTGGTGGT AAGgtaatg
SynORF 3	agCTTACCACCTGGAGATGAAAGTGTCCAGATGCTGAAGATGGTAAGACAGgtaatg
Hox a3	agAGAAGCTTCTGGGAGCCGCGGTCTGAAGGCTACGTGTGCTGCCTGGTCATTCAAAGT GTCAATTTTAGGTCCAGAAGTGTCCAAACCACAAGTTCTCAAAACTCTGAAAAATGGCTCC CTCCATGTTAAGAGTGCCTGGACACTGGAAAAAAAGATTCCCTGAGCACCTGAGgtaatg
Hox a11	agATCCCTCACCCACCGGGGAGTGGGGGGAGGCGTCAGGAGTTGCGCTCTCTTGCCGC CCTCAGAGCACTCGTGGACCAGGAGGATGTAGCTGAGCAAAGGAGAGCTGCCCGGGGG CGCACCCCAGCCTTTCTGCGCGCGGGGAGGCCCCCCAGCCAACATGAGTTACACCGGC GATTACGTGCTTTCGGTGAGAACACCGAGTGACGATCTGTTGCAGgtaatg
SPINK	agATGACCCTTCCAGTCCCAGGCTTCTGAAGAGATGTGCTAAgtaatg
SPINK short	agATGTGCTAAgtaatg
SRY	agATGCAAGTTTCATTACAAAAGTTAACGTAACAAAGAATCTCGTAGAAATGAGTTTTGGAT AGTAAGgtaatg
SRY short	agATGAGTTTTGGATAGTAAGgtaatg

5’-

AGgtgagtctatgggacccttgatgttttctttccccttctttttctatggttaagttcatgtcataggaaggggagaagtaacagggtac
acatattgaccaaatcagggtaattttgcatttgtaattttaaaaaatgctttcttctttttaatatacttttttgtttatcttatttctaatactttccc
taatctctttctttcagggcaataatgatacaatgtatcatgccgagtaacgctgtttctctaacttgtagACCACCACATAAAA
CATACCAGATGAAAGTCTGGAGAGGTGAAGAATACGACCACCATGTGGTGGTAAGGTAA
TGTCCTAAAACATACCAGATGAAAGTCTGGAGAGGTGAAGAATACGACCACCTAGGACA
TTACgcaccattctaaagaataacagtgataatttctgggttaaggcaatagcaatatttctgcatataaatatttctgcatataaatt
gtaactgatgtaagaggtttcatattgctaatagcagctacaatccagctaccattctgcttttatttatggttgggataaggctggatta
ttctgagtccaagctaggccctttgctaatcatgttcatacctcttatcttcctcccacagCCACC**ATG…**-3’

Supplementary Figure 4: Nucleotide sequence of splice cassette. Introns depicted in lowercase letters. 3’ splice sites highlighted in red and 5’ splice sites in yellow. The Tet-aptamer sequence is marked in blue. The synORF sequence, which can be replaced by any sequence in Supplementary Table 3, is underlined. Bold letters indicate the start codon of the respective luciferase gene.

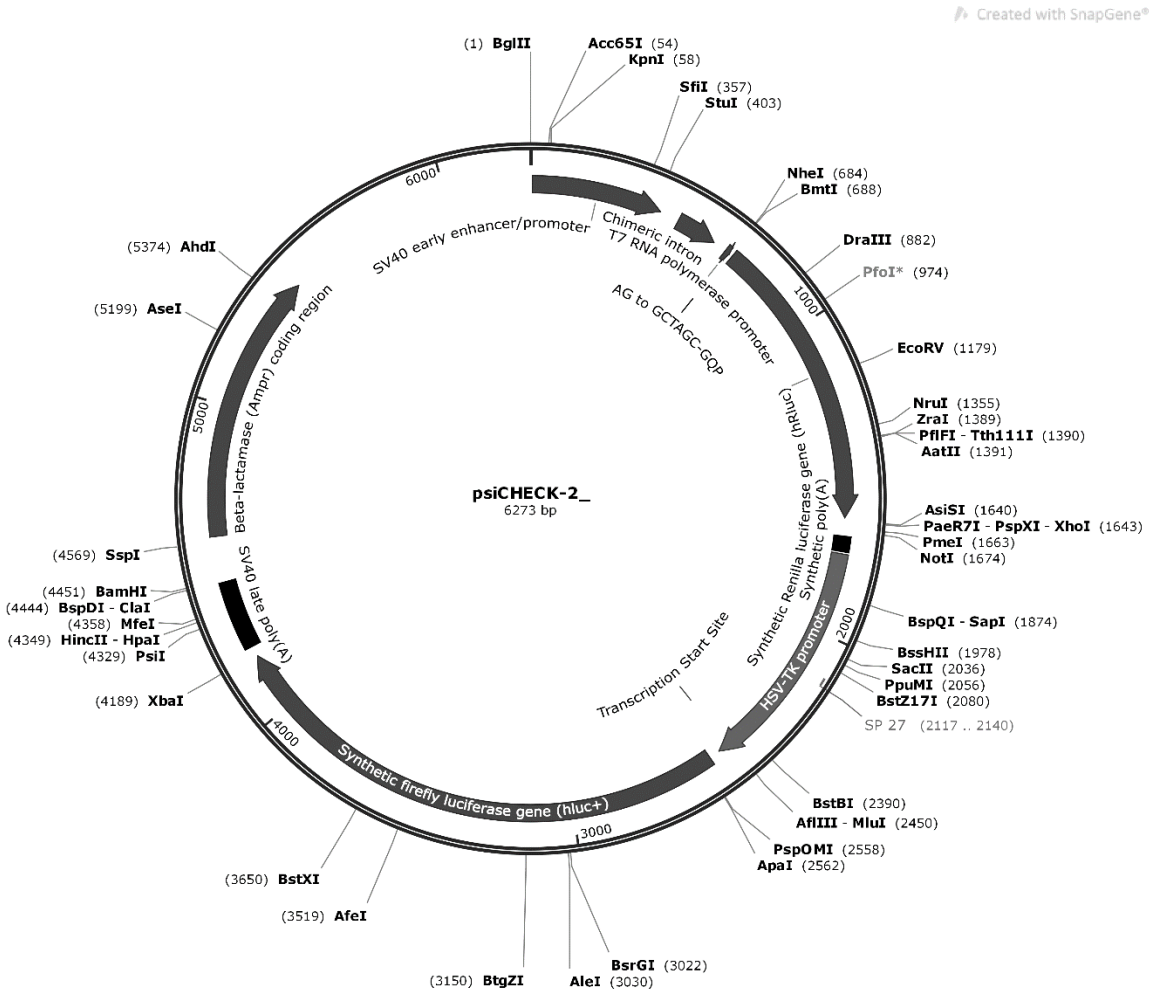

Supplementary Figure 5: psiCheck™-2 vector (Promega). Used for measurements in HeLa cells to control gene expression levels. The vector encodes for the Renilla luciferase (hRluc) and the firefly luciferase (hLuc+). It also conveys an ampicillin resistance.

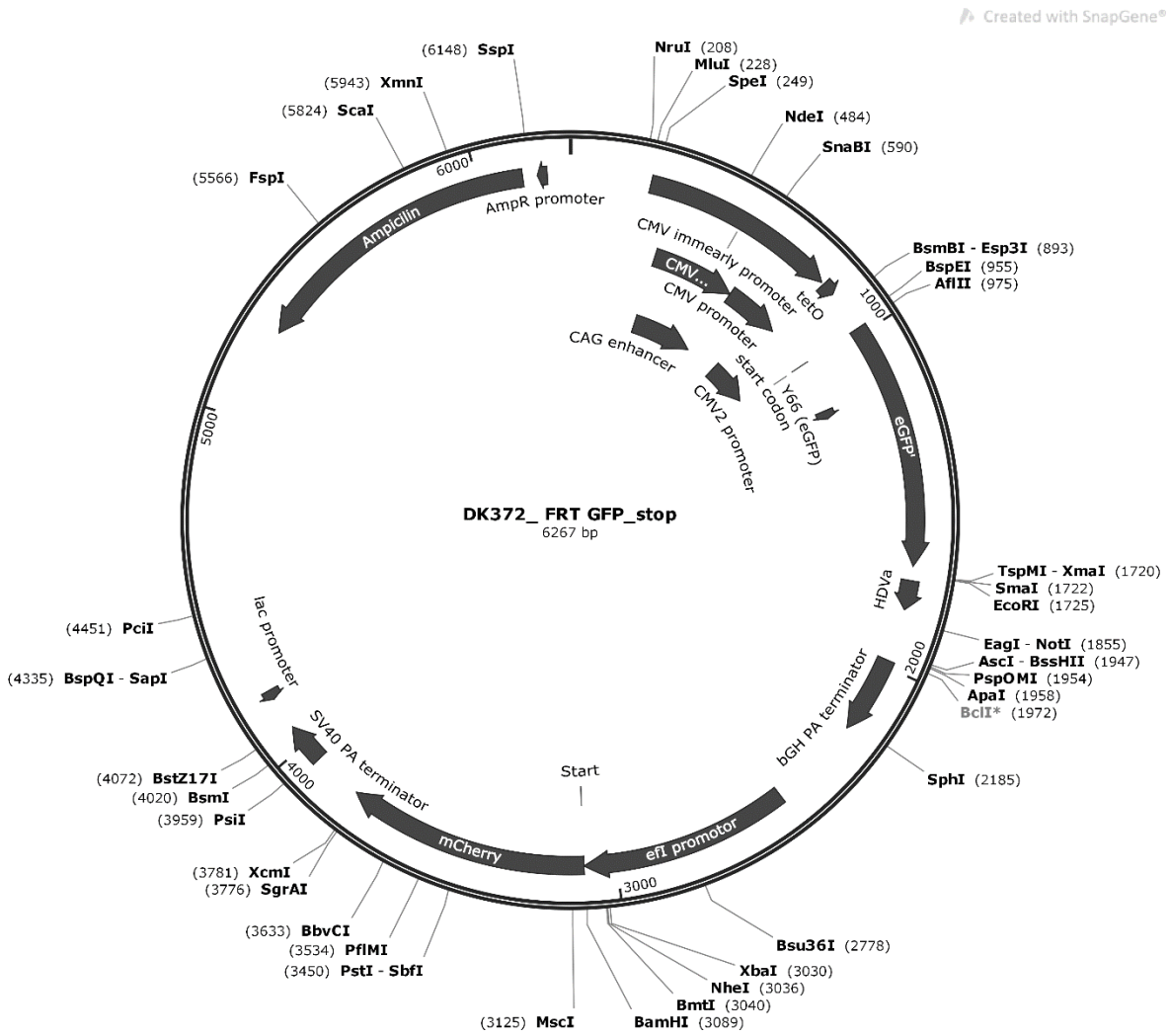

Supplementary Figure 6: Modified psiCheck™-2 vector (Promega). Used for measurements in HeLa cells to control gene expression levels. The vector encodes for the enhanced green fluorescent protein (eGFP) and the red fluorescent protein (mCherry). It also conveys an ampicillin resistance.

11. Acknowledgements

Mit großer Freude und Erleichterung beende ich an dieser Stelle meine Dissertation und möchte die Gelegenheit nutzen, mich bei einigen zu bedanken! Dieses Projekt war nicht nur eine akademische Herausforderung für mich, sondern auch eine Reise voller Lernmomente, Durchhaltevermögen und auch vieler lustiger Momente.

Mein aufrichtiger Dank gilt in erster Linie meinem Betreuer Prof. Dr. Jörg Hartig. Vielen Dank, dass ich Teil Deiner Arbeitsgruppe sein durfte. Die Arbeit war sehr abwechslungsreich und ich durfte mich immer austoben, wie ich es wollte. Vielen Dank für die Betreuung unterwegs, die Tipps und Möglichkeiten, die dann jetzt am Ende zu dieser doch recht spannenden Arbeit geführt haben.

Herzlichen Dank auch an Prof. Dr. Valentin Wittmann für die Übernahme des Zweitgutachtens und die Betreuung und die Gespräche während meiner Promotion. Das gemeinsame Projekt hat mich von Anfang an begeistert und wir konnten es doch recht erfolgreich abschließen.

Bjarne, es war mir eine Ehre mit dir zusammen zu arbeiten! Vielen Dank für deine Unterstützung und den Zuspruch und die ein oder andere Fotosession! :D

Ein herzliches Dankeschön geht ebenso an meine Familie für die Unterstützung auch durchs ganze Studium hindurch. #MeinOsten

Liebe geht raus an meine Freunde die mir nicht nur in den akademischen Höhen, sondern vor allem auch in den Tiefen mit Rat, Tat und mit viel Humor und Ablenkung zur Seite standen. Die Trixies haben mich mit Trash immer wieder in die Realität zurückgeholt, wenn denn mal ein Upsi passiert ist. Sowohl emotionale, intellektuelle als auch wohlfeile Abende gehen auf das Konto der Trixies <3. Ihr Fünf seid meine persönlichen Superhelden, die mich auch durch jede Schreibblockade begleitet haben. Yannick, ich liebe dich!

Und wie könnte ich meine Dankbarkeit ausdrücken, ohne meinem treuen Begleiter zu huldigen – meinem Computer. Trotz zahlreicher Tastaturattacken, verzweifelter Blicke in den Bildschirm und mancher emotionalen Ausbrüche ist er stets loyal geblieben.

Danke an das alte Labor L969! Ihr seid der Grund warum ich in diese Arbeitsgruppe gekommen bin. Aber auch großen Dank an die aktuelle AG für die hilfreichen Tipps, die überzogenen Kaffeepausen, die genialen Feiern und die wirklich gute Zusammenarbeit. Ich habe gern mit euch gearbeitet.

Besonderen Dank an alle, die mir während der Arbeit geholfen haben (Peter, Lissy, Josi, Vera, Malte), ihr wart mir eine riesen Hilfe!! Und Danke an alle, die ein Teil dieser unvergesslichen Reise durch meine Promotion waren. <3